

**Dissertation zur Erlangung des Doktorgrades
der Fakultät für Chemie und Pharmazie
der Ludwig-Maximilians-Universität München**

**Roles of PIP aquaporins in lateral root development
and stress responses in *Arabidopsis thaliana***

Jin Zhao

aus

Shenyang, China

2013

Erklärung

Diese Dissertation wurde im Sinne von § 7 der Promotionsordnung vom 28. November 2011 von PD Dr. Anton Schäffner betreut.

Eidesstattliche Versicherung

Diese Dissertation wurde eigenständig und ohne unerlaubte Hilfe erarbeitet.

München, am 04.06.2013

(Jin Zhao)

Dissertation eingereicht am	04.06.2013
1. Gutachter:	PD Dr. Anton Schäffner
2. Gutachter:	Prof. Dr. Jörg Durner
Mündliche Prüfung am	10.07.2013

ABSTRACT

Aquaporins are water channel proteins belonging to the major intrinsic protein (MIP) family. They facilitate water transport across cellular membranes. In plants, plasma membrane intrinsic proteins (PIPs) represent abundant aquaporins located at the plasma membrane. Here I study (i) the impact of PIP-dependent tissue hydraulics on lateral root (LR) development and (ii) metabolomic changes provoked by the loss of *PIP* genes in control, drought and heat scenarios employing the model plant *Arabidopsis thaliana*.

LR development is crucial for the establishment of a mature root system. The developmental processes leading to the initiation of the lateral root primordium (LRP) in defined pericycle cells in the inner root tissue, to its expansion and finally to the penetration of the overlaying tissue are predominantly regulated by a local accumulation of the phytohormone auxin. Although tissue hydraulics should affect these steps, the role of PIP aquaporins in LR development has not yet been studied. Expression assays reveal that most *PIP* genes are repressed by exogenous auxin treatment. In many cases, this repression is dependent on the transcription factor AUXIN RESPONSE FACTOR 7 (ARF7) mediating auxin responses. The spatio-temporal expression patterns of most *PIP* genes during LR development using *proPIP::GUS* reporter lines demonstrate that the highly expressed isoforms *PIP2;1* and *PIP2;2* are progressively excluded from the tip of LRP while being maintained at its base and in the underlying stele. *PIP1;2* and *PIP2;7* are repressed only at the tip of the LRP throughout its growth, and they are also present in the overlaying tissue. *PIP1;1* and *PIP2;4* are exclusively expressed in the overlaying tissue. Their expression in the overlaying tissue is somewhat weaker than in flanking regions of the root. In contrast, *PIP2;8* is highly induced later during LR development at the base of LRP and the underlying stele in an auxin-independent manner. A tissue-scale mathematical model (developed by Leah Band, University of Nottingham) further predicts the delayed lateral root emergence (LRE) in loss-of-function *pip* mutants, in which LRP-expressed isoforms are affected. Consistent with the model prediction, *pip2;1*, *pip2;2*, *pip1;2* and *pip2;7* exhibit retarded LRP outgrowth. However, *pip1;1*, *pip2;4* and *pip2;8* cannot confirm the current model which predicts accelerated LRE, since all mutants exhibit delayed LRE. Taken together, these findings indicate that LRE requires the spatio-temporal distribution of PIP aquaporins regulated by both auxin-dependent and independent pathways.

Drought and heat are key factors of climate change scenarios affecting plant water relations. In this study, the involvement of PIP aquaporins in coping with such conditions is addressed by analyzing the altered stress responses at metabolic level upon loss of *PIP2;1*, *PIP2;2* and

ABSTRACT

PIP2;4 isoforms. Non-targeted metabolomics analysis using ultra-high resolution Fourier Transform Ion Cyclotron Resonance Mass Spectrometry (FT-ICR-MS) approach reveals that the metabolic profiles are affected by both environmental conditions and *PIP* mutations. Among the significantly changed m/z peaks identified in *pip* mutants compared to wild-type plants most are related to a specific condition. The changes of putative soluble sugars, sulfur-containing metabolites and some unknown peaks due to the loss of PIP isoforms could reflect the metabolic regulations upon reduction of cellular water permeability.

CONTENTS

ABSTRACT	I
ABBREVIATIONS	VI
1. INTRODUCTION	1
1.1 Water transport and aquaporins in plants	1
1.1.1 Water uptake and transport	1
1.1.2 Plant aquaporins	2
1.1.2.1 Structure and substrate selectivity	2
1.1.2.2 MIP subfamilies in plants	3
1.1.2.3 Transcript and protein levels of PIP aquaporins in <i>Arabidopsis</i>	3
1.1.2.4 Regulations and functions of PIP aquaporins in <i>Arabidopsis</i>	5
1.1.2.4.1 Water transport in roots and leaves	5
1.1.2.4.2 Response of PIP aquaporins to various environmental stimuli	6
1.1.2.4.3 Root growth and development	8
1.1.2.4.3.1 Elongation of the primary root and root hairs	8
1.1.2.4.3.2 Lateral root development	9
1.2 Aims of this work	10
2. REGULATION OF PIP AQUAPORINS IS REQUIRED TO FACILITATE LATERAL ROOT EMERGENCE	11
2.1 Results	14
2.1.1 The majority of root <i>PIP</i> genes are repressed by exogenous auxin	14
2.1.2 Regulation of root <i>PIPs</i> by auxin is dependent on ARF7	14
2.1.3 Auxin alters spatial expression of <i>PIP</i> aquaporins during LR development	17
2.1.4 Primordium-expressed <i>PIP</i> aquaporins are major isoforms in the whole stele	19
2.1.5 Spatial expression of <i>PIP</i> aquaporins is required during LRE	23
2.1.6 Expression of <i>PIP2;8</i> during LR formation is not regulated by auxin	27
2.1.7 Twenty-one transcription factors were identified as interesting candidates regulating <i>PIP2;8</i> expression during LR development	32
2.1.8 <i>PIP2;8</i> function is also required for promoting LRE	36
2.2 Discussion	37

CONTENTS

2.2.1 Fine-tuned regulation of aquaporin-dependent tissue hydraulics by auxin facilitates LRE.....	37
2.2.2 Auxin-responsive <i>PIPs</i> are regulated by ARF7 and parallel pathways.....	38
2.2.3 Understanding a novel aquaporin-dependent regulation of LRE requires identification of regulators of <i>PIP2</i> ;8 expression	39
2.2.4 LRE phenotypes of some <i>pip</i> mutants help to refine crucial parameters in the current mathematical model.....	41
2.2.5 Mutations in <i>PIPs</i> do not affect LR number under normal growth conditions	43
3. INVOLVEMENT OF PIP AQUAPORINS IN RESPONSE TO ALTERED ENVIRONMENTAL CUES.....	45
3.1 Experimental design.....	45
3.1.1 Genotype selection.....	45
3.1.2 Growth conditions and stress application	45
3.1.3 Replicate arrangement and harvest	47
3.1.4 Non-targeted metabolome analysis using FT-ICR-MS	48
3.2 Results.....	49
3.2.1 Several data-processing strategies of statistical analyses emerge from the quality control of the metabolic profile datasets.....	49
3.2.2 Both stress conditions and <i>PIP</i> mutations affect metabolic profiles	52
3.2.3 Loss of major PIP isoforms results in specific metabolic changes under different environmental conditions.....	55
3.3 Discussion	63
3.3.1 Loss of major PIPs is associated with altered accumulation of putative osmoprotectants and glucosinolate biosynthesis.....	63
3.3.2 Heat stress in combination with high air humidity seems to trigger specific metabolic responses.....	66
3.3.3 Integration of metabolome and transcriptome data helps to better understand the metabolic responses caused by <i>PIP</i> mutations	68
4. MATERIALS AND METHODS.....	69
4.1 Materials.....	69
4.1.1 Plant materials	69
4.1.2 Media and solutions.....	69

CONTENTS

4.1.3 Restriction enzymes and modifying enzymes	69
4.1.4 Bacterial strains	71
4.1.5 Vectors	71
4.1.6 Antibiotics	72
4.1.7 Plant hormones and hormone response inhibitor	72
4.2 Methods	73
4.2.1 Plant growth conditions	73
4.2.2 Hormone treatments.....	73
4.2.3 qPCR (quantitative Polymerase Chain Reaction).....	74
4.2.4 Generation of double/quadruple mutants.....	74
4.2.4.1 Crossing	74
4.2.4.2 Verification of homozygous double/quadruple mutants	75
4.2.4.2.1 PCR-based genotyping	75
4.2.4.2.2 Reverse Transcription Polymerase Chain Reaction (RT-PCR).....	75
4.2.5 Complementation of <i>pip2;1</i> mutants	76
4.2.6 <i>E. coli</i> transformation and preparation of plasmid DNA.....	77
4.2.7 <i>Agrobacterium</i> transformation	77
4.2.8 Histochemical GUS assay	78
4.2.9 Vibratome sectioning	78
4.2.10 Application of gravitropic stimulus and sampling	79
4.2.11 Microscopy	79
4.2.12 SOM (self-organizing map) analysis	80
4.2.13 Metabolite extraction and FT-ICR-MS measurements.....	80
4.2.14 FT-ICR-MS data processing	82
4.2.15 Assignment of possible metabolite identities	83
5. REFERENCES	85
6. SUPPLEMENTARY MATERIALS	97
6.1 Regulation of PIP aquaporins is required to facilitate lateral root emergence.....	97
6.2 Involvement of PIP aquaporins in response to altered environmental cues	100
ACKNOWLEDGEMENTS.....	111
CURRICULUM VITAE.....	113

ABBREVIATIONS

6-BA	6-benzylaminopurine
ABA	abscisic acid
ACC	1-aminocyclopropane-1-carboxylic-acid (ethylene precursor)
AGI	<i>Arabidopsis</i> Genome Initiative
ARF	auxin response factor
BL	brassinolide
BR	brassinosteroid
C	control condition
cDNA	complementary DNA
d	day
d35S	double enhanced cauliflower mosaic virus 35S
DH	combination of drought and heat stress
dm	<i>pip2;1 pip2;2</i> double mutant
DMSO	dimethyl sulfoxide
DNA	deoxyribonucleic acid
dNTP	deoxynucleotide-5'-triphosphates
DTT	dithiothreitol
<i>E. coli</i>	<i>Escherichia coli</i>
EDTA	Ethylene Diamine Tetra-acetic Acid
e-FP Browser	electronic fluorescent pictographic browser
ER	endoplasmic reticulum
FT-ICR-MS	Fourier Transform Ion Cyclotron Resonance Mass Spectrometry
GFP	Green Fluorescent Protein
GUS	β-Glucuronidase
h	hour
H	heat stress
IAA	indole-3-acetic acid
IE	independent experiment
kb	kilo base pair
kDa	kiloDalton
k _x	permeability of boundary x

ABBREVIATIONS

k_{xinit}	initial permeability of boundary x
k_{2g}	rate of decrease of boundary 2 permeability due to auxin
LR	lateral root
LRE	lateral root emergence
LRP	lateral root primordium / primordia
min	minute
MIP	Major Intrinsic Protein
MS	Murashige and Skoog
m/z	mass-to-charge ratio
NIP	NOD26-like Intrinsic Protein
PCIB	p-chlorophenoxy-isobutyric acid
pgi	post-gravitropic induction
PIP	Plasma membrane Intrinsic Protein
ppm	parts per million
qPCR	quantitative PCR
RNA	ribonucleic acid
rpm	rotations per minute
RT-PCR	Reverse Transcription Polymerase Chain Reaction
SCF	Skp, Cullin, F-box (complex)
SIP	Small basic Intrinsic Protein
SOC	Super Optimal broth with Catabolic repressor
SOM	self-organizing map
TAE	Tris-Acetate-EDTA
TAIR	The <i>Arabidopsis</i> Information Resource
T-DNA	transfer DNA
TF	transcription factor
TIP	Tonoplast Intrinsic Protein
tm	<i>pip2;1 pip2;2 pip2;4</i> triple mutant
v/v	volume per volume
w/v	weight per volume
wt	wild type

1. INTRODUCTION

1.1 Water transport and aquaporins in plants

1.1.1 Water uptake and transport

In plants, roots are mostly responsible for water uptake from the surrounding environment (e.g. soil, hydroponic culture) to fulfill the organisms' water requirements. Once water enters a root, it moves radially across outer tissues to reach the xylem (Figure 1), and eventually achieves long-distance transport and distribution into mesophyll and epidermal cells of leaves.

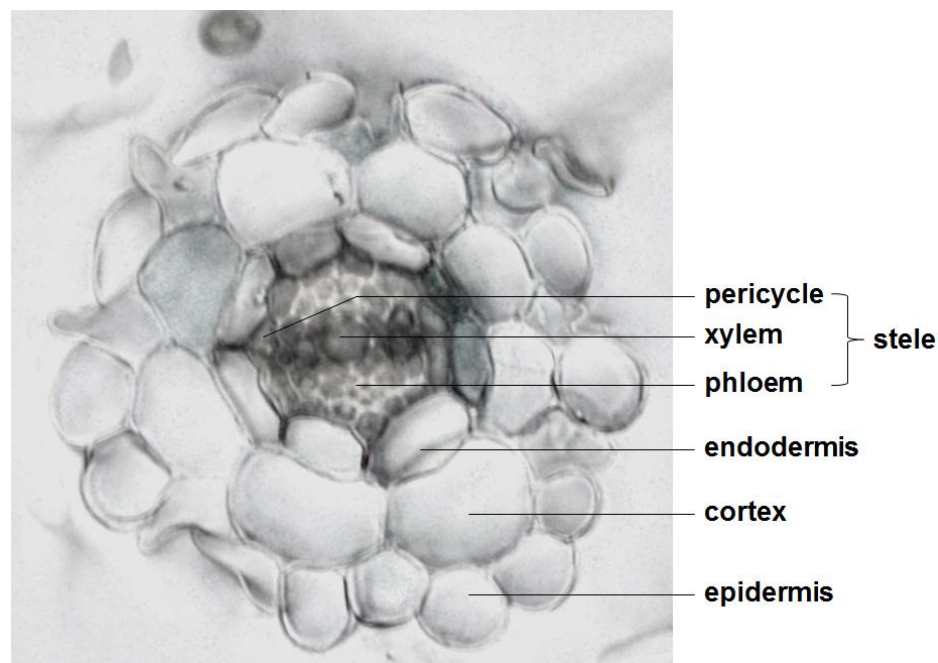


Figure 1 Cross section of an *Arabidopsis* root. The section is positioned with the xylem in a horizontal manner. The line for pericycle points to a xylem-pole pericycle cell. Section thickness: 30 μm .

The water movement in plants' living tissues follows three routes: apoplastic (within cell wall continuum), symplastic (cytoplasmic continuities and plasmodesmata) and transcellular (across cell membranes) paths (Steudle, 2001). They are co-present, and their contributions vary depending on the conditions. For example, symplastic and transcellular paths are dominant when the apoplastic passage is blocked by the Casparian band (found in root endodermal cells), which is thought to be completely impermeable to water.

INTRODUCTION

In contrast to apoplastic and symplastic paths, which do not require water to cross membranes, the transcellular path involves water transport across plasma and intracellular membranes. Although lipid bilayer membranes are permeable for water to some extent, the presence of water-conducting channels, so-called aquaporins, at the membranes largely enhances their water permeability. This is an essential feature when high rates of transcellular water transport are required in plants.

1.1.2 Plant aquaporins

1.1.2.1 Structure and substrate selectivity

Aquaporins were initially discovered in human erythrocytes (Moon *et al.*, 1993; Preston and Agre, 1991), and further found in most living organisms (Gomes *et al.*, 2009). They belong to the major intrinsic protein (MIP) family and exhibit conserved structural features across organisms (Fujiyoshi *et al.*, 2002; Jung *et al.*, 1994; Törnroth-Horsefield *et al.*, 2006): an aquaporin monomer is a 23-31 kDa protein containing six transmembrane helices connected by five loops (A to E), with N- and C-terminal domains protruding into the cytosol (Figure 2). Two highly conserved asparagine-proline-alanine (NPA) motifs, together with aromatic/Arg (ar/R) constriction, contribute to the substrate selectivity and control water molecules passing the channel in a single-file manner.

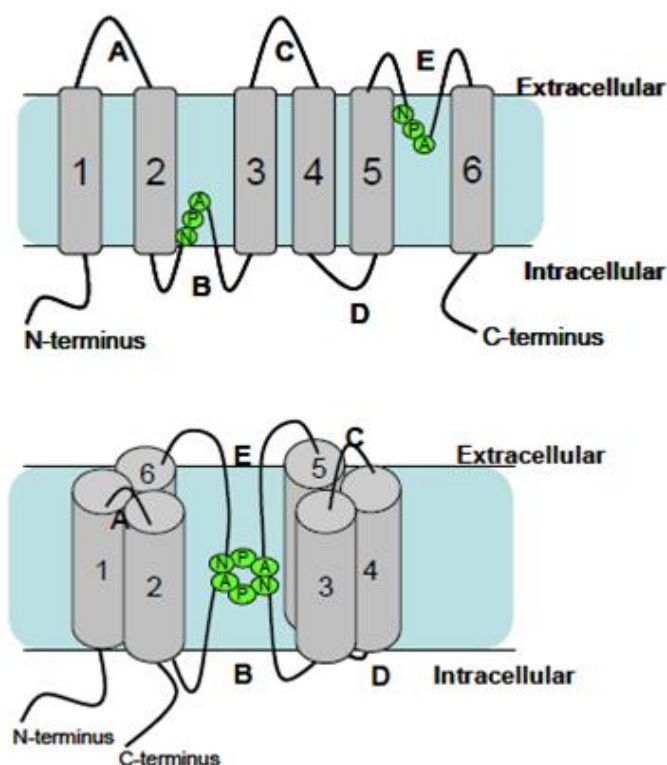


Figure 2 Schematic representation of an aquaporin monomer located at the plasma membrane. Six grey bars indicate the trans-membrane helices (1 to 6), which are connected by three extracellular (A, C, E) and two intracellular (B, D) loops. Two conserved NPA motifs located at loop B and E, respectively, fold into the lipid bilayer to form a seventh transmembrane helix. A single aqueous pathway contributes to the substrate selectivity and forces water molecules to pass the channel in a single-file manner.

INTRODUCTION

Although aquaporins were initially designated as water channels, some isoforms have been shown to facilitate the transport of other small uncharged molecules as well, including urea (Gerbeau *et al.*, 1999), glycerol (Biela *et al.*, 1999), carbon dioxide (Uehlein *et al.*, 2003), hydrogen peroxide (Bienert *et al.*, 2007), ammonia (Holm *et al.*, 2005), boric acid (Takano *et al.*, 2006) and silicic acid (Ma *et al.*, 2006).

1.1.2.2 MIP subfamilies in plants

Compared with 13 aquaporins in mammals, plant aquaporins show a larger number of isoforms with 35 homologs in *Arabidopsis thaliana* (Johanson *et al.*, 2001; Quigley *et al.*, 2002). These 35 isoforms fall into four subfamilies on the basis of sequence homology and subcellular localization (Figure 3). The plasma membrane intrinsic proteins (PIPs) and the tonoplast intrinsic proteins (TIPs) represent the most abundant aquaporins located in the plasma membrane and the tonoplast, respectively. The PIP subfamily contains 13 isoforms, which can be further divided into PIP1 (five isoforms) and PIP2 (eight isoforms) subgroups. The nodulin-26-like intrinsic proteins (NIPs) are close homologs of nodulin-26 in soybean (*Glycine max*), an aquaporin highly expressed in the peribacteroid membrane of N₂-fixing symbiotic root nodules (Fortin *et al.*, 1987; Rivers *et al.*, 1997). Nine isoforms of NIPs identified in *Arabidopsis* are expressed in the plasma and endoplasmic-reticulum (ER) membranes (Wallace *et al.*, 2006). The fourth subfamily is small basic intrinsic proteins (SIPs). Three SIP isoforms are present in *Arabidopsis*, harboring in the ER membranes (Ishikawa *et al.*, 2005).

1.1.2.3 Transcript and protein levels of PIP aquaporins in *Arabidopsis*

Expression and protein levels of PIP aquaporins at different developmental stages and in various organs in *Arabidopsis* provide fundamental information of their possible functions. Expression of PIPs during seed germination and in different organs, including roots, leaves and flowers, has been determined using cDNA microarray or real-time quantitative PCR (qPCR). In dry seeds, all PIP isoforms exhibit very low expression level, whereas PIP1;2 is highly induced in two-day-old germinating seeds. Other PIP genes, including PIP1;1, PIP1;4, PIP2;1, PIP2;2, PIP2;6 and PIP2;7, are also upregulated, but to a lesser extent compared with PIP1;2 (Vander Willigen *et al.*, 2006). Interestingly, most of germination-upregulated genes are also major PIP isoforms found in different organs post-germination. PIP1;1, PIP1;2, PIP2;1 and PIP2;2 exhibit both high transcript and protein levels in roots. The qPCR and

INTRODUCTION

quantitative proteome analysis have demonstrated that PIP1;2 and PIP2;1 represent the major isoforms whereas PIP1;1 and PIP2;2 are less abundant ones in leaves. *PIP1;2* and *PIP2;1* have been shown to be highly expressed in flowers as well. PIP2;7 is also ubiquitously present, but its abundance is lower than that of PIP1;2 and PIP2;1. Although PIP2;6 has the highest transcript level in leaves among PIP isoforms, its protein level is considerably low. Both transcript and protein levels of remaining PIP isoforms are comparably low in roots, leaves and flowers (Alexandersson *et al.*, 2005; Boursiac *et al.*, 2005; Monneuse *et al.*, 2011). In addition to expression data obtained by determining the transcript or protein abundance, the expression pattern of *PIP2* isoforms in different organs was analyzed using transcriptional *proPIP2::GUS* fusions (Da Ines, 2008; Javot *et al.*, 2003; Postaire *et al.*, 2010; Prado *et al.*, 2013). The observations confirmed their expression in different organs, and provided more specific expression details, including that *PIP2;4* is specifically expressed in roots, however, none of *PIP2* genes is shoot-specific.

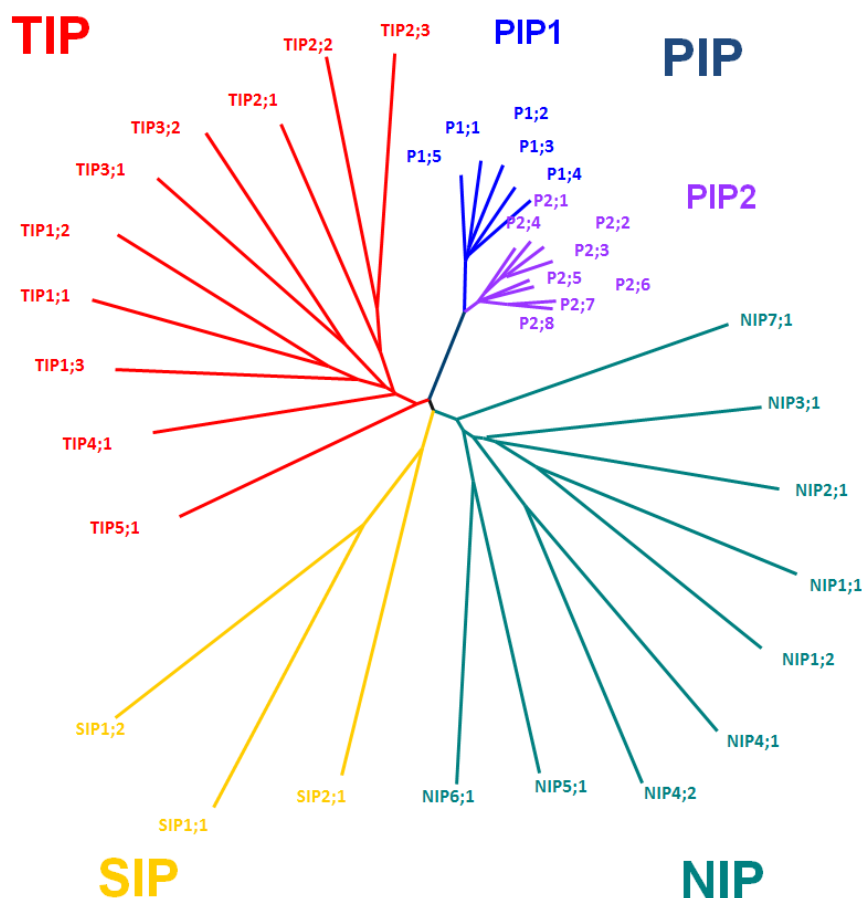


Figure 3 Phylogenetic tree of 35 aquaporin isoforms in *Arabidopsis thaliana* and the four subfamilies PIPs, TIPs, NIPs and SIPs.

1.1.2.4 Regulations and functions of PIP aquaporins in *Arabidopsis*

1.1.2.4.1 Water transport in roots and leaves

Heterologous expression in *Xenopus* oocytes or yeast is a common approach to determine water channel activity of aquaporins. Among PIP2 isoforms, PIP2;1, PIP2;2, PIP2;3, PIP2;6 and PIP2;7 have been individually examined using *Xenopus* oocyte system showing that they largely enhance the water permeability of oocyte membrane (Daniels *et al.*, 1994; Kammerloher *et al.*, 1994; Weig *et al.*, 1997). Three PIP1 isoforms, PIP1;1, PIP1;2 and PIP1;3, also display water transport activities (Kammerloher *et al.*, 1994). Although the water transport properties of the remaining PIP isoforms have not been determined, they are assumed to have the same specificity as the tested ones due to the high sequence conservation. The water transport capacity of most PIP isoforms characterized using the *Xenopus* oocyte system suggests that they function in regulating water relations *in planta*. Employing mercury as a general aquaporin blocker (Daniels *et al.*, 1996), the contribution of overall aquaporins to hydraulics in roots and leaves has been initially examined. Indeed, mercury treatment results in reduced hydraulic conductivity in roots and rosettes in *Arabidopsis* (Postaire *et al.*, 2010; Sutka *et al.*, 2011), indicating that aquaporins play an important role in plant water relations. However, mercury application has disadvantages for aquaporin function analysis, e.g. the contribution of a single isoform to water transport cannot be examined and its toxicity exerts side effects on other physiological processes (Zhang and Tyerman, 1999). Therefore, reverse genetic approaches are used allowing functional analysis of specific PIP isoforms. By generating a PIP1 anti-sense line (reduced transcript levels of PIP1;1 and PIP1;2) in *Arabidopsis*, it has been shown for the first time that PIPs facilitate water transport in plant cells. The isolated leaf protoplasts of the anti-sense line exhibit decreased osmotic water permeability. In parallel, the transgenic line increases its root growth to compensate the cellular hydraulic changes (Kaldenhoff *et al.*, 1998). In recent years, the application of single aquaporin knockouts became a powerful tool to investigate the role of individual PIP isoforms in water relations. By employing two independent *pip2;2* mutants, it has been shown that this root abundant isoform plays a role in osmotic water transport at both the single-cell and whole-root levels (Javot *et al.*, 2003). Water permeability measurement using a *pip1;2* mutant has revealed that the mutation causes reduction in hydrostatic hydraulic conductivity, but not osmotic water transport in roots, whereas it significantly affects the osmotic water permeability of isolated mesophyll protoplasts (Postaire *et al.*, 2010). In addition, both *pip2;1* and *pip2;2* single mutants exhibit reduced water relocation from roots to leaves and

distribution in leaves using a non-invasive deuterium tracer, indicating the important role of these major isoforms in the whole-plant hydraulics (Da Ines *et al.*, 2010).

1.1.2.4.2 Response of PIP aquaporins to various environmental stimuli

Abiotic stresses, such as drought, high salinity, extreme temperatures and limited oxygen availability, have negative impacts on plant growth and productivity. Many studies have been performed to uncover the molecular, biochemical and physiological reactions in response to these environmental stimuli by employing the model plant *Arabidopsis*. As the plants' water status is challenged under stress conditions, the regulations of PIPs can be essential for water homeostasis responding to these stresses.

The remarkable reduction of hydraulic conductivity at the whole-organ and single-cell levels is one of the early responses to salt, cold and low oxygen in *Arabidopsis* roots (Boursiac *et al.*, 2005; Lee *et al.*, 2012; Martínez-Ballesta *et al.*, 2003; Sutka *et al.*, 2011; Tournaire-Roux *et al.*, 2003). This reduction is thought to relate to transcriptional and post-translational regulations of PIPs under these challenging conditions. Long-term (4-24 h) salt exposure represses root abundant *PIP* isoforms, like *PIP1;1*, *PIP1;2*, *PIP2;1* and *PIP2;2* (Boursiac *et al.*, 2005). Furthermore, cycling of *PIP2;1* is enhanced (Martinière *et al.*, 2012) and internalization of this isoform from the cell surface was observed as well (Boursiac *et al.*, 2005; Prak *et al.*, 2008). The rapid internalization of *PIP2;1* in response to salinity is due to dephosphorylation at two C-terminal sites (Ser280 and Ser283) mediated by reactive oxygen species (ROS)-dependent signaling pathways (Boursiac *et al.*, 2008). Similarly, downregulation of *PIP* genes and phosphorylation changes are involved in response to low temperature (Jang *et al.*, 2004; Lee *et al.*, 2012). In addition, low oxygen availability triggers repression of *PIP* genes and closure of the water channels due to cytosol acidosis (Liu *et al.*, 2005; Tournaire-Roux *et al.*, 2003).

Water deficit is one of the most frequently occurred stresses in the field causing marked reduction of crop yield (Boyer, 1982). The plants' responses to water deficit have been widely documented. Drought stress induces the production of the hormone abscisic acid (ABA) and its signaling pathway, resulting in stomatal closure and reduced transpiration (Kang *et al.*, 2002; Mustilli *et al.*, 2002; Pei *et al.*, 2000; Wasilewska *et al.*, 2008). Proline and soluble sugars are accumulated as osmoprotectants (Hummel *et al.*, 2010; Rizhsky *et al.*, 2004; Singh *et al.*, 1972; Sperdouli and Moustakas, 2012; Urano *et al.*, 2009). Drought responses also involve the regulation of hydraulic conductivity. The leaf hydraulic conductivity is rapidly reduced in response to drought or ABA treatment (Martre *et al.*, 2002). A recent study has

INTRODUCTION

shown that the hydraulic-conductivity reduction in leaves in response to drought is derived from the decrease of osmotic water permeability in bundle-sheath cells (single layer of parenchymatous cells surrounding the entire leaf vasculature), but not mesophyll cells (Shatil-Cohen *et al.*, 2011). In addition, the transcriptional and post-translational regulations of PIP aquaporins at the organ or whole-plant level have been examined and revealed that most of *PIP* genes are again downregulated, and the protein content and activity are modified as well. Ten out of 13 *PIP* genes are repressed, whereas *PIP1;4*, *PIP2;5* and *PIP2;6* are either induced or not responsive under drought stress (Alexandersson *et al.*, 2005; Jang *et al.*, 2004). This is commonly observed in five *Arabidopsis* accessions (Alexandersson *et al.*, 2010). Interestingly, the general downregulation of *PIP* genes can be restored to the expression levels similar to control condition after rehydration (Alexandersson *et al.*, 2005). With respect to the post-translational regulations, several PIP isoforms, including PIP2;1 and PIP2;2, have been shown to dephosphorylate after 30 min of ABA treatment (Kline *et al.*, 2010). This phosphorylation change suggests that the internalization of these abundant isoforms may occur as an early response to drought similar to salinity. Moreover, the trafficking of PIP2;1 from ER to plasma membrane is also inhibited, and the ER-retained PIP2;1 is eventually degraded through the ubiquitin-proteasome system (Lee *et al.*, 2009). PIPs have also been shown to play an important role in recovery from drought stress in *Arabidopsis* (Martre *et al.*, 2002). Transgenic plants with antisense inhibition of PIP1 and PIP2 expressions exhibit similar transpiration rates, hydraulic conductance and leaf water potential to wild-type plants under drought stress, whereas these parameters are significantly lower in transgenic plants than in wild type after rewatering.

In comparison with the progresses made on regulations and functions of PIPs in response to water deficit, little is known about the involvement of PIPs in response to heat stress. It has been demonstrated that high temperature causes reduction of leaf water potential in *Arabidopsis* (Koussevitzky *et al.*, 2008). In tomato, not only leaf water potential, but also root hydraulic conductivity is reduced (Morales *et al.*, 2003). These changes in water relations suggest that aquaporins could be regulated by high temperature. A heat-induced transcription factor RELATED TO APETALA 2.4B (RAP2.4B) has been identified to control the expression of major *PIP* isoforms (*PIP1;1*, *PIP1;2*, *PIP2;1* and *PIP2;2*) together with its duplication RAP2.4 (Rae *et al.*, 2011). This suggestive evidence indicates that the transcriptional regulation of PIPs may contribute to the hydraulic changes under heat stress.

Many studies have focused on how plants respond to single abiotic stresses. The knowledge of plants' responses to combinational stress, however, should provide more profound

INTRODUCTION

information as plants are simultaneously exposed to several different stresses in the field. In particular, high temperature is frequently associated with drought stress. Thus, the experimental data of molecular, biochemical and physiological changes upon combination of drought and heat have been rapidly accumulating in recent years (Koussevitzky *et al.*, 2008; Macková *et al.*, 2013; Rizhsky *et al.*, 2004; Signarbieux and Feller, 2012). These data have demonstrated that stress combination triggers specific cellular processes. Proline, which acts as a major osmoprotectant during drought stress, is not accumulated in response to the combination of drought and heat (Rizhsky *et al.*, 2004). A recent study has described that the stress combination specifically induces enzymes involved in reactive oxygen detoxification, carbon fixation and malate metabolism (Koussevitzky *et al.*, 2008). In addition, heat stress exerts more significant effect on reduction of leaf water potential in the presence of drought than the non-drought condition (Koussevitzky *et al.*, 2008; Signarbieux and Feller, 2012).

Taken together, plants seem to benefit from diminishing both the amount and activity of PIP aquaporins in response to various environmental stimuli. However, the mechanisms of PIPs' involvement in plants' adaptations to these conditions, such as drought, are only partially understood. Little is known about the role of PIPs in response to heat stress and its combination with drought. Further analysis addressing multiple-level regulations of PIPs and PIP-dependent changes at the metabolome and transcriptome levels will help to better understand the involvement of PIPs in response to these environmental scenarios.

1.1.2.4.3 Root growth and development

1.1.2.4.3.1 Elongation of the primary root and root hairs

Plant tissues grow when cell walls relax and extend in response to the cell's turgor pressure (Cosgrove, 1993). Sustained growth is primarily driven by solute uptake and maintenance of cell osmotic potential, and requires sufficient water inflow to keep turgor above the yield threshold (Boyer and Silk, 2004). Thus, water transport should be an important aspect of growth and development.

Only a few studies have demonstrated that PIP-dependent water transport might be involved in root growth and development in *Arabidopsis*. It has been shown that mutation in *PIP2;4* results in longer root hairs under control and phosphate deficiency conditions, suggesting the role of PIP2;4 in root hair development (Lin *et al.*, 2011). In addition, *PIP2;7* (expressed in the root elongation zone) is downregulated by the treatment of ethylene precursor 1-aminocyclopropane-1-carboxylic-acid (ACC), an inhibitor of root elongation (Markakis *et al.*,

2012), suggesting that this isoform may play a role in facilitating water transport into the rapidly elongating root cells.

1.1.2.4.3.2 Lateral root development

Plants rely on the root system to acquire water and nutrients. The acquisition efficiency is determined by the degree of repetitive branching of the primary root, so-called lateral root (LR) formation, which is therefore an important agronomic trait.

Lateral root primordia (LRP) originate from small numbers of pericycle cells located deep within the primary root (Figure 1 and 11) (Casimiro *et al.*, 2003). These cells undergo a series of cell divisions and expansions to form dome-shaped LRP, which eventually break through the overlaying tissue to achieve their emergence (Péret *et al.*, 2009b). Auxin is the most important hormone signal regulating the whole developmental process (Overvoorde *et al.*, 2010; Péret *et al.*, 2009a). It acts as the inductive signal during LR initiation (Casimiro *et al.*, 2001), mediates the patterning of LRP into a dome shape (Friml *et al.*, 2003), and favors cell separation in the overlaying tissue to promote emergence (Swarup *et al.*, 2008). In addition to auxin, other plant hormones, such as cytokinin, ethylene and ABA, are also involved in regulating LR development (Laplaze *et al.*, 2007; Ivanchenko *et al.*, 2008; De Smet *et al.*, 2006).

Although the significance of PIP-mediated water transport during LR development has not been explored, several lines of experimental evidence support this association. Firstly, LRP growth is symplastically isolated from the primary root vasculature (Oparka *et al.*, 1995), suggesting that cell expansions of LRP involve efficient transcellular water fluxes. Secondly, a recent study has discovered that auxin exerts specific effect on cell-wall biomechanics of the overlaying tissue to promote emergence (Swarup *et al.*, 2008). The auxin influx carrier LIKE AUXIN RESISTANT 1 3 (LAX3) is specifically expressed in the cortical and epidermal cells that overlay LRP. Auxin induces *LAX3*, and its high expression reinforces the accumulation of auxin, which further regulates the expression of a set of cell wall remodeling enzymes in the LRP overlaying cells to favor cell separation. A blockage of lateral root emergence (LRE) is observed in *lax3* loss-of-function mutant. However, it remains unclear whether the regulation of cell-wall properties in the overlaying tissue is sufficient to achieve the smooth emergence of LRP. It is believed that changes of hydraulic and cell-wall properties are highly associated during plant tissue growth. For example, the hypocotyl elongation of etiolated soybean seedlings has been previously shown to require the increase of both hydraulic conductivity and cell wall extensibility, which are induced by auxin (Boyer and Wu, 1978). Thirdly, some

PIP isoforms have been determined to contribute to water relations at the whole-root and single-cell levels (Javot *et al.*, 2003; Postaire *et al.*, 2010). These indications suggest that, in parallel to cell wall remodeling, PIP-dependent water transport could also play an important role in LR development, likely regulated by auxin, which is similar to the hypocotyl elongation process.

1.2 Aims of this work

In general, the goal of this work was to expand our understanding of the roles of PIP aquaporins in regulating growth and development and in response to altered environmental cues.

The first part aimed at determining the regulation of PIPs and its effects on LR development, namely (1) establishing a link between expression (and function) of PIPs and auxin-regulated LR development using molecular biological and biochemical approaches; (2) uncovering how this developmental process is affected by the presence of PIPs and auxin by employing a mathematical model and mutant analysis; (3) identifying whether PIPs are regulated by signals other than auxin during LR development (based on international collaborations with the groups of Malcolm Bennett from the University of Nottingham and Christophe Maurel from CNRS Montpellier).

The roles of PIPs in response to heat stress and its combination with drought are poorly understood. To address this from a new perspective, a systems biology approach was used to analyze whether the loss of ubiquitous and organ-specific PIP isoforms would provoke metabolic changes and alter the plants' stress responses. The second part of this work focused on determining the differential metabolic responses in *pip2;1 pip2;2* and *pip2;1 pip2;2 pip2;4* mutants under control, drought and heat scenarios. By comparing the metabolic profiles of wild type and these *pip* mutants upon such conditions acquired from a non-targeted approach employing Fourier Transform Ion Cyclotron Resonance Mass Spectrometry (FT-ICR-MS), significantly changed metabolites and possibly affected metabolic pathways associated with the *PIP* mutations should be identified (collaboration with Research units of Environmental Simulation and Analytical BioGeoChemistry, Helmholtz Zentrum München).

2. REGULATION OF PIP AQUAPORINS IS REQUIRED TO FACILITATE LATERAL ROOT EMERGENCE

Roots are crucial for acquisition of water and nutrients and soil anchorage. Establishment of a mature root system requires well-controlled lateral root (LR) development. Therefore, many studies have been performed to characterize the regulatory mechanisms of this process. The *Arabidopsis* root has a simple structure consisting of one layer of epidermis, cortex and endodermis, which surround the central stele (Figure 1 and 11). This feature makes the *Arabidopsis* root an ideal object to investigate LR development.

The whole developmental process can be divided into four phases: pre-initiation (or priming), initiation, patterning and emergence. Auxin and its signaling pathways have been identified to control or influence each of these phases (Overvoorde *et al.*, 2010; Péret *et al.*, 2009a).

LR formation is initiated from a small subset of pericycle founder cells, which are exclusively adjacent to the xylem poles (Figure 1 and 11) (Casimiro *et al.*, 2003). Different from other pericycle cells, the ones neighboring the xylem poles are stem cells, maintaining the capacity to divide (Beeckman *et al.*, 2001; DiDonato *et al.*, 2004). These pericycle cells are primed by the auxin response maxima arising in their adjacent protoxylem cells shortly after exiting the root apical meristem, in the basal meristem zone (De Smet *et al.*, 2007). Although three pericycle cell files at a xylem pole can be primed and divide, only the middle cell file significantly contributes to LR formation (Kurup *et al.*, 2005). The nuclei of two primed, longitudinally adjacent founder cells migrate to the common cell wall, and activation of auxin efflux/influx carriers, such as PIN FORMED proteins (PINs) and AUXIN RESISTANCE 1 (AUX1), generates a local auxin accumulation in these cells (Ditengou *et al.*, 2008; Laskowski *et al.*, 2008). Auxin signaling activates cell cycle-related genes to promote LR initiation (Himanen *et al.*, 2002; Nieuwland *et al.*, 2009). Auxin is perceived *via* TRANSPORT INHIBITOR RESPONSE 1 / AUXIN SIGNALING F-BOX PROTEINS (TIR1/AFBs) receptors and triggers the interaction between TIR1/AFBs and AUXIN / INDOLE-3-ACETIC ACID proteins (AUXIAAs), which bind the auxin-responsive transcription factors to block their activities at low auxin concentration (Dharmasiri *et al.*, 2005a; Dharmasiri *et al.*, 2005b; Greenham *et al.*, 2011; Kepinski and Leyser, 2005). The interaction recruits AUXIAAs to the SCF complex for 26S proteasome-dependent degradation, leading to derepressing the AUXIAAs bound transcription factors (Tan *et al.*, 2007). One of the most important AUXIAAs during LR initiation is IAA14 (INDOLE

ACETIC ACID14) / SLR1 (SOLITARY ROOT1) (Fukaki *et al.*, 2002). IAA14/SLR1 represses the activity of transcription factors termed auxin response factors (ARFs) (Guilfoyle and Hagen, 2007). The ARF family comprises 23 members; five out of 23 ARFs are known to function as transcription activators (ARF5, 6, 7, 8 and 19) and the remaining ones likely act as transcription repressors (Tiwari *et al.*, 2003). During LR initiation, the elevated level of auxin degrades IAA14/SLR1 to derepress ARF7 and ARF19 (Fukaki *et al.*, 2005), which are thought to activate expression of cell cycle-related genes and eventually result in cell divisions (Feng *et al.*, 2012; Goh *et al.*, 2012; Okushima *et al.*, 2007). Consistent with this, the *arf7* single mutant exhibits significantly reduced number of LRs, and the *arf7 arf19* double mutant strengthens the LR phenotype of *arf7* (Okushima *et al.*, 2007; Okushima *et al.*, 2005; Wilmoth *et al.*, 2005).

The pericycle founder cells first divide anticlinally and asymmetrically into shorter and longer daughter cells at the center and flanks of the new lateral root primordium (LRP), respectively (Casimiro *et al.*, 2001; Dubrovsky *et al.*, 2001; Malamy and Benfey, 1997). The auxin response maxima are observed in the central small daughter cells (Benková *et al.*, 2003). The expression of receptor-like kinase ARABIDOPSIS CRINKLY 4 (ACR4) in small daughter cells plays an important role in cell-division inhibition of longitudinally surrounding pericycle cells (De Smet *et al.*, 2008). The anticlinal asymmetric cell divisions are followed by periclinal asymmetric cell divisions to create a two-cell-layer LRP. Additional cell divisions and cell expansions radially and distally pattern the LRP into a dome shape. An auxin gradient is established in the growing LRP, and its response maxima dynamically move from the central daughter cells to the tip of multilayered LRP (Figure 4) (Benková *et al.*, 2003), which is dependent on the function of some PIN proteins (auxin efflux carriers). The auxin response maxima are thought to mediate the patterning of newly forming LRP (Friml *et al.*, 2003).

Since the LRP originates deep within the primary root, the developing LRP has to push through the overlaying tissue to emerge (Péret *et al.*, 2009b). It has been demonstrated that auxin originating from the growing LRP induces different signaling pathways in different overlaying cell layers to regulate lateral root emergence (LRE) (Swarup *et al.*, 2008). IAA14/SLR1- ARF7/ARF19 signaling components activate the expression of the auxin influx carrier LIKE AUX1 3 (LAX3), resulting in cell wall remodeling of cortical and epidermal cells overlaying LRP (as introduced in 1.1.2.4.3.2). In endodermal cells (LAX3 absent), auxin triggers degradation of IAA3/SHY2 (SHORT HYPOCOTYL 2), instead of IAA14/SLR1, to reprogram the cell walls. These differences suggest different cell-wall compositions between

endodermal and cortical/epidermal cells. Nevertheless, auxin-dependent regulation of cell-wall mechanics in the overlaying tissue leads to cell separation to promote LRE. These findings indicate the tight coordination of LRP growth and emergence through auxin actions to minimize tissue damage during LR development.

Auxin derived from different origins regulates LR initiation and emergence. Auxin is synthesized both in shoots and roots. The auxin generated in the root tip is required for LR initiation, and LRE necessitates shoot-derived auxin synthesis and transport (based on phloem path) (Bhalerao *et al.*, 2002; Casimiro *et al.*, 2001; Wu *et al.*, 2007).

LR formation can be induced by gravitropic stimulus (Lucas *et al.*, 2008), thus making gravistimulation a powerful tool for LR development study. Following a 90° gravitropic stimulus, LRs develop in a highly synchronized manner at the outer edge of a bending root (Péret *et al.*, 2012). According to the morphological changes, the LRP growth and development (from first anticlinal asymmetric division to emergence) are divided into eight stages (Figure 4) (Malamy and Benfey, 1997). Stage I primordia are first detected 18 h post-gravitropic induction (pgi); then primordia for each subsequent stage are detected approximately every 3 h, until emergence at stage VIII 42 h pgi. These observations allow us to characterize LR development at a high temporal resolution.

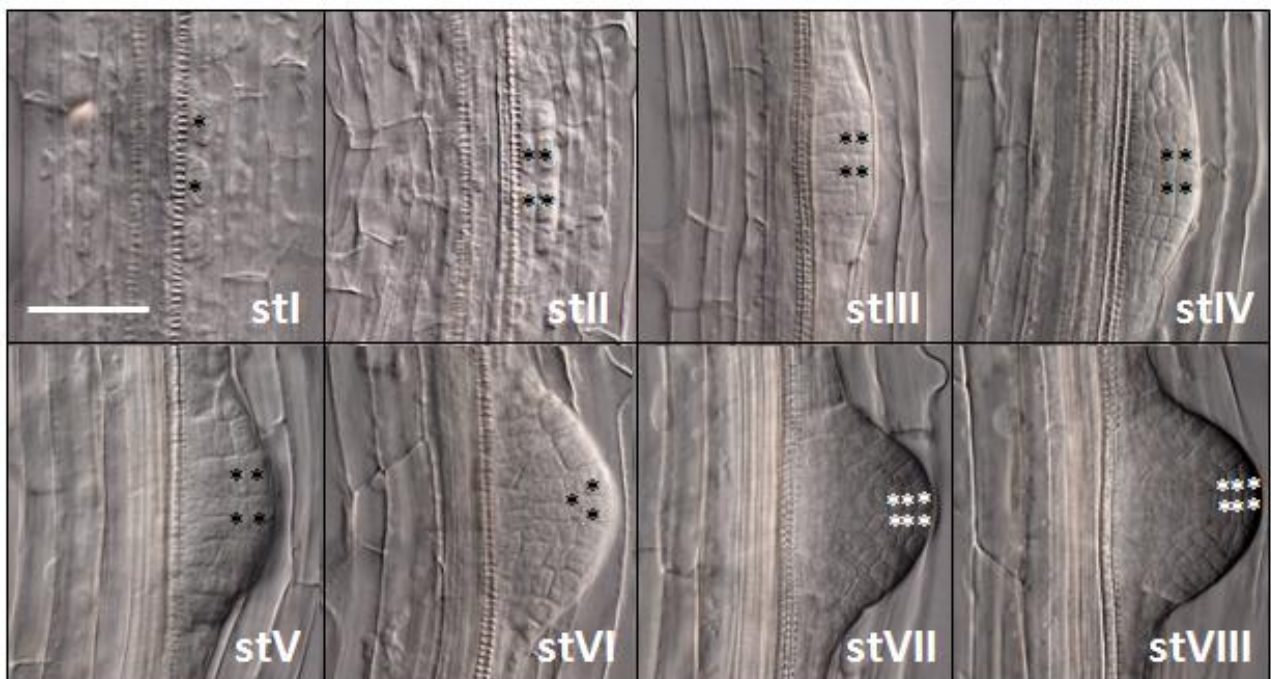


Figure 4 LRP Morphology and dynamic establishment of auxin response maxima at each developmental stage. The Roman numbers indicate eight stages of LRP growth and development (Malamy and Benfey, 1997). The black and white asterisks indicate the LRP cells with auxin response maxima at each stage (Benková *et al.*, 2003). Scale bar represents 50 μ m.

2.1 Results

2.1.1 The majority of root *PIP* genes are repressed by exogenous auxin

Dynamic expression of *PIP* genes during LR development and in response to auxin were initially examined using qPCR in a collaborative effort in order to investigate whether PIP aquaporins play a role in this process.

Ute Voß (University of Nottingham) determined the high-resolution expression profile of all 13 *PIP* isoforms during LR development, which was achieved by micro-dissecting root bends every 6 hours pgi. qPCR result revealed that 10 out of 13 genes were repressed during LR development whereas *PIP1;4* and *PIP2;5* showed no or little induction. In contrast, *PIP2;8* was induced up to tenfold 36 h pgi (Péret *et al.*, 2012).

In parallel, I analyzed the expression profile of 13 *PIP* isoforms in response to exogenous auxin together with Benjamin Péret (University of Nottingham). Treatment of whole roots with 1 µM of the naturally occurring auxin indole-3-acetic acid (IAA) induced an overall inhibition of *PIP* gene expression (Figure 5). All genes except *PIP1;3* were repressed after 6 h IAA treatment. This repression was sustained in most cases, however, transcript abundance of *PIP2;5* and *PIP2;8* recovered, overshooting their previous levels by up to fourfold 24 h after treatment. *PIP1;3* was induced throughout IAA treatment (Figure 5b).

The similar expression profiles of *PIP* genes observed following gravity and auxin treatment suggest that auxin is responsible for the repression of *PIP* gene expression during LR development. The temporal differences (e.g. expression of *PIP1;3* is repressed during LR development, however, induced by exogenous auxin) are likely to reflect the synchronous and asynchronous cellular responses to endogenous and exogenous auxin sources, respectively. Nevertheless, this result revealed that auxin represses the expression of the majority of *PIP* genes in the *Arabidopsis* root.

2.1.2 Regulation of root *PIPs* by auxin is dependent on ARF7

ARF proteins function as transcription factors that control the expression of auxin-responsive genes (Guilfoyle and Hagen, 2007). Previous studies have demonstrated that ARF7 plays a key role in mediating cell cycle activation during LR initiation and cell separation of the overlaying tissue during LRE (Okushima *et al.*, 2007; Okushima *et al.*, 2005; Swarup *et al.*, 2008; Wilmoth *et al.*, 2005). Thus, I determined the effects of the *arf7* loss-of-function on *PIP* expression upon auxin treatment together with Benjamin Péret (University of Nottingham).

PIP AQUAPORINS – LATERAL ROOT EMERGENCE

For *PIP1;1*, *PIP1;4*, *PIP2;1*, *PIP2;2* and *PIP2;7* showing sustained auxin-dependent repression, a diminution of hormone effects was observed in the *arf7* mutant background. Interestingly, auxin-induction of *PIP1;3* and *PIP2;5* was also ARF7-dependent. Expression of the remaining *PIPs* was similar between the Col-0 and *arf7* genetic backgrounds in response to IAA application (Figure 6). These data indicate that, in many cases, auxin-regulated *PIP* expression is dependent on ARF7.

In addition, water-transport properties of auxin-treated roots were characterized by Guowei Li (CNRS Montpellier). As a result of general repression of *PIP* expression, root hydraulic conductivity in Col-0 was reduced by auxin at both whole-organ and single-cell levels. IAA application also reduced the cortical cell turgor. Interestingly, both hydraulic conductivity and cortical cell turgor were insensitive to auxin inhibition in the *arf7* mutant background (Péret *et al.*, 2012). Taken together, auxin regulates both expression and function of *PIP* aquaporins in the *Arabidopsis* root in an ARF7-dependent manner.

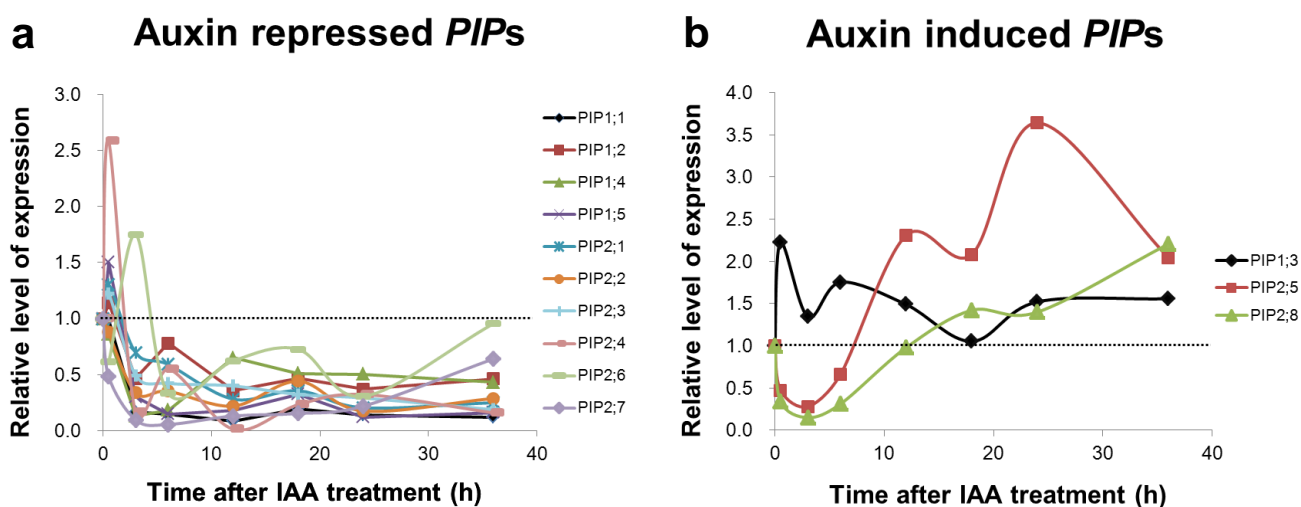


Figure 5 Exogenous auxin represses expression of most *PIP* aquaporins. The expression levels of *PIP* genes were determined in the whole root after treatment with auxin (1 μ M IAA) for 0.5 h, 3 h, 6 h, 12 h, 18 h, 24 h and 36 h. (a) Ten *PIPs* are repressed by auxin (*PIP1;1*, *PIP1;2*, *PIP1;4*, *PIP1;5*, *PIP2;1*, *PIP2;2*, *PIP2;3*, *PIP2;4*, *PIP2;6* and *PIP2;7*). (b) *PIP1;3* shows little induction whereas *PIP2;5* and *PIP2;8* are induced by auxin.

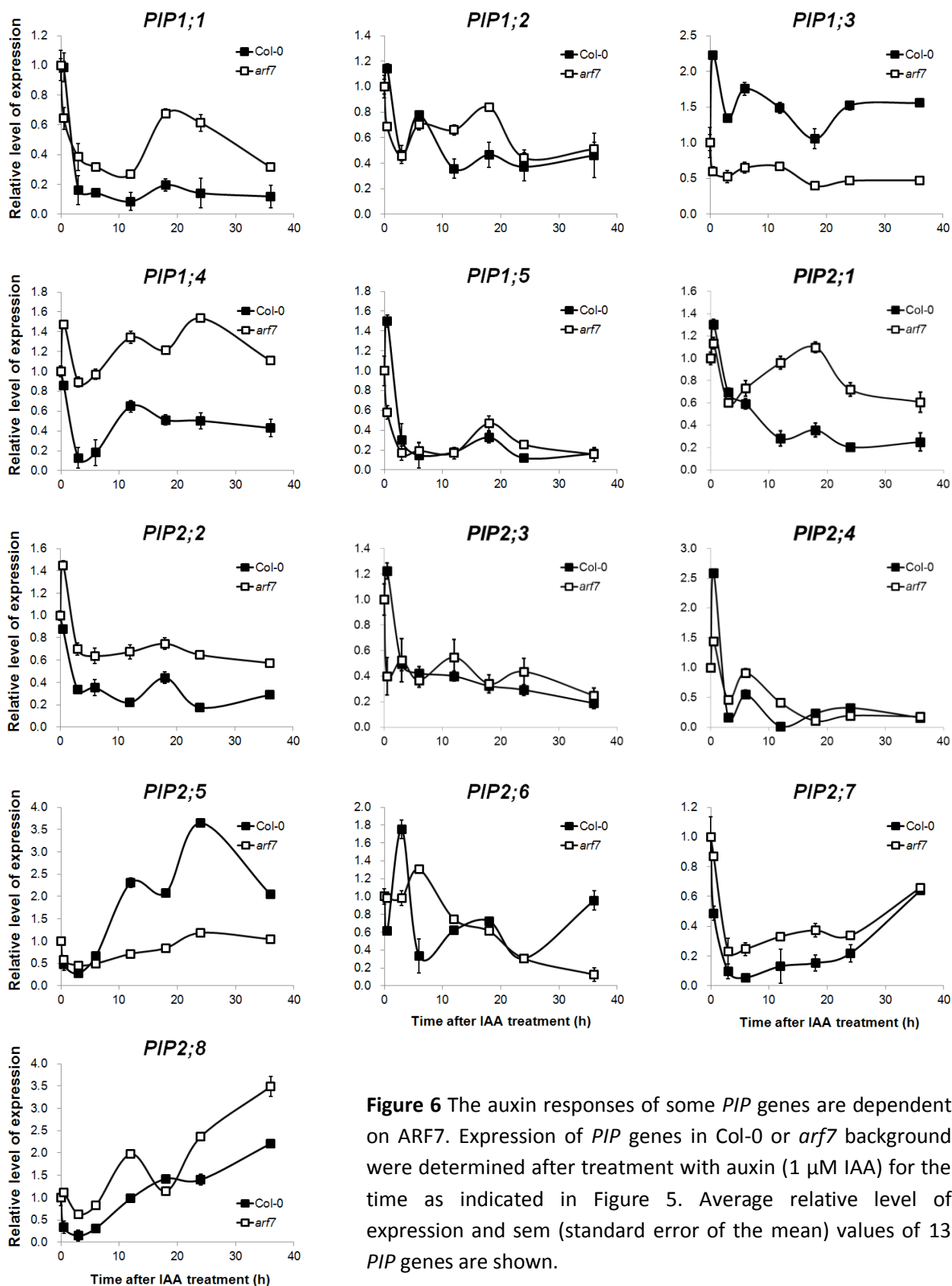


Figure 6 The auxin responses of some *PIP* genes are dependent on *ARF7*. Expression of *PIP* genes in *Col-0* or *arf7* background were determined after treatment with auxin (1 μ M IAA) for the time as indicated in Figure 5. Average relative level of expression and sem (standard error of the mean) values of 13 *PIP* genes are shown.

2.1.3 Auxin alters spatial expression of *PIP* aquaporins during LR development

The expression and functional studies suggest that auxin-regulated PIPs may play an important role during LR development. To investigate this further, expression patterns of all *PIP2* genes and two major *PIP1* genes (*PIP1;1* and *PIP1;2*) were analyzed using transcriptional *proPIP:GUS* fusions.

PIP2;1, one of the most abundant aquaporins in roots (Alexandersson *et al.*, 2005; Monneuse *et al.*, 2011) was first examined. Expression studies revealed that *PIP2;1* was highly expressed in the stele and less in outer root layers. During LRE, *PIP2;1* was expressed in the early-stage LRP, but from stage III onwards its expression was progressively excluded from LRP tip. GUS signals of *proPIP2;1:GUS* line were observed only at the base of late-stage LRP (Figure 7a). This expression pattern was confirmed by observations in the translational *proPIP2;1:PIP2;1-mCHERRY* complementing *pip2;1* mutant (Figure S1). Importantly, the spatio-temporal expression of *PIP2;1* during LRE was exactly opposite to the expression of the auxin response reporter DR5 (Benková *et al.*, 2003). As another major root aquaporin, expression pattern of *PIP2;2* (Alexandersson *et al.*, 2005; Monneuse *et al.*, 2011) was similar to that of *PIP2;1* during LRE (Figure 7b).

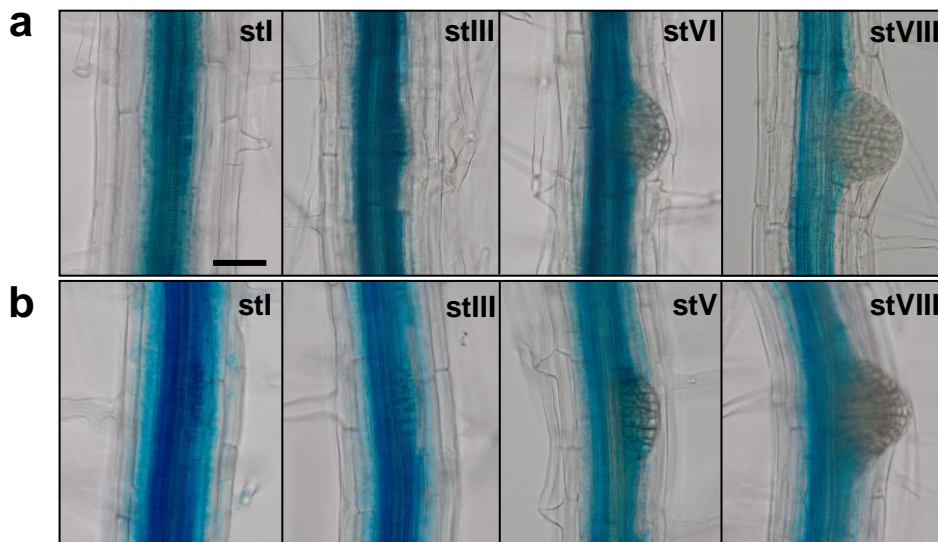


Figure 7 Expression of *PIP2;1* and *PIP2;2* oppositely mirrors auxin accumulation in the LRP. (a) *proPIP2;1:GUS* fusion. (b) *proPIP2;2:GUS* fusion. These reporter lines were stained for 25 min (a) and 5 min (b), respectively. Two independent *proPIP:GUS* lines of each *PIP* gene displayed similar expression pattern during LR development. The developmental stages are indicated by Roman numbers. Scale bar represents 50 μ m.

PIP1;2 and *PIP2;7* were expressed both in LRP and in the overlaying tissue (Figure 8a, c). To eliminate the influence of overlaying tissue on the LRP observation, a shorter staining time was applied (it had been observed that LRP could be more quickly stained than the overlaying tissue in these reporter lines). Similar expression patterns of *PIP1;2* and *PIP2;7* during LR development were observed. They were present in the early-stage LRP and maintained their expression in the whole LRP except for the sites of auxin response maxima (Figure 8b, d). In addition, the expression of *PIP1;2* and *PIP2;7* in the overlaying tissue at LR formation sites were somewhat weaker than the regions lacking LRP (Figure 8a, c).

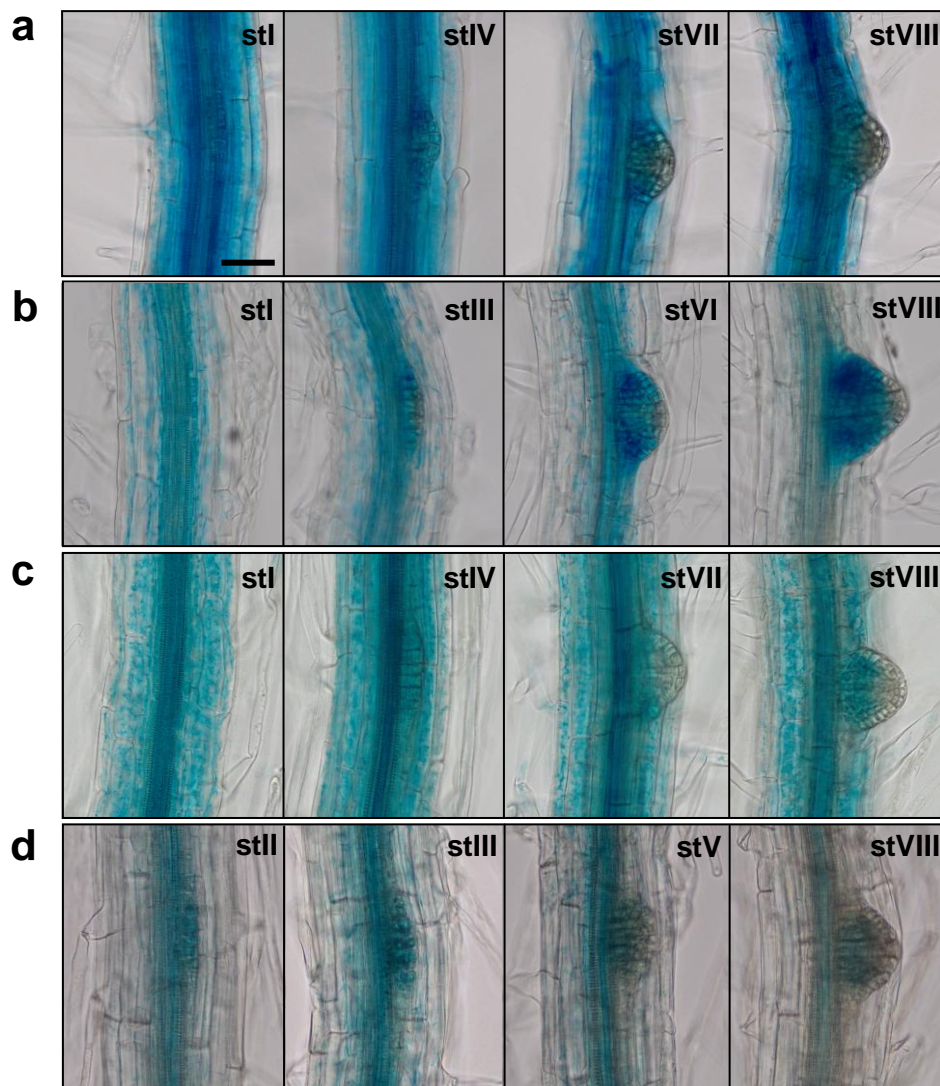


Figure 8 *PIP1;2* and *PIP2;7* are expressed both in the LRP and the overlaying tissue during LR development. Their expression in the LRP is only repressed at its tip. (a, b) *proPIP1;2:GUS* fusion. (c, d) *proPIP2;7:GUS* fusion. These reporter lines were stained for 35 min (a), 15 min (b), 5.5 h (c) and 3 h (d), respectively. Two independent *proPIP:GUS* lines of each *PIP* gene displayed similar expression pattern during LR development. The developmental stages are indicated by Roman numbers. Scale bar represents 50 μ m.

In the remaining *proPIP:GUS* fusion lines, no *PIP* aquaporins were expressed in the early-stage LRP. Expression of *PIP1;1* and *PIP2;4* was observed exclusively in the overlaying tissue. Their GUS signals in the overlaying tissue at LR formation sites again appeared to be weaker compared with the regions lacking LRP (Figure 9a, b). This suggests that overlaying tissue-accumulated auxin may result in repression of these *PIPs*. *PIP2;3* was expressed in the pericycle, and its expression at LR formation sites was repressed throughout LR development (Figure 9c). *PIP2;5*, *PIP2;6* and *PIP2;8* were largely restricted to the stele (Figure 9d-f). Interestingly, *PIP2;8* was highly induced from stage IV onwards at the base of the LRP and in the underlying stele (Figure 9f), consistent with its high-resolution expression profile showing tenfold induction during late-stage LR development (Péret *et al.*, 2012).

As expression of *PIP* genes is regulated during LR development as well as by exogenous auxin, I examined whether treatment of 1 μ M auxin (IAA) or 10 μ M auxin response inhibitor (p-chlorophenoxy-isobutyric acid, PCIB) altered the expression pattern of *PIPs* present in the LRP and/or overlaying tissue, where auxin accumulates during LRE. IAA treatment resulted in strong reduction of the *proPIP2;1:GUS* signal, whereas PCIB treatment led to an increase of the *proPIP2;1:GUS* signal and extended the spatial pattern into the outer root layers (Figure 10a). Similar results were also observed in the reporter lines of *PIP1;1*, *PIP1;2*, *PIP2;2* and *PIP2;7* after IAA or PCIB treatment (Figure 10b-e). However, *proPIP2;4:GUS* line was not responsive to both treatments (Figure 10f). The transcriptional regulation of the *proPIP2;4:GUS* construct in response to exogenous auxin did not reflect the qPCR analysis (Figure 5). Nevertheless, these observations suggest that auxin accumulation causes the reduction of *PIP* expression in the LRP and/or overlaying tissue during LRE.

2.1.4 Primordium-expressed *PIP* aquaporins are major isoforms in the whole stele

It is known that LRP initiates exclusively from pericycle cells located at either of the xylem poles in *Arabidopsis* (Figure 1 and 11) (Casimiro *et al.*, 2003). Precise expression pattern of *PIP* aquaporins in the stele will provide more insight into their potential contribution to LR development. The cross-section of GUS-stained roots revealed that *PIP1;2*, *PIP2;1*, *PIP2;2*, *PIP2;3* and *PIP2;7* were expressed in the whole stele. Interestingly, they showed a higher expression level at the xylem poles and adjacent pericycle cells, where LRP originate, except for *PIP2;7* (Figure 11a-e). Together with the observations that *PIP1;2*, *PIP2;1*, *PIP2;2* and

PIP2;7 were also expressed in the primordium during LR formation, these results highlight their potential significance during LR development.

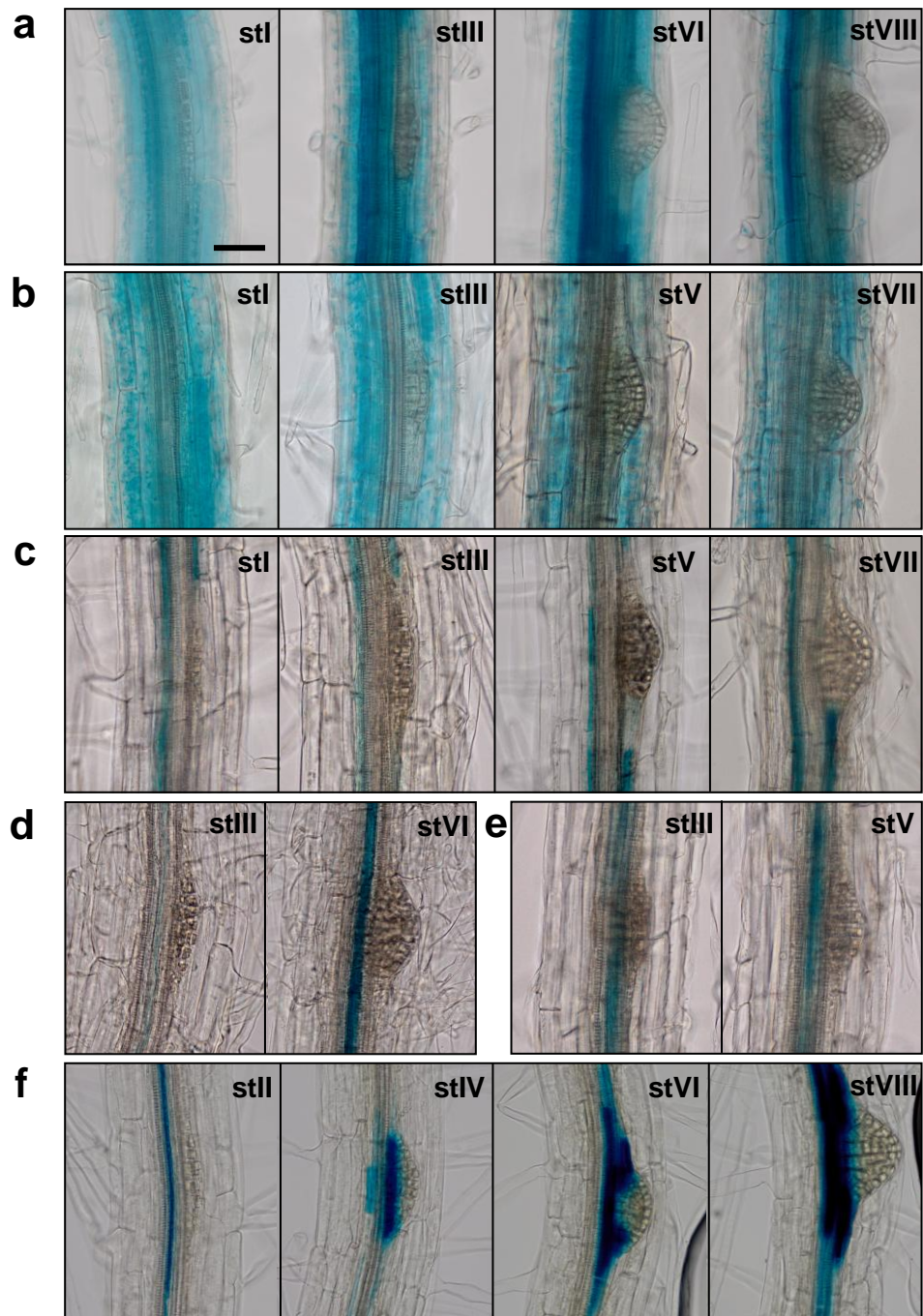


Figure 9 Six *PIP* aquaporins show no expression in the early-stage primordium during LR formation. (a) *proPIP1;1:GUS* fusion. (b) *proPIP2;4:GUS* fusion. (c) *proPIP2;3:GUS* fusion. (d) *proPIP2;5:GUS* fusion. (e) *proPIP2;6:GUS* fusion. (f) *proPIP2;8:GUS* fusion. These reporter lines were stained for 2 h (a-b) and overnight (c-f), respectively. Two independent *proPIP:GUS* lines of each *PIP* gene displayed similar expression pattern during LRE. The developmental stages are indicated by Roman numbers. Scale bar represents 50 μ m.

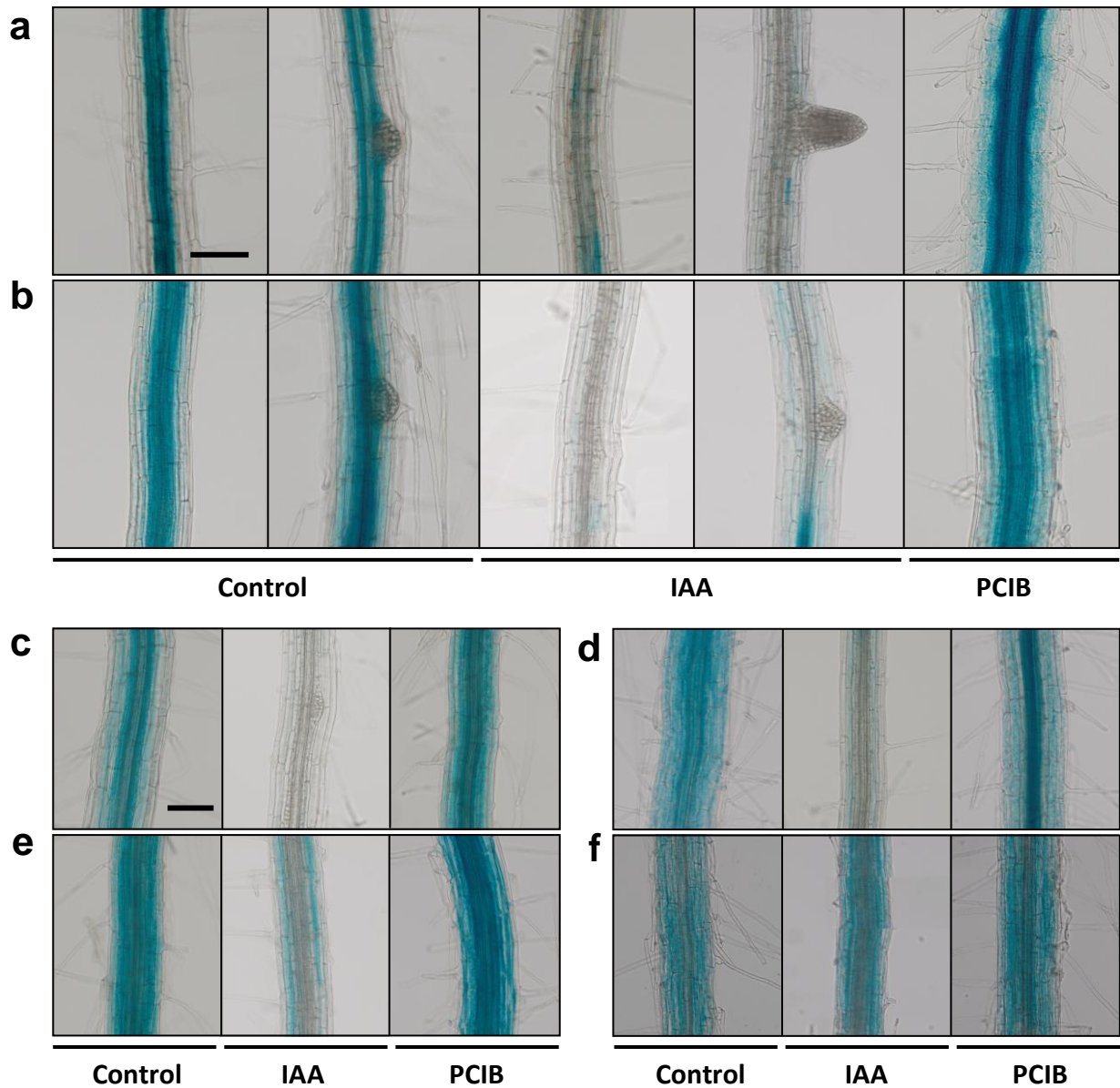


Figure 10 Auxin controls the *PIP* aquaporins expressed in the LRP and/or overlaying tissue. Control: seven-day-old seedlings transferred to normal MS medium. IAA: seven-day-old seedlings transferred to MS plates supplemented with 1 μM IAA for 48 h. PCIB: seven-day-old seedlings transferred to MS plates supplemented with 10 μM PCIB for 24 h. (a) *proPIP2;1:GUS* fusion. (b) *proPIP2;2:GUS* fusion. (c) *proPIP1;2:GUS* fusion. (d) *proPIP2;7:GUS* fusion. (e) *proPIP1;1:GUS* fusion. (f) *proPIP2;4:GUS* fusion. Two independent *proPIP:GUS* lines of each *PIP* gene displayed similar expression pattern after IAA or PCIB treatment. Scale bar represents 100 μm.

PIP AQUAPORINS – LATERAL ROOT EMERGENCE

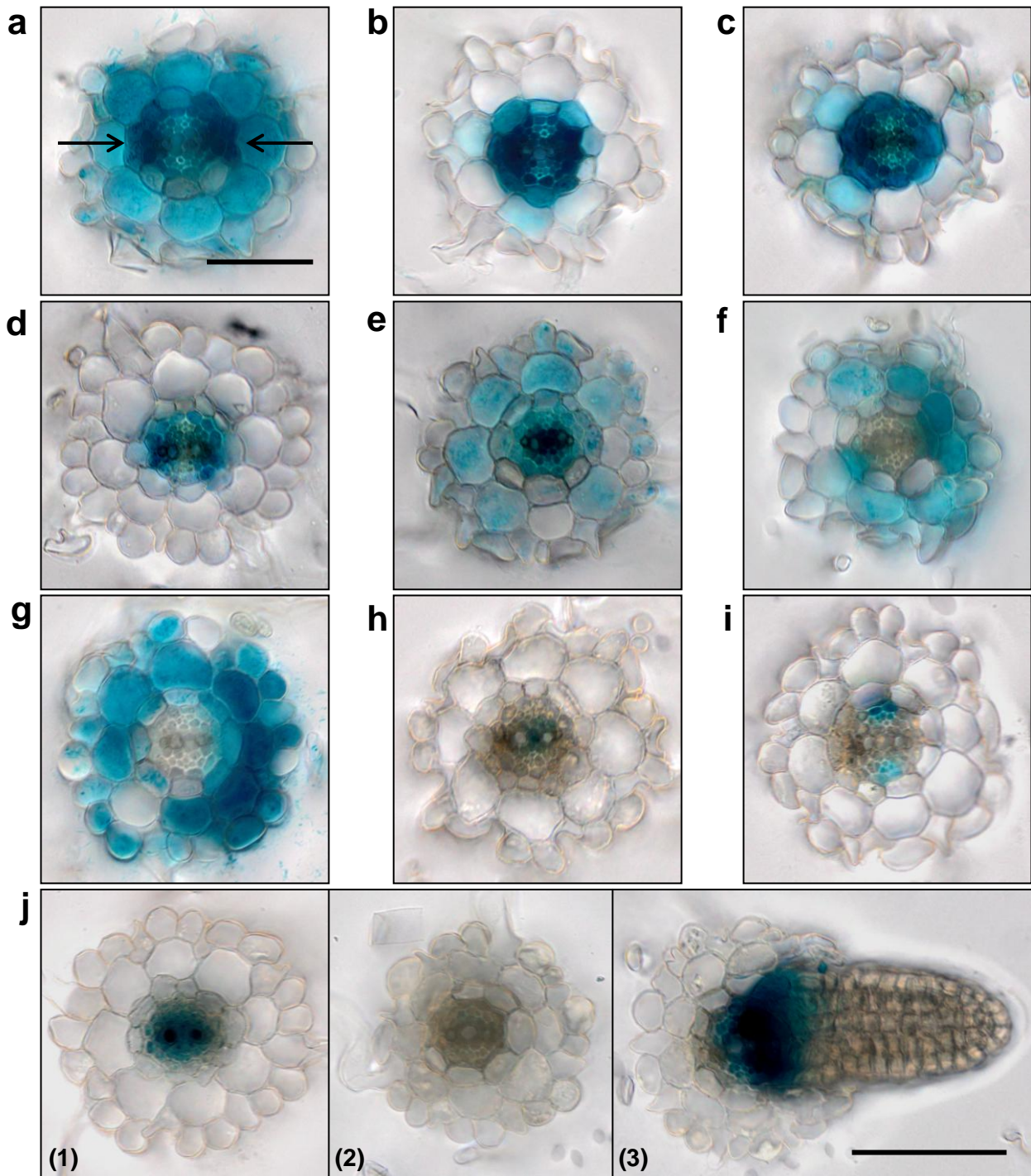


Figure 11 Expression patterns of *PIP* aquaporins in the stele. Root cross-sections were prepared after GUS staining (the staining time of individual reporter lines were the same as indicated in Figure 7, 8 and 9). (a) *proPIP1;2:GUS* fusion. (b) *proPIP2;1:GUS* fusion. (c) *proPIP2;2:GUS* fusion. (d) *proPIP2;3:GUS* fusion. (e) *proPIP2;7:GUS* fusion. (f) *proPIP1;1:GUS* fusion. (g) *proPIP2;4:GUS* fusion. (h) *proPIP2;5:GUS* fusion. (i) *proPIP2;6:GUS* fusion. (j) *proPIP2;8:GUS* fusion; three images show the expression pattern of *PIP2;8* at the root tip (1), older root region lacking LR (2) and the LR formation site (3), respectively. Two independent *proPIP:GUS* lines of each *PIP* gene displayed similar expression pattern in the stele. All sections are positioned with xylem poles in a horizontal manner indicated by arrows in (a). Section thickness: 30 μm. Scale bars represent 50 μm.

In the remaining *proPIP:GUS* fusion lines, *PIP1;1* and *PIP2;4*, which were expressed in the overlaying tissue, were not present in the stele (Figure 11f, g); *PIP2;5* showed a low expression in the metaxylem and cambium cells (Figure 11h); the expression of *PIP2;6* was specifically observed at the phloem poles and their neighboring pericycle cells (Figure 11i). *PIP2;8* was expressed in the stele of young root (from root tip to where metaxylem differentiation starts), but not in the older part except for LR formation sites, where *PIP2;8* was highly expressed at the base of the late-stage primordium, or emerged LR, and the underlying stele (Figure 11j). These data suggest that *PIP2;8* may also play an important role during LR development.

2.1.5 Spatial expression of *PIP* aquaporins is required during LRE

The expression patterns of *PIP* aquaporins (Figure 7-9 and 11) suggest that LR development involves a fine spatial and temporal control of water exchanges between the stele, LRP and overlaying cells.

To gain further understanding of the biomechanics of LRE and how this process is affected by the presence of auxin and *PIP* aquaporins, a tissue-scale model was established (Leah Band, University of Nottingham). This two-dimensional model is based on water movement between stele, LRP and the overlaying tissue (Figure 12). It is assumed that emergence is driven by increasing osmotic pressure within dividing primordium cells, which drives water into the LRP. The turgor pressure then increases the stress in the LRP boundary, which eventually yields and extends, enabling the LRP to force through the overlaying tissue. The predicted LRE time depends on the magnitude of different water fluxes, which is determined by the water potential difference and boundary permeability (k_1 to k_4). The presence of aquaporins increases the boundary permeability whereas auxin accumulation leads to its decrease. Thus, the model provides a way to deduce how LRE is affected by the aquaporin distribution and its regulation by auxin.

The model revealed how boundary permeabilities affect the emergence time: owing to the assumed direction of water fluxes (Figure 12), reducing k_2 or k_4 promotes emergence by decreasing water movement into the overlaying tissue (less resistance for primordium outgrowth); in contrast, reducing k_1 inhibits emergence by decreasing water flow into the primordium, whereas reducing k_3 has an opposite effect on emergence by decreasing water outflow towards the stele. However, auxin seems to have a contradictory effect on aquaporin regulation affecting the emergence time, i.e. it promotes emergence by reducing aquaporin

activity in the overlaying tissue (reducing k_2), and also inhibits emergence by reducing aquaporin activity in the primordium (reducing k_1). To understand these opposing effects, the influence of auxin was removed from the model (making k_1 and k_2 constant). This delayed the emergence by 8.7 h, indicating an overall accelerating effect of auxin on LRE (Péret *et al.*, 2012).

Combining these predictions with the distribution of individual PIP isoforms at a LR formation site (Figure 12), the model was used to simulate the importance of the dynamic PIP expression during LRE. Knockout of the PIPs expressed in the primordium, *PIP2;1* and *PIP2;2* in this context, would reduce permeability k_1 and k_3 and auxin's influence on k_1 . Reducing k_1 dominates over the influence of reducing k_3 , so that LRE should be delayed. In contrast, the loss-of-function mutants *pip1;1* and *pip2;4* would reduce k_2 and k_4 and auxin's influence on k_2 . As a result, reducing water flow into the overlaying tissue should promote LRE. Mutation in *PIP1;2* or *PIP2;7* should affect all boundary permeabilities. The model predicted that the effects of boundary permeabilities on LRE by affecting k_1 and k_3 would counteract those due to k_2 and k_4 . Therefore, a slight delay in LRE could be expected.

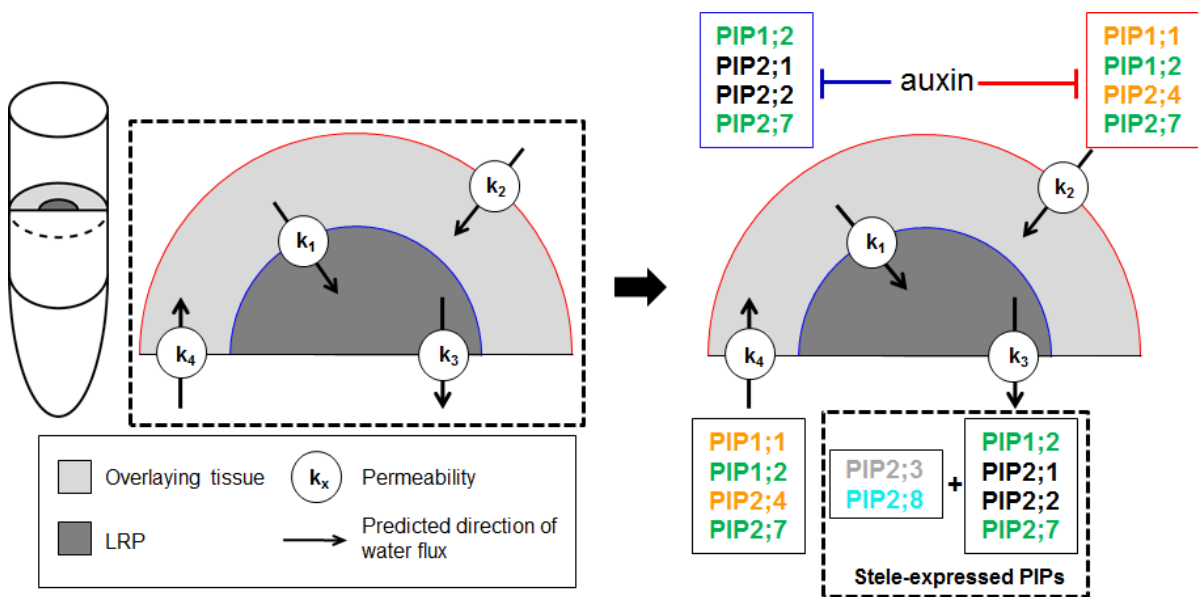


Figure 12 Two-dimensional tissue-scale model of LRE (Péret *et al.*, 2012) and distribution of PIP aquaporins at a LR formation site based on the expression pattern study. Left panel: the model represents the cross-section of an LRP (dark grey) protruding into the outer tissue (light grey). The arrows show the predicted direction of water fluxes between compartments; the magnitude of each water flux depends on the difference in water potential and the boundary's permeability (k_1 to k_4). Right panel: distribution of individual PIP isoforms in different compartments, which may contribute to the boundary permeabilities during LRE. PIP isoforms in black indicate that they are present only in the primordium, the ones in orange show expression only in the overlaying tissue and the ones in green are expressed in both compartments.

To test the model predictions and simulations, I examined the LRE rate in various aquaporin knockout mutants, which should affect different boundary permeabilities based on their expression patterns. Firstly, the effects of mutations in *PIP2;1* and/or *PIP2;2* on LRE were studied. Taking advantage of synchronization of LR formation, roots of wild type and mutants were given a gravitropic stimulus and LRP were counted and staged at 18 and 42 h pgi. Wild-type (Col-0) plants accumulated stage I and II LRP 18 h pgi and stage VII and VIII LRP 42 h pgi respectively (Figure 13a). LR initiation and first divisions were not affected in the *pip2;1-1* and *pip2;1-2* mutants, but showed an accumulation of stage II to VIII LRP 42 h pgi, which indicated that LRP emergence was delayed (Figure 13b, c). The *pip2;1-1* and *pip2;1-2* mutants transformed with a 4.6 kb genomic fragment containing the full *PIP2;1* gene displayed a wild-type LRE phenotype upon LR induction (Figure 13d, e), demonstrating that the LRE defect was due to disruption of the *PIP2;1* gene. In addition to the defective emergence time, the LRP of *pip2;1* mutant was flattened compared with the dome-shaped LRP observed in the wild type (Figure 14). It has been shown that expression of auxin-regulated *PIP2;1* was ARF7-dependent (Figure 6). Interestingly, similar LRE kinetics in *arf7* and *arf7 pip2;1* mutants were observed (Figure 13f, g), consistent with the ARF7-dependence of *PIP2;1*. Two independent *pip2;2* mutants accumulated stage V to VIII LRP 42 h pgi, indicating a less profound delay in LRE (Figure 13h, i). The LRE in the *pip2;1 pip2;2* double mutant also occurred significantly later than in the wild type (Figure 13j). The similar phenotype observed in the double mutant and *pip2;1* single mutants suggests *PIP2;1* being dominant during LRE in comparison with *PIP2;2*. Hence, loss of function in *PIP2;1* and *PIP2;2* resulted in defective LRE, consistent with the model predictions.

Subsequently, I analyzed the effects of mutations in *PIP1;2* and/or *PIP2;7* on LRE. LR initiation and first divisions were not affected, but LRE was delayed 42 h pgi by accumulation of stage V to VIII LRP in *pip1;2* and *pip2;7* mutants (Figure 15b-d). Obviously, this delay was less significant than the LRE phenotype in *pip2;1* mutants. Mutations in both genes strengthened the delay in LRE in either single mutant (Figure 15e). These observations were again consistent with the model predictions.

Interestingly, when the LRE rate of the *pip1;2 pip2;1 pip2;2 pip2;7* quadruple mutant was examined, mutations in these four primordium-expressed genes did not result in a further delay in LRE, but were similar to the *pip2;1* single mutants (Figure 15f).

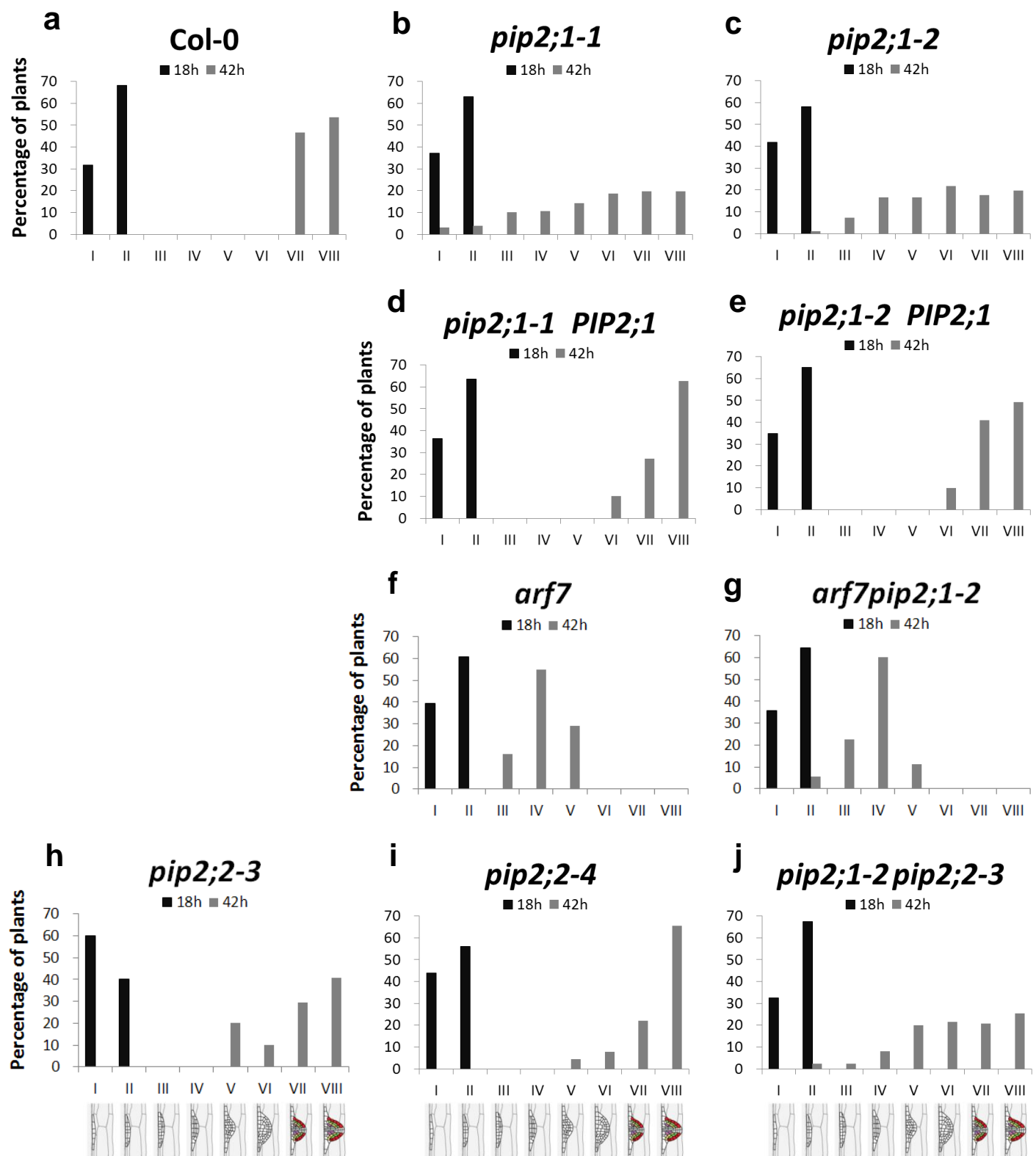


Figure 13 LRE is delayed in the *pip2;1* and *pip2;2* mutants. LRE phenotyping was achieved by synchronizing lateral root formation with a gravistimulus. Primordia were grouped according to developmental stages 18 h pgi (black bars) and 42 h pgi (grey bars). Percentage of plants was calculated from the total number of seedlings harvested from three independent experiments (n=90-100).

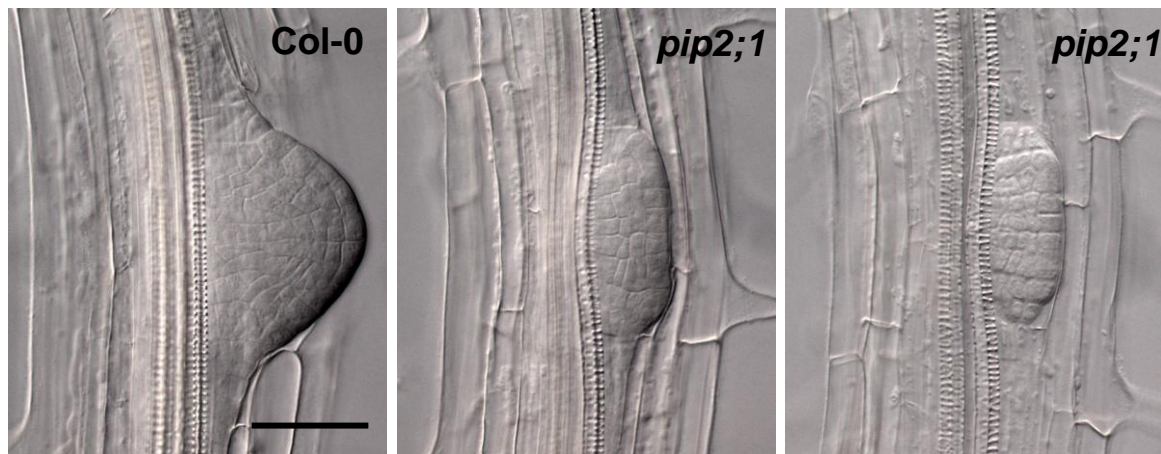


Figure 14 Flattened LRP shape in the *pip2;1-2* mutant compared with the dome-shaped wild-type primordium at 42 h pgi. Scale bar represents 50 μ m.

Surprising results were observed in *pip1;1* and *pip2;4* mutants. According to the model predictions, loss of *PIP1;1* or *PIP2;4*, which would lead to reducing permeabilities k_2 and k_4 and reducing water flow into the overlaying tissue, should facilitate LRE. However, the experimental data demonstrated a retardation of primordium outgrowth in the *pip1;1* or *pip2;4* single mutant 42 h pgi (Figure 15g, h). This was similar to the LRE phenotype observed in the mutants, LRP-expressed *PIPs* of which had been affected. *pip1;1 pip2;4* double mutant displayed a stronger delay in LRE (Figure 15i), confirming the surprising observation in the single mutants. These results indicated that the estimates of some parameter values or other assumptions in the current model are not accurately describing all factors, which require further modifications (see 2.2.4).

2.1.6 Expression of *PIP2;8* during LR formation is not regulated by auxin

In contrast to the majority of repressed aquaporins, *PIP2;8* is upregulated at a later phase of LR development (Péret *et al.*, 2012) as well as by exogenous auxin (Figure 5b). I noticed that *PIP2;8* was upregulated up to tenfold during LR development, but only to threefold after auxin treatment. In addition, *PIP2;8* was not expressed at the auxin accumulation site during LRE (Benková *et al.*, 2003; Swarup *et al.*, 2008). Therefore, I examined whether the expression pattern of *PIP2;8* was altered by treatment of IAA or PCIB. As expected, its expression was not responsive to application of IAA or PCIB (Figure 16a). Instead, the enhancement of LR number as a result of auxin treatment accounted for the up to threefold

upregulation of *PIP2;8* (Figure 16b). These observations suggest that the induction of *PIP2;8* is controlled by signal(s) other than auxin.

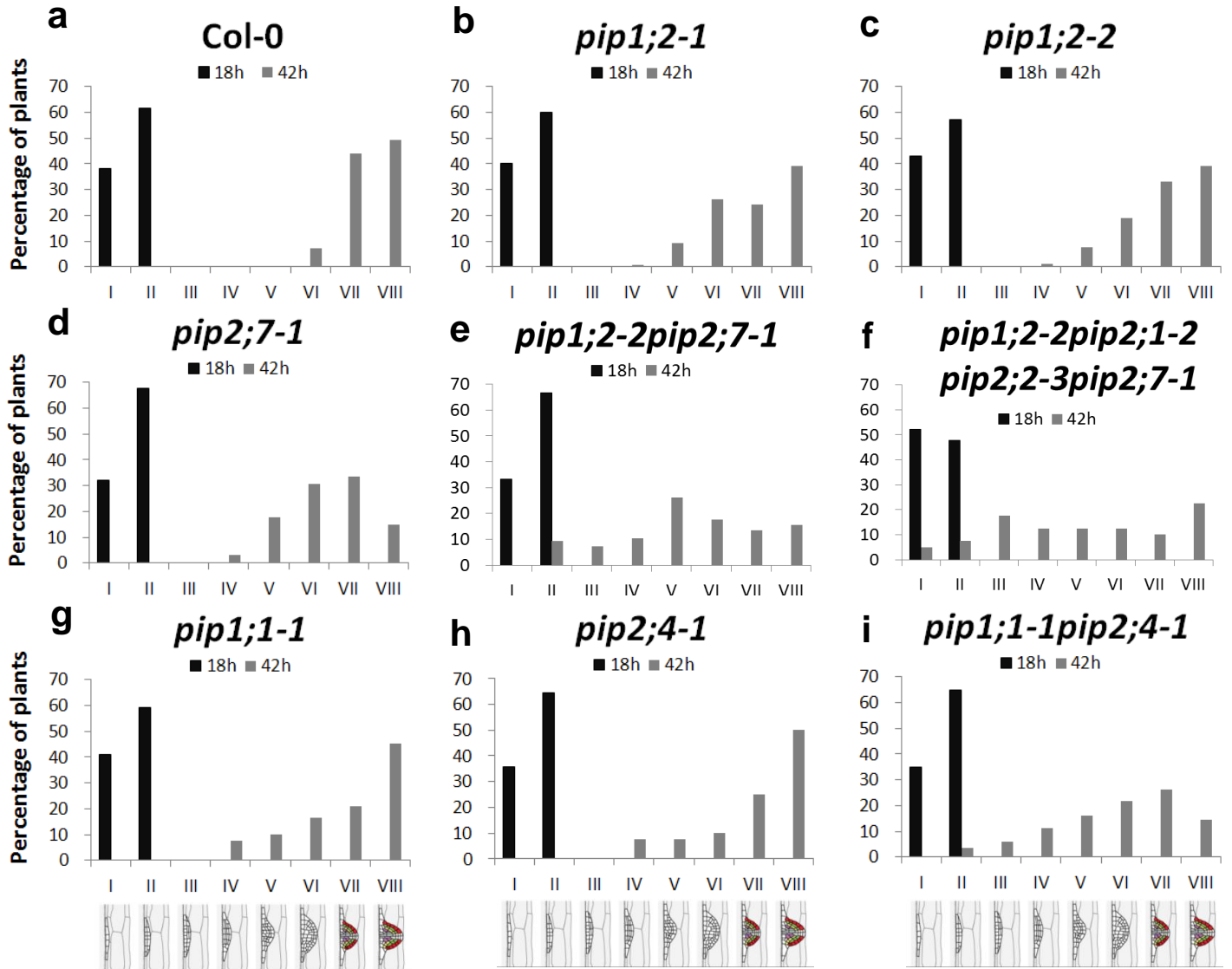


Figure 15 Delayed LRE in the *pip1;2*, *pip2;7*, *pip1;1* and *pip2;4* single or double mutants. LRE phenotyping was achieved as described in Figure 13. Primordia were grouped according to developmental stages 18 h pgi (black bars) and 42 h pgi (grey bars). Percentage of plants was calculated from the total number of seedlings harvested from three independent experiments (n=90-100).

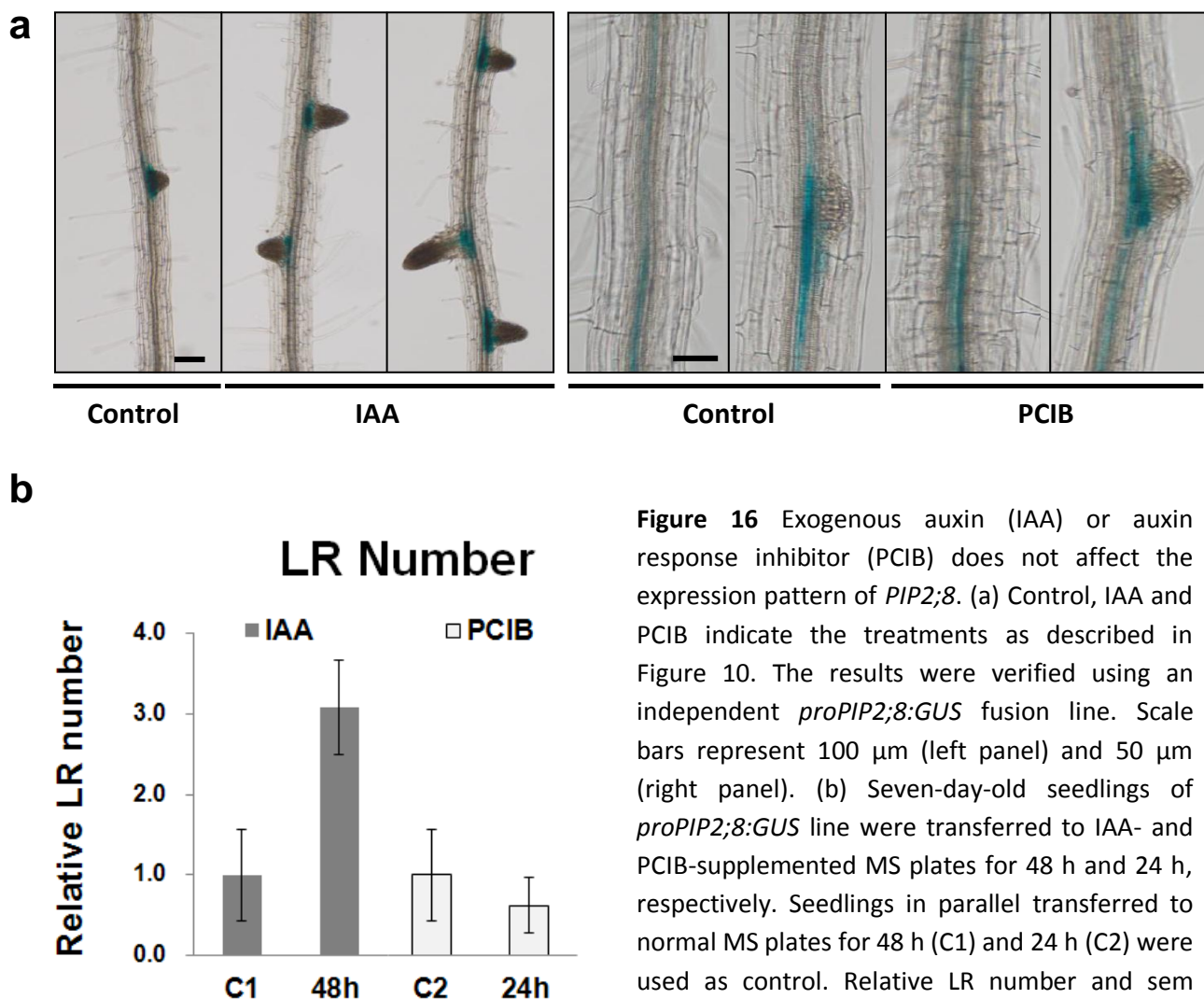


Figure 16 Exogenous auxin (IAA) or auxin response inhibitor (PCIB) does not affect the expression pattern of *PIP2;8*. (a) Control, IAA and PCIB indicate the treatments as described in Figure 10. The results were verified using an independent *proPIP2;8:GUS* fusion line. Scale bars represent 100 μm (left panel) and 50 μm (right panel). (b) Seven-day-old seedlings of *proPIP2;8:GUS* line were transferred to IAA- and PCIB-supplemented MS plates for 48 h and 24 h, respectively. Seedlings in parallel transferred to normal MS plates for 48 h (C1) and 24 h (C2) were used as control. Relative LR number and sem (standard error of the mean) values are shown.

Previous studies have described the roles of other plant hormones in regulating LR development: cytokinin inhibits LR initiation and disrupts LRP morphogenesis (Laplace *et al.*, 2007); very low concentrations of ethylene ($<0.04 \mu\text{M}$) promote LR formation whereas higher doses inhibit this process but facilitate emergence of existing LRP (Ivanchenko *et al.*, 2008); ABA is a negative regulator of LRE (De Smet *et al.*, 2006) and brassinosteroid (BR) positively regulates LR formation (Bao *et al.*, 2004). To further address the signal(s) resulting in the distinct expression pattern of *PIP2;8*, the effects of these hormones on the expression of *PIP2;8* were tested. Similar to auxin, 48 h treatment of cytokinin (6-benzylaminopurine and kinetin), 0.1 μM ethylene precursor ACC or brassinolide (BL) did not affect the expression pattern of *PIP2;8* (Figure 17a-d, f). To validate whether the hormone treatments worked, LR

number (LRP and emerged LRs) of treated and control seedlings were counted (together with Marion Kirchner and Robert Rampmaier, Ludwig-Maximilians-Universität München). As a negative regulator of LR formation, treatment of cytokinin or ACC resulted in fewer LRs, whereas BL had an opposite effect on LR production, which is consistent with the positive role of BR during this process (Figure S2). Different from these hormones, ABA fully repressed GUS signals of the *proPIP2;8:GUS* line even after 24 h of treatment (Figure 17a, e). Taken together, none of the plant hormones tested in this work induced *PIP2;8* expression as observed during LR development; ABA acted as a negative regulator of *PIP2;8* expression.

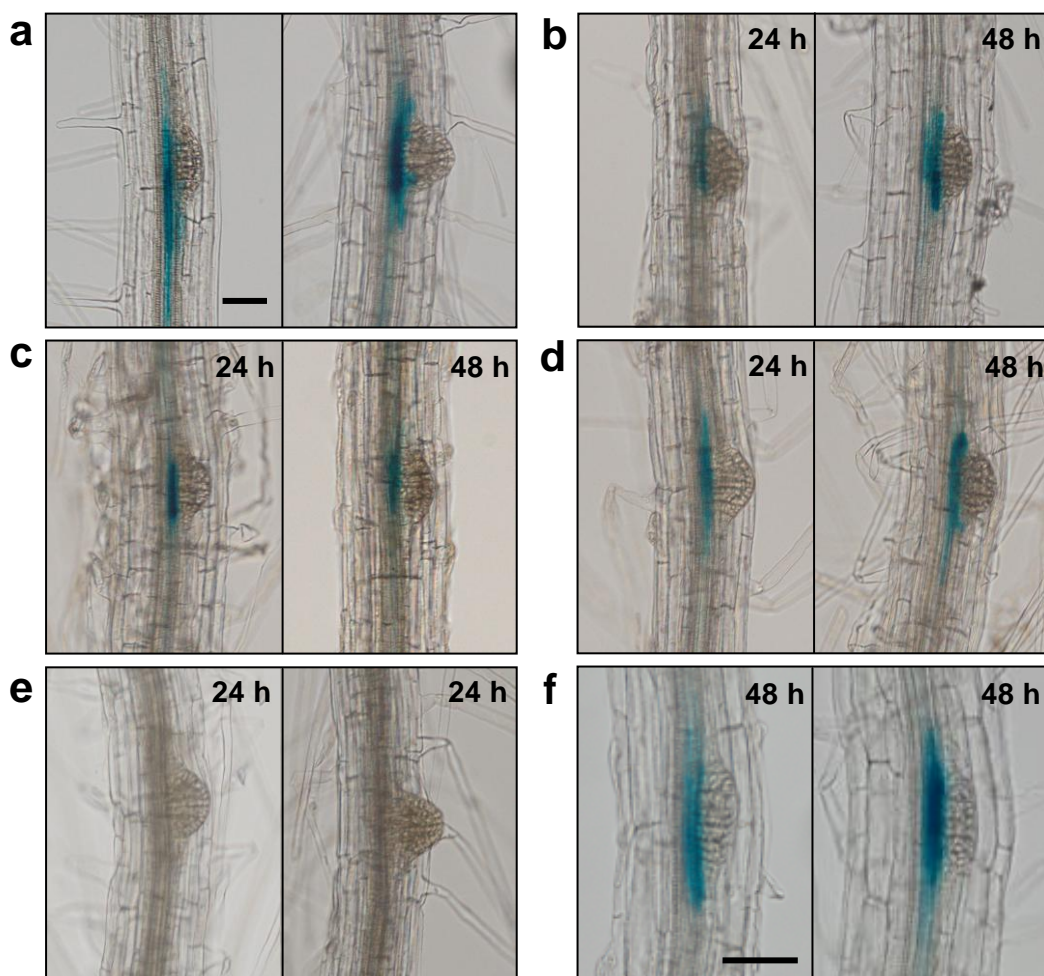


Figure 17 *PIP2;8* expression is repressed by ABA, but not regulated by cytokinin, ethylene or BR. Seven-day-old seedlings of *proPIP2;8:GUS* fusion line were transferred to normal MS plates (a) or to MS plates supplemented with 0.1 μ M ACC (b), 0.1 μ M 6-benzylaminopurine (c), 0.5 μ M kinetin (d), 0.1 μ M ABA (e) and 10 nM BL (f) and grown for 24 h or 48 h as indicated. Two independent *proPIP2;8:GUS* fusion lines in response to each plant hormone exhibited similar results. Scale bars represent 50 μ m.

Since exogenous ABA repressed expression of *PIP2;8*, it might have a negative physiological role in upregulating *PIP2;8* expression, i.e. the gene induction at late stages of LR formation could result from a locally reduced ABA level. Thus, a high-resolution LR transcriptomic dataset established using micro-dissecting root bends every 3 hours pgi (provided by Ute Voß, University of Nottingham) was employed to check the dynamic expression of ABA biosynthesis genes during LR development. This would yield the information on ABA level alteration. In *Arabidopsis*, ABA biosynthesis takes place in plastid and cytosol and consists of several enzymatic reactions, in which ABA1 (ABA deficient 1), ABA2 (ABA deficient 2), ABA3 (ABA deficient 3), ABA4 (ABA deficient 4), NCED3 (nine-cis-epoxycarotenoid dioxygenase 3) and AAO3 (abscisic aldehyde oxidase 3) are involved (Bittner *et al.*, 2001; González-Guzmán *et al.*, 2002; Iuchi *et al.*, 2001; Marin *et al.*, 1996; Nambara and Marion-Poll, 2005; Seo *et al.*, 2004). Among them, *ABA3*, *ABA4* and *NCED3* were downregulated upon LR induction. In particular, the expression of NCED3, which is commonly thought to be the rate-limiting enzyme during ABA biosynthesis, was strongly reduced 15 h pgi and sustainably low thereafter (Figure 18). It has been shown that the ABA level of NCED3 anti-sense line is significantly lower than that of wild type (Iuchi *et al.*, 2001). Thus, the repression of *NCED3* suggests a decrease of the ABA level during LR development, which may trigger the induction of *PIP2;8*.

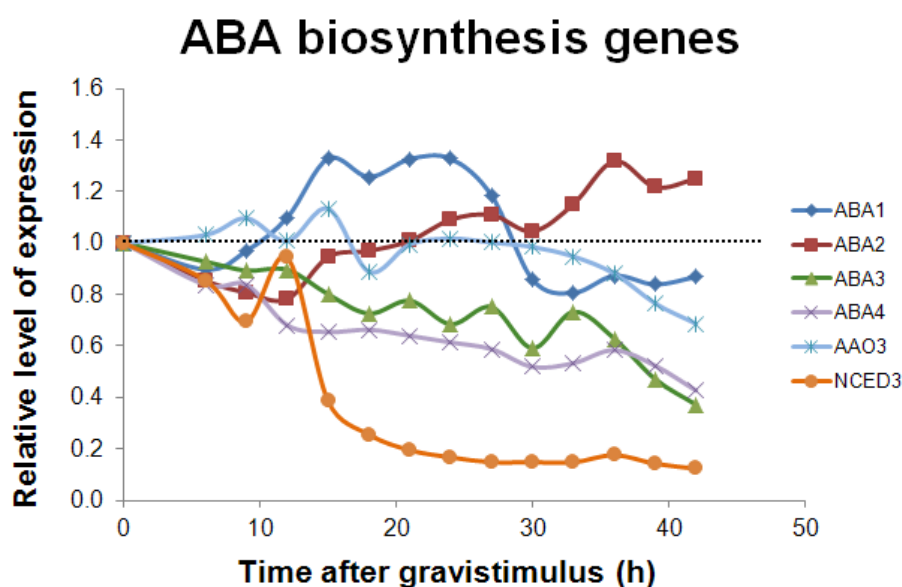


Figure 18 High-resolution expression profiles of genes involved in ABA biosynthesis after gravistimulation of lateral root formation.

2.1.7 Twenty-one transcription factors were identified as interesting candidates regulating *PIP2;8* expression during LR development

It has been shown that expression of most auxin-regulated *PIP* genes are controlled by transcription factor ARF7 (Figure 6). To further investigate how the distinct expression of *PIP2;8* is regulated during LR development, the high-resolution transcriptomic dataset was again used to explore the candidate(s), which might control *PIP2;8* expression based on their expression profiles upon LR induction. Transcription factors (TFs) were first selected to reduce the large number of genes in the dataset using Gene Ontology (GO) analysis in MAPMAN (Version 3.5.1). The TFs were further filtered to eliminate genes showing slight changes throughout LR development and the ones which had their maximum expression level at the last time-point (42 h pgi) (see 4.2.12). The remaining 224 TF genes, together with *PIP2;8*, were subjected to self-organizing map (SOM) analysis (collaboration with Dietrich Trümbach from the Institute of Developmental Genetics, Helmholtz Zentrum München) and were grouped into 16 clusters according to the similarity of expression profiles after gravistimulation (Figure 19a). All TF genes showing positive and negative correlations with the expression profile of *PIP2;8* are theoretically interesting candidates. However, as an initial investigation of *PIP2;8* regulating TFs, only positively correlated TF genes, i.e. those exhibiting similar expression profiles to *PIP2;8* or upregulation earlier than *PIP2;8*, will be targeted in this work. SOM analysis revealed that *PIP2;8* fell into cluster (0,0) together with 34 TF genes (Figure 19b). Fifteen genes in cluster (0,1) and one gene in cluster (1,0) also showed similar expression profiles to *PIP2;8*, but their expression maxima were shifted to earlier time-points upon LR induction (Figure 19b). Those genes grouped into the remaining clusters, showing either a decreased expression to a very low level after the peak or potentially negative correlation with *PIP2;8*, will not be further discussed.

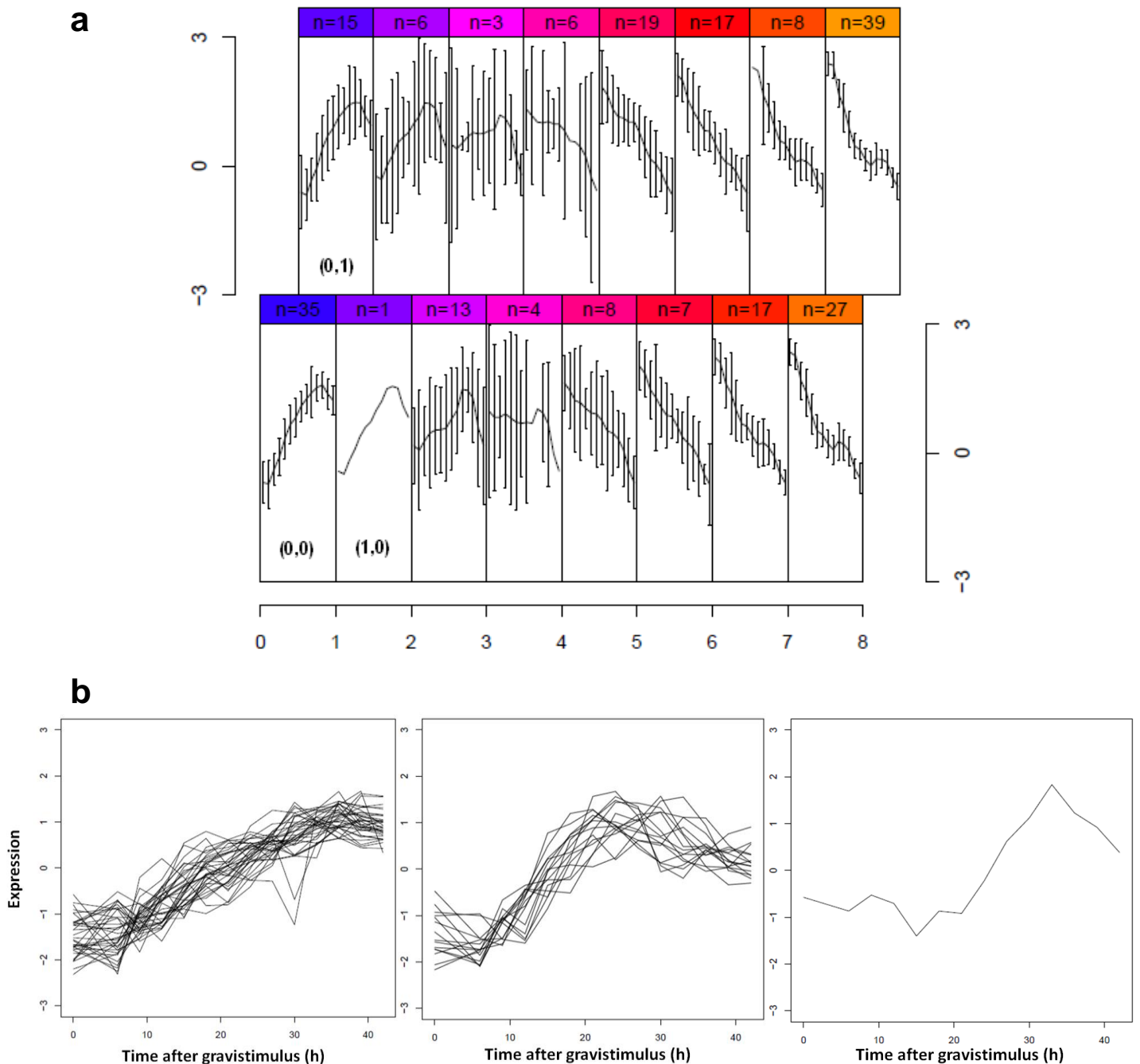


Figure 19 Self-organizing map (SOM) analysis revealed the selected TFs as candidates for regulating the expression of *PIP2;8* during LR development. (a) 224 TF genes, together with *PIP2;8*, are grouped into 16 clusters (8×2) according to the similarity of expression profiles upon LR induction. In each cluster, the curve represents the mean gene expression levels of all time-points upon gravistimulus, and a vertical line at each time-point is shown as standard deviation. The number highlighted in each box indicates the number of genes belonging to the corresponding cluster. (b) From left to right: overlay of expression profiles of genes in cluster (0,0), (0,1) and (1,0), respectively.

To find out the final candidate genes from 50 initially selected TFs (Table 1 and S1), further filtering was performed based on several criteria including their tissue expression profile, roles in regulating transcription and ABA responsiveness (Figure 20).

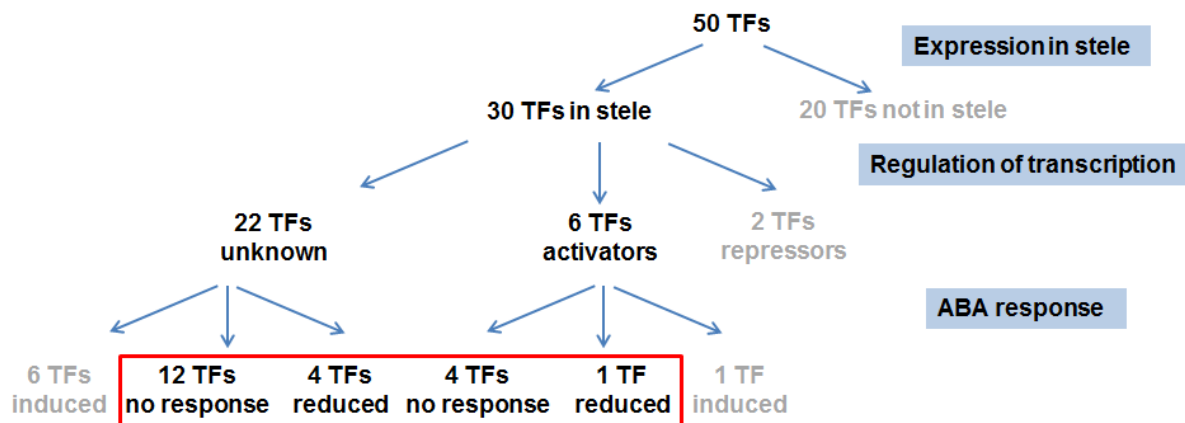


Figure 20 Scheme for selection of most interesting TF genes, which might induce *PIP2;8* expression during LR development, from 50 initial candidates obtained from SOM analysis. Three selection criteria are highlighted in light-blue. Red frame indicates the final candidate regulators of *PIP2;8* expression selected *via* three steps.

Firstly, final candidate(s) should be expressed in the stele, where upregulation of *PIP2;8* at late stages of LR formation mainly occurs. Thirty out of 50 TFs have been shown to express in the stele (Brady *et al.*, 2011). Secondly, final candidate(s) among 30 stele-expressed TFs should function as transcription activator to regulate *PIP2;8* expression. According to the gene annotations by TAIR (www.arabidopsis.org), only six and two TFs are known to act as transcription activators and repressors, respectively. Although the roles of the remaining 22 TF genes in regulating transcription remain unclear, they have been considered as potential transcription activators to ensure that all possible candidates are included for the subsequent filtering procedure. Thirdly, the hormone assay demonstrating ABA represses *PIP2;8* suggested that final candidate(s) should also be downregulated by ABA. However, ABA is not necessarily involved in regulation of *PIP2;8* expression during LR development, as only few hormones have been tested in this work. Unknown signal(s), such as a direct inducer, may exist to contribute to the distinct *PIP2;8* expression. Thus, final candidate(s) among 28 known or potential transcription activators should be either downregulated or not responsive after ABA treatment, but not induced by ABA. The expression data obtained from public databases (Genevestigator and e-FP Browser) demonstrated that five and seven out of 28 TF

PIP AQUAPORINS – LATERAL ROOT EMERGENCE

genes are significantly reduced and induced by ABA ($p<0.05$), respectively, and the remaining 16 TFs do not respond to ABA treatment (Table 1 and S1). Taken together, the 21 TFs, which are expressed in the stele, act as (potential) transcription activators and are not ABA-inducible, were identified as final candidates (Table 1). These final candidates, particularly five known transcription activators (AT1G20910, AT3G16770, AT3G54810, AT5G65310 and AT5G66320), will be subjected to further investigation of their roles in controlling expression of *PIP2;8* during LR development.

Table 1 TF genes selected as final candidates for positively controlling *PIP2;8* expression during LR development.

AGI code	SOM cluster	Stele expression	Regulation of transcription	Response to hormones tested in this work		Response to other factors (hormones or stresses)
				ABA	other hormones	
AT1G20910	(0,0)	yes	activator	no		
AT3G16770	(0,0)	yes	activator	no	cytokinin, ethylene	jasmonic acid
AT3G54810	(0,0)	yes	activator	no		
AT5G65310	(0,0)	yes	activator	reduced		
AT5G66320	(0,0)	yes	activator	no		nitrate inducible
AT1G20700	(0,0)	yes	unknown	no		
AT1G30330	(0,0)	yes	unknown	no	auxin	
AT2G34140	(0,0)	yes	unknown	no	auxin, ethylene	
AT2G41710	(0,0)	yes	unknown	no		
AT2G44940	(0,0)	yes	unknown	no		
AT3G16280	(0,0)	yes	unknown	reduced		
AT3G25710	(0,0)	yes	unknown	no		phosphate starvation
AT4G14770	(0,0)	yes	unknown	no		
AT4G30410	(0,0)	yes	unknown	reduced	auxin	
AT5G60200	(0,0)	yes	unknown	no		
AT5G65640	(0,0)	yes	unknown	no		
AT1G72360	(0,1)	yes	unknown	reduced	ethylene	
AT3G11280	(0,1)	yes	unknown	reduced		gibberellin, salicylic acid
AT3G16500	(0,1)	yes	unknown	no	auxin	nitrogen starvation
AT5G15130	(0,1)	yes	unknown	no		
AT5G17800	(0,1)	yes	unknown	no		

2.1.8 PIP2;8 function is also required for promoting LRE

The spatio-temporal expression of *PIP2;8* at LR formation sites (Figure 9f), in particular compared with its low or non-existent expression in the remaining root, suggests that *PIP2;8* may play a role in LRE. Based on the expression pattern of *PIP2;8*, the mathematical model predicted that its mutation should promote LRE due to the reducing boundary permeability k_3 and decreasing water outflow towards the stele (Figure 12). To test this, the LRE rate in *pip2;8* mutants was examined. In comparison with the wild type (Col-0 or Col-4), LR initiation and first divisions were not affected, but primordial outgrowth was retarded by accumulation of stage II to VIII LRP 42 h pgi in *pip2;8-1* or *pip2;8-2* mutant (Figure 21a-d). These observations were inconsistent with the model prediction, but nevertheless demonstrate that optimal LRE also requires PIP2;8 function.

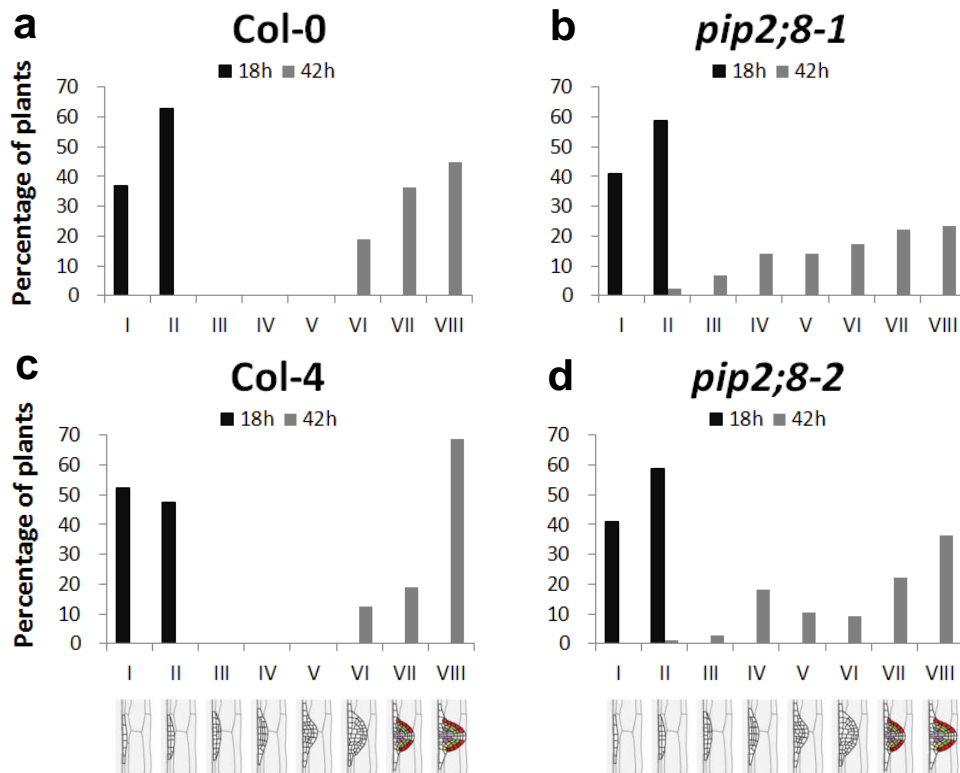


Figure 21 LRE is delayed in *pip2;8* mutants. *pip2;8-1* is Col-0 background and *pip2;8-2* is Col-4 background. LRE phenotyping was achieved as described in Figure 13. Primordia were grouped according to developmental stages 18 h pgi (black bars) and 42 h pgi (grey bars). Percentage of plants was calculated from the total number of seedlings harvested from three independent experiments (n=90-100).

2.2 Discussion

2.2.1 Fine-tuned regulation of aquaporin-dependent tissue hydraulics by auxin facilitates LRE

Auxin acts as a key regulator of LR development (Overvoorde *et al.*, 2010). It induces cell divisions during initiation, patterns the newly forming LRP (Casimiro *et al.*, 2001; Friml *et al.*, 2003) and triggers the cell wall remodeling in the overlaying tissue to facilitate new organ emergence (Swarup *et al.*, 2008). The results of this work demonstrate that auxin also controls aquaporin-dependent tissue hydraulics to promote LRE.

Auxin regulates root tissue hydraulics by coordinating the repression of *PIP* gene expression in the LRP and overlaying tissue. Application of exogenous auxin downregulates most of the *PIP* genes, including those expressed in the LRP and overlaying tissues (Figure 5). Accordingly, root hydraulic conductivity at both whole-root and single-cell levels decrease (Péret *et al.*, 2012). Expression-pattern analysis employing PIP reporter lines further revealed an auxin-directed spatio-temporal distribution of PIPs during LR development (Figure 7-10). These observations suggest that LRE involves the spatial and temporal control of tissue hydraulics through regulating PIP distribution by auxin.

To probe the regulatory mechanism of how auxin control of aquaporin activity affects LRE, a tissue-scale mathematical model had been developed (Figure 12) (Péret *et al.*, 2012). It suggested that optimal LRE requires water transport into the overlaying tissue to be repressed as a result of auxin accumulation, whereas aquaporins would promote water transfer from the overlaying cells into the primordium. These opposing effects on LRE have therefore to be precisely tuned in time and space to explain an overall beneficial effect of auxin and repression of PIPs in different compartments. Model simulations have provided insights into this integrated process. The model predicted that knockout of specific *PIPs* should result in a delayed LRE due to either a reducing water flow into the growing primordium (*pip2;1* or *pip2;2* mutant) or overall effects of reducing water flow in both growing primordium and overlaying tissues (*pip1;2* or *pip2;7* mutant). The LRE phenotypes observed in the mutants were consistent with model predictions (Figure 13 and 15). Interestingly, the model also predicted that LRE should be delayed when PIP2;1 is ectopically expressed under the control of a constitutive promoter and therefore independent of auxin. The ectopically expressed PIP2;1 is not only present in the LRP, but also in the overlaying tissue. This PIP2;1 distribution would facilitate water fluxes into the overlaying tissue, resulting in this tissue

providing a greater resistance to primordium expansion. The experimental data determining the LRE rate in *d35S:PIP2;1* line again validated the model prediction (Péret *et al.*, 2012). Thus, due to the opposite effect of PIP expression in different tissues, this is a very special case that loss-of-function mutant and constitutive overexpression line show a similar phenotype.

2.2.2 Auxin-responsive PIPs are regulated by ARF7 and parallel pathways

A previous study has demonstrated that ARF7, together with ARF19, mediates the expression of *LAX3* to promote LRE (Swarup *et al.*, 2008). In this work, this transcription factor was shown to also regulate expression and function of PIP aquaporins during LRE (Figure 6 and 13f, g). The expression pattern of ARF7 provides additional evidence for the ARF7-dependence of some auxin-responsive PIPs. *ARF7* is expressed in the stele and in the whole LRP, but after emergence from the parental root, its expression dissipates from the meristematic region (Okushima *et al.*, 2005). Some ARF7-dependent PIPs, *PIP2;1*, *PIP2;2* and *PIP2;7*, exhibit similar expression patterns. However, another LRP-expressed isoform *PIP1;2* is repressed by auxin independently of ARF7. The expression pattern of ARF7 indicates that this transcription factor is absent from the overlaying tissue during LR development (Okushima *et al.*, 2005). For the auxin-regulated PIPs, which are exclusively expressed in the overlaying tissues, *PIP2;4* expression is ARF7-independent, whereas *PIP1;1* is expressed dependently on ARF7 function. The ARF7-dependence of *PIP1;1* expression seems contradictory to the observation that their expression patterns during LR development have no overlays. Nevertheless, these results suggest that auxin regulates PIPs with similar expression patterns through different pathways.

The data on ARF7-dependence showing that *PIP1;1*, *PIP2;1*, *PIP2;2* and *PIP2;7* function downstream of the ARF7 pathway and the observation that *PIP1;2* and *PIP2;4* could be targeted by parallel pathways help to interpret the observed LRE phenotypes in double mutants. Given that two genes are involved in the same pathway, mutations in both genes would result in similar plant phenotype to that caused by the mutation in either gene; in contrast, mutations in two genes would give an additive phenotype when they are controlled by independent pathways. Mutant analysis based on the synchronization of LR formation upon gravistimulation demonstrated that the *pip2;1 pip2;2* double mutant exhibited a similar LRE phenotype as *pip2;1*, whereas *pip1;2 pip2;7* and *pip1;1 pip2;4* strengthened the delayed

LRE compared with the single mutants (Figure 13 and 15). These observations nicely fit the two-pathway assumption.

The ARF7-related transcription factor ARF19 may contribute to regulating ARF7-independent PIPs. ARF19 is another key component taking part in auxin-regulated LR formation (Okushima *et al.*, 2007; Wilmoth *et al.*, 2005) and is ubiquitously expressed in the primary root and LRs (LRP and emerged LRs) (Okushima *et al.*, 2005). Monitoring the effects of *arf19* loss-of-function on expression of ARF7-independent PIPs upon auxin treatment will provide the evidence whether their auxin responses are dependent on the ARF19 function. Taken together, these results suggest that auxin exerts complicated effects on regulation of *PIP* expression to regulate LRE.

2.2.3 Understanding a novel aquaporin-dependent regulation of LRE requires identification of regulators of *PIP2;8* expression

In comparison with most *PIP* isoforms, *PIP2;8* shows distinct behaviours during LR development, including strong induction from stage IV onwards in the stele and independence of auxin. Together with the delayed LRE in *pip2;8* mutants, these observations suggest that an auxin-independent pathway also targets at regulating aquaporins (i.e. inducing *PIP2;8*) to promote LRE.

Better understanding such a novel regulation of LRE needs to address the questions which and how signal(s) precisely regulate the expression of *PIP2;8* during LR development. The hormone assay demonstrated that ABA, a negative regulator of LR development, repressed the expression of *PIP2;8* (Figure 17). Consistent with this, LRE phenotypes of ABA-treated Col-0 and *pip2;8* mutants are highly similar (Figure 21 and 22). Upregulation of *PIP2;8* could result from a reduction of the ABA level upon LR induction, which releases the repression of *PIP2;8* expression. A remarkable downregulation of *NCED3* (that encodes the rate-limiting enzyme in the ABA biosynthesis pathway) during LR development was observed (Figure 18), which is consistent with the assumption that the ABA level is reduced. However, *NCED3* has been shown to be specifically expressed at the base of a LR (Tan *et al.*, 2003) similar to the site of *PIP2;8* expression. This observation suggests that the base of a LR is an active site of ABA biosynthesis, which contradicts the assumption above. Therefore, the involvement of ABA in *PIP2;8* induction requires further experimental support. Comparison of *PIP2;8* expression during LR development between wild type and mutants defective in ABA biosynthesis (e.g. *nced3*) (Ruggiero *et al.*, 2004) and/or ABA response (e.g. *ABA insensitive*

mutants) (Finkelstein and Somerville, 1990) will provide straightforward evidence whether ABA deficiency releases the repression of *PIP2;8*.

Instead of such a release of repression, a direct upregulation of *PIP2;8* by so far unknown inducer(s) could be possible. Public expression databases such as Genevestigator and e-FP Browser are normally powerful tools to identify candidate regulators of gene expression. However, they are not applicable for investigating the inducer(s) of *PIP2;8* expression since the hybridization signals of *PIP2;8* and *PIP2;7* are not distinct on Affymetrix microarray, on which the majority of public data depend. Nevertheless, the responsiveness of *PIP2;8* to plant hormones other than the ones tested in this study (auxin, cytokinin, ethylene, BR and ABA), such as strigolactone and gibberellin (negative regulators of LR development), is to be determined (Gou *et al.*, 2010; Ruyter-Spira *et al.*, 2011). In recent years, some signaling peptides (Fernandez *et al.*, 2013; Kumpf *et al.*, 2013; Meng *et al.*, 2012) and nitric oxide (NO) (Méndez-Bravo *et al.*, 2010) have been shown to be involved in regulating LR development. They may also lead to specific induction of *PIP2;8*.

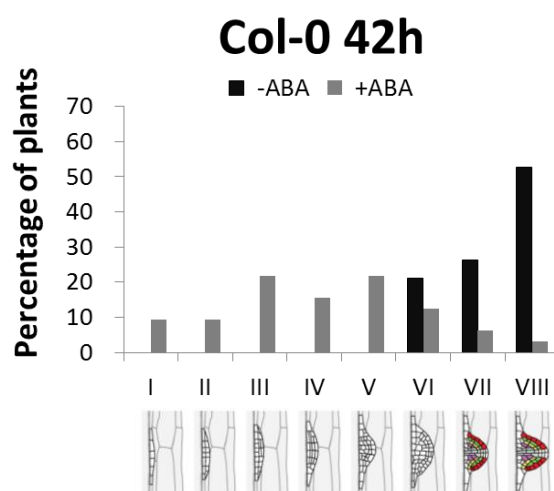


Figure 22 LRE is delayed in Col-0 seedlings treated with exogenous ABA. Three-day-old seedlings were transferred to MS plates containing 0.1 μ M ABA or normal MS plates. Gravistimulus was applied immediately after the transfer for 42 h. Primordia were grouped according to developmental stages in treated (grey bars) or non-treated (black bars) seedlings. Percentage of plants was calculated from the total number of 30 seedlings.

SOM analysis and further filtering procedures have identified 21 transcription factors as candidates that might control *PIP2;8* expression during LR development due to their parallel or preceding upregulation with *PIP2;8*. One should be aware that transcription factors, which anti-correlate with *PIP2;8* expression profile (i.e. highly reduced at late-stage LR development), exhibit stele expression and function as transcription repressors, are equally interesting candidates. Two strategies can be employed to further investigate whether and

which candidate determines *PIP2;8* expression: (1) compare the expression pattern of *PIP2;8* during LR development between wild-type and TF-mutant backgrounds (introduce *proPIP2;8:GUS* into different TF mutants); (2) compare the expression profile of *PIP2;8* between different genetic backgrounds based on qPCR (particularly at crucial time-points, e.g. 36 h pgi). The identification of the final TF controlling *PIP2;8* expression could in turn help to find out the chemical inducer(s) of *PIP2;8*, because the regulation of the final TF might be better annotated and the public expression databases could be used to search for the candidate inducer(s).

2.2.4 LRE phenotypes of some *pip* mutants help to refine crucial parameters in the current mathematical model

Although the modeling approach has allowed us to correctly simulate the LRE phenotypes upon many modifications of boundary permeabilities, in particular the similar LRE defects caused by both gain- and loss-of-function of *PIP2;1*, some experimental data, which disagreed with model simulations, suggest that estimates of crucial parameter values are inaccurate and require further modifications.

The delayed LRE observed in *pip1;1* and *pip2;4* mutants is contradictory to the model prediction. Since *PIP1;1* and *PIP2;4* are exclusively expressed in the overlaying tissue (Figure 9a, b and 11f, g), they should contribute to the boundary permeabilities k_2 and k_4 , which affect the water fluxes into the overlaying tissue (Figure 12). Furthermore, boundary permeability k_2 is reduced during LRE due to auxin accumulation, whereas k_4 is not regulated by auxin. Therefore, the simulation of LRE phenotype in *pip1;1* or *pip2;4* mutant involves the value changes of model parameters including initial k_2 (k_{2init} , distinguished from minimum k_2 as a result of auxin repression), k_4 and rate of decrease of k_2 due to auxin (k_{2g}). Simulations by Leah Band (University of Nottingham) revealed that reducing k_{2init} and k_4 causes faster emergence whereas reducing k_{2g} causes delayed emergence (Table 2). The faster emergence in *pip1;1* or *pip2;4* predicted by the current model considered the effects of reducing k_{2init} and k_4 dominating over reducing k_{2g} , but the delayed LRE observed in *pip1;1* and *pip2;4* mutants implied that reducing k_{2g} should have a more pronounced effect than reducing k_{2init} and k_4 on emergence time. Taking this into account, the model prediction of emergence time in *pip1;1* or *pip2;4* mutant would be greatly improved with slight reductions of k_{2init} and k_4 (e.g. $k_{2init}=k_4=0.6$) and a very small value of k_{2g} (Table 2). However, the meaning of such modification in parameter values is questionable since the knowledge of contributions of

individual overlaying-tissue PIPs to boundary permeabilities k_{2init} and k_4 during LRE and the relationship between changes in k_{2init} and k_{2g} (the degree of k_{2g} reduction is associated with how much k_{2init} would be reduced) is still lacking. Although quantitative analysis of PIP proteins in the whole root could give some hints (Monneuse *et al.*, 2011), this data cannot be simply used to assess the contribution of individual PIPs to boundary permeabilities during LRE for two main reasons: (1) protein abundance is not equal to its real-time activity (for example, PIP2;2 is more abundant than PIP2;1 in the whole root whereas PIP2;1 appears to function more dominantly at the particular LR formation sites); (2) one isoform could have different expression levels in LRP and overlaying tissues and, therefore, exert different contributions to boundary permeabilities (such as PIP1;2 and PIP2;7). Nevertheless, the currently available data on transcript and protein levels of PIP1;1 and PIP2;4 could be employed for subsequent simulations. In addition, optimal estimates of these parameters could be identified from the simulation which most nicely agrees with the experimental data.

Table 2 The influence of different boundary permeabilities (k_{2init} and k_4) and the decreasing rate of k_{2init} (k_{2g}) on the predicted emergence time.

	k_{2init}	k_{2g}	k_4	Emergence time
Wild type	1	0.0028	1	28 hours
Partial contribution of PIP(s) to k_x^* & auxin influences k_{2init}	0.6	0.0028	0.6	22.7 hours
Partial contribution of PIP(s) to k_x & auxin no longer influences k_{2init}	0.6	0	0.6	44.7 hours
Full contribution of PIP(s) to k_x & auxin no longer influences k_{2init}	0.2	0	0.2	17 hours

* k_x represents k_{2init} and k_4 .

The significance of boundary permeability k_3 -mediated water flux during LRE may have been overlooked in the current model. k_3 -dependent water flux is predicted to flow from primordium into the stele (it is commonly known that water moves towards the stele where long-distance transport occurs), and plays the least important role in affecting the emergence time (Péret *et al.*, 2012). However, the spatio-temporal expression of *PIP2;8* at LR formation

sites and retarded LRE observed in *pip2;8* mutants suggest that k_3 -dependent water transport could be equally important as other water fluxes. This raises the possibility that the direction of water flux between stele and primordium driven by the water potential difference may revert at LR formation sites, namely from stele into primordium, to meet the water requirement in the rapidly growing LRP for cell expansions. Although the experimental data supporting this speculation is challenging to obtain, the observations in this work will direct the parameter modification towards strengthening the importance of k_3 and considering dynamic changes of water potential difference between primordium and stele.

In addition to optimization of the current parameters, new factors might be required to further develop the mathematical model. The regulatory signals other than auxin (e.g. the inducer of *PIP2;8* expression) could be integrated. Furthermore, since the current tissue-scale model provides the simplest representation of LRE, considering the growing primordium and the overlaying tissue as two homogeneous fluid-like compartments and lumping the effects of cell-wall extension and cell-to-cell reorganization into the boundaries surrounding each tissue region (Péret *et al.*, 2012), it would be important to build a cell-scale, three-dimensional model. Such a model would facilitate the simulations of the emergence time and, more importantly, help to better understand the complexity of LRE biomechanics.

2.2.5 Mutations in *PIPs* do not affect LR number under normal growth conditions

Mutant analysis has demonstrated that LRE was delayed in various *pip* mutants (Figure 13, 15 and 21), including *pip2;1*. In addition, a flattened LRP was observed in *pip2;1* (Figure 14). However, *pip2;1* mutants exhibited similar primary root length and LR number as Col-0 under normal growth conditions (Figure S3a, b). Preliminary characterization of LR density (LR number/primary root length) in *pip2;1 pip2;2* double mutant and *pip2;8* single mutant, which exhibited similar delay in LRE to *pip2;1*, also showed no significant difference from wild type (Figure S3c). These data indicate that, although a longer time is required for LRE, the entire growth program in these mutants is not hampered.

It has been demonstrated that retardation of LRP outgrowth in the *pip1;2 pip2;1 pip2;2 pip2;7* quadruple mutant (mutations in four LRP-expressed *PIPs*) was similar to the *pip2;1* single mutants (Figure 13b, c and 15f). The unexpected observation showing no further delay of LRE in the quadruple mutant motivates further study to examine whether LR number/density

of this mutant is altered. In addition, the subsequent investigation of lateral root length in Col-0 and various *pip* mutants would provide some insights into the role of PIPs in the post-emergence LR growth.

It could also be interesting to characterize LR phenotypes of *pip* mutants under various nutrient conditions. Suboptimal nutrient availability in the soil modifies root architecture through regulating endogenous hormones and their signaling pathways. For example, high concentration of nitrate causes a lower auxin level and higher levels of cytokinin and ethylene, leading to an inhibitory effect on LR growth (Takei *et al.*, 2004; Tian *et al.*, 2009; Walch-Liu *et al.*, 2006); phosphate deficiency induces LR formation by upregulation of the key auxin signaling component TIR1 to increase the auxin sensitivity (Perez-Torres *et al.*, 2008). In parallel, root hydraulic conductivity is also affected under these conditions. Re-supply of nitrate after deprivation largely induces the root hydraulic conductivity in *Lotus japonicas* (Prosser *et al.*, 2006). A similar treatment upregulates the aquaporin gene expression in tomato (Wang *et al.*, 2001). Phosphate deficiency reduces root hydraulic conductivity in wheat, suggesting that regulation of aquaporins may occur (Clarkson *et al.*, 2000). The difference of LR phenotypes between wild type and *pip* mutants under these conditions would increase our understanding of the biological significance of aquaporin functions during lateral root development.

3. INVOLVEMENT OF PIP AQUAPORINS IN RESPONSE TO ALTERED ENVIRONMENTAL CUES

3.1 Experimental design

3.1.1 Genotype selection

The expression data obtained from different sources, including published qPCR results (Alexandersson *et al.*, 2005; Boursiac *et al.*, 2005), public database “Genevestigator” and GUS staining patterns (Da Ines, 2008; Prado *et al.*, 2013), demonstrated that *PIP2;1* and *PIP2;2* are highly and ubiquitously expressed isoforms, and *PIP2;4* is an isoform specifically expressed in roots in *Arabidopsis*. In addition, the water channel activity of *PIP2;1* and *PIP2;2* has been determined (Kammerloher *et al.*, 1994), and their post-translational modifications and regulations are well-characterized. Based on these information, *pip2;1 pip2;2* double mutant (dm) and *pip2;1 pip2;2 pip2;4* triple mutant (tm) were selected, in comparison with Col-0 (wt), to determine the plants’ metabolic changes in response to different environmental conditions. Seeds of these genotypes were propagated before use under control condition as indicated in Table 3.

3.1.2 Growth conditions and stress application

Plants were raised in two identical climate simulation chambers, where realistic conditions for plant growth, including irradiance (spectrum and intensity), temperature, humidity and chamber atmosphere (CO₂, O₃), can be provided (Seckmeyer and Payer, 1993; Thiel *et al.*, 1996). In addition, the central control system allows a well-defined operation and accurate climatic conditions to ensure reproducibility between independent experiments (collaboration with the Environmental Simulation Research unit, Helmholtz Zentrum München).

Plants of three genotypes (dm, tm and wt) were grown under control condition (C) for 20 days (Figure 23 and Table 3). A flooding system was employed to achieve uniform watering: plants were distributed in square basins and flooded with water up to 60 % of the pot height for 15 minutes. The amount and timing of water pumping in/out are well-controlled and automatic (Figure 24). After a flooding on day 20, watering was stopped to the plants used for drought and heat treatment (DH) in chamber 2 (Figure 23). The soil moisture was regularly monitored during the following drought stress. When the soil water content decreased to 20.7

PIP AQUAPORINS – RESPONSES TO ALTERED ENVIRONMENTAL CUES

± 2.7 % on day 27, both drought-treated and well-watered plants in chamber 2 were subject to heat stress (33 °C; H) for 6 hours (from 11:00 a.m. to 5:00 p.m.). It is known that temperature increase dramatically reduces relative air humidity. In order to maintain the same vapour pressure deficit (VPD) at the level before application of heat stress, the relative air humidity was accordingly adjusted to 82 %. The combination of high temperature and high air humidity ensured that heat stress could be separated from an additional drought stress in the ambient air. The plants in chamber 1 were continuously grown under control condition (Figure 23 and Table 3).

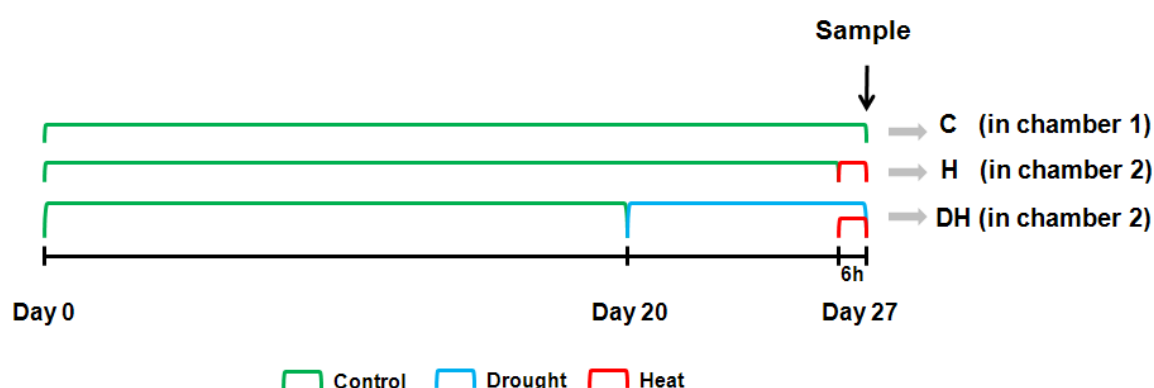


Figure 23 Scheme for drought and/or heat stress application used in this work. The black line and bars represent plant growth and treatment durations. Three different conditions are shown by color-coded brackets. C, H and DH are abbreviated for control, heat stress and combination of drought and heat stress, respectively.

Table 3 Details of control, drought and heat conditions in the climate simulation chambers.

	Control	Drought	Heat
Watering status	regular watering	no watering	regular watering
Temperature	22 °C	22 °C	33 °C
Relative humidity	70 %	70 %	82 %
VPD (Vapour Pressure Deficit)	0.793 kPa	0.793 kPa	0.793 kPa
Light/dark cycle	11 h* / 13 h	11 h / 13 h	11 h / 13 h
Light intensity	200 $\mu\text{E m}^{-2} \text{s}^{-1}$	200 $\mu\text{E m}^{-2} \text{s}^{-1}$	200 $\mu\text{E m}^{-2} \text{s}^{-1}$

* Light was on from 8:30 a.m. to 7:30 p.m..

3.1.3 Replicate arrangement and harvest

Under each environmental scenario, five replicates of each genotype were generated. To exclude any potential position effect among genotypes and replicates, they were randomly distributed in each treatment area to ensure that one genotype did not have the same neighboring genotypes in other instances (Figure 25).

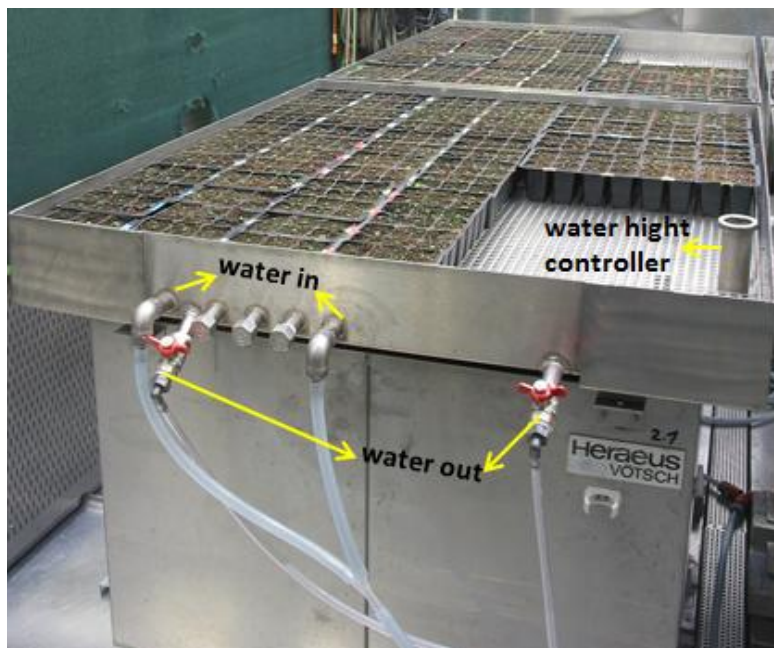


Figure 24 Flooding system designed to achieve uniform watering. Four square watering basins (1 m × 1 m) can be placed in one chamber. The pipes for water pumping in and out are mounted as indicated. The timing is automatically controlled by timers, and the water height controller is set to 60 % of pot height to avoid excess water pumping in.

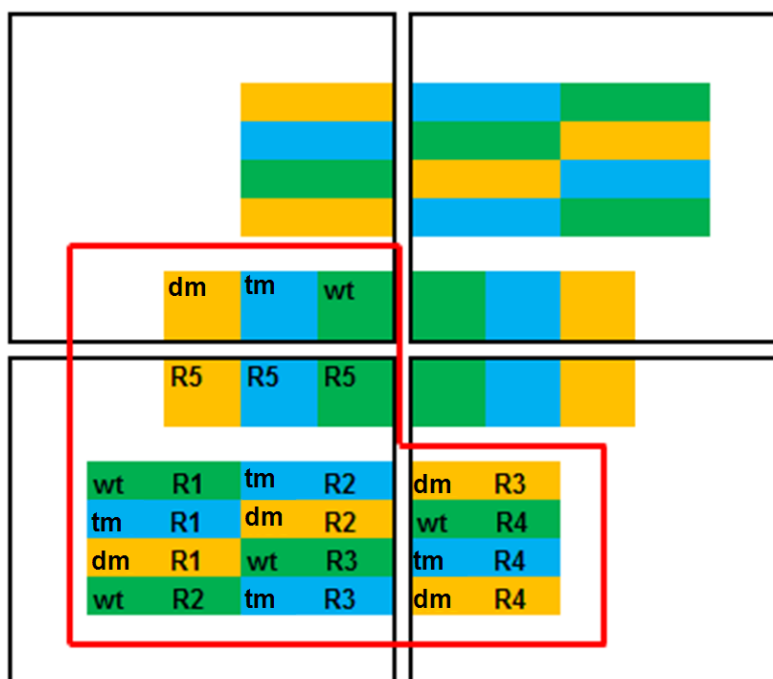


Figure 25 Scheme for random arrangement of genotypes and replicates under H and DH to exclude the position effect. Four black frames represent the watering basins where plants are placed. The arrangement of genotypes and replicates for DH is shown (inside the red frame). The distribution of plants for H mirrors this arrangement. R is abbreviated for replicate.

Treated and control samples were harvested on day 27 starting at 5:00 p.m.. Rosettes from eight plants were pooled as one replicate, and collected into a sampling bag. The difference of harvest time between replicate 1 and 5 was at most 15 minutes. All harvested samples were immediately frozen in liquid nitrogen and stored at -80 °C until use.

3.1.4 Non-targeted metabolome analysis using FT-ICR-MS

The Fourier Transform Ion Cyclotron Resonance Mass Spectrometry (FT-ICR-MS) is an unbiased analytical approach that allows the parallel detection of a large number of compounds with different masses in biological samples. It provides ultra-high resolution and accurate m/z determinations, therefore enables pattern analysis as well as prediction of empirical formula and molecular identities of the m/z peaks (Gougeon *et al.*, 2009; Stenson *et al.*, 2003; Tziotis *et al.*, 2011).

An FT-ICR-MS (Bruker, Germany) equipped with a 12 Tesla magnet was used for non-targeted metabolome analysis. Each sample was measured in both negative (loss of proton) and positive (addition of cation, e.g. H^+ or Na^+) ionization modes (collaboration with the Research unit of Analytical BioGeoChemistry, Helmholtz Zentrum München). After processing and statistical analyses of the acquired data (done by Theresa Faus-Kessler from the Institute of Developmental Genetics and Veronica von Saint Paul from the Institute of Biochemical Plant Pathology, Helmholtz Zentrum München), the formulas and putative metabolite identities of significantly changed m/z peaks associated with *PIP* mutations were identified.

3.2 Results

The metabolic profiles of three genotypes under different environmental scenarios were obtained from FT-ICR-MS measurements. The negative- and positive-mode datasets, each of which joined all samples from two independent experiments (IEs), were subjected to statistical analyses (see 4.2.14).

3.2.1 Several data-processing strategies of statistical analyses emerge from the quality control of the metabolic profile datasets

To control the quality of FT-ICR-MS measurements, the intensity of internal standard di-alanine (added after metabolite extraction) and the sum of total peak intensities were monitored to detect variation of ionization efficiency. In the negative-mode dataset, di-alanine exhibited increasing peak intensities throughout the measurements in both IEs (Figure 26a), indicating enhanced ionization efficiency along the measurement order. The increase of total peak intensities, similar to di-alanine, was also observed in IE1. However, in IE2, the mean of total peak intensities steeply dropped from $7e+10$ in replicate 1 and 2 to $3e+10$ in the remaining replicates (Figure 26b). In the positive-mode dataset, the changes of di-alanine intensity and total peak intensities were similar, showing decreasing peak intensities throughout the measurements in IE1 and a “sudden increase” effect in IE2 (Figure S4). The changing ionization efficiency and replicate-separated intensity differences resulted in significant variations between replicates and could eventually affect the identification of significantly changed metabolites. To suppress this effect, the mean intensity of each peak over all replicates was used and the measurement order was taken into account during the downstream principle component analysis (PCA) and analysis of variance (ANOVA), respectively.

I also noticed that total peak intensities displayed pseudo-periodic “up-down-up” variations in both datasets (Figure 26b and S4b). When DH-treated samples of three genotypes were combined, their mean intensities were higher than those of non-drought (H and C) samples for each replicate in IE1 (Figure 27b). In addition, the dilution series (1:30, 1:50, 1:75, 1:100, 1:125 and 1:150) assay, which was performed in negative mode using two wild-type samples under C and DH, respectively, showed that the DH-treated sample exhibited higher peak intensities of some endogenous metabolites (not drought inducible) and total peak intensities than the C-treated sample regardless of dilution ratios (Figure S5). These observations

suggested the difference in metabolite concentrations between DH-treated and non-drought samples was most likely a consequence of their fresh-weight differences. Due to water loss, the fresh weights of DH-treated samples were 30 % (on average) lower than non-drought ones, whereas the wild type and *pip* mutants had similar fresh weights under each condition (Table S2). As a consequence, the metabolites in DH-treated samples should be more concentrated when the same amounts of fresh powder (100 mg) were used for extraction. Normalization using fresh weight would reduce this difference between DH-treated and non-drought samples. However, not all peaks in DH-treated samples suffer from an identical concentration effect since the peak intensity is not fully determined by its concentration, but also the chemical property and complexity of biological matrices (Han *et al.*, 2008; Lei *et al.*, 2011; Wang *et al.*, 2003). More importantly, this study aimed at determining the altered metabolic responses upon loss of major PIP isoforms, i.e. the metabolic differences between different genetic backgrounds under each condition rather than those between different conditions in each genotype. Therefore, instead of normalization with fresh weight, mutant/wt ratios were used with the replicates and measurement order taken into account during downstream PCA and ANOVA to compensate for the observed differences in fresh weight and ionization efficiency.

As an internal standard added after metabolite extraction, the peak intensity of di-alanine should not be affected by the metabolite-concentration difference as discussed above. However, it seemed that DH-treated samples exhibited higher mean peak intensities of di-alanine than the non-drought samples (Figure 27a), which was probably due to the matrix effect or drought induction of alanine (Allan *et al.*, 2008).

Pairwise xy-plots and Pearson correlation analysis of all peak intensities (excluding missing values) were in parallel employed to check extract reproducibility in each group (a “group” contains all replicates collected from one genotype under one condition). In the negative-mode dataset, high reproducibility between replicates within each IE was achieved, yielding a correlation coefficient of $R^2 > 0.90$ in most cases. Relatively lower correlations ($0.80 < R^2 < 0.90$) were observed between the first two replicates and the remaining three ones in IE2. Some peaks, visualized by formation of additional lines or “clouds” in corresponding pairwise-plots, exhibited higher intensities in replicate 1 and 2, but lower ones in replicate 3, 4 and 5 (Figure 28), consistent with the drop of total peak intensities at the interface of replicate 2 and 3 in IE2. In addition to extract reproducibility within each IE, it was also examined between replicates from different IEs. As expected, two extracts from different IEs exhibited lower reproducibility, with varying correlation coefficients ranging from 0.65 to 0.80 (Figure 28).

Similarly, higher extract reproducibility within each IE and lower reproducibility between extracts from different IEs were also observed in the positive-mode dataset (Figure S6).

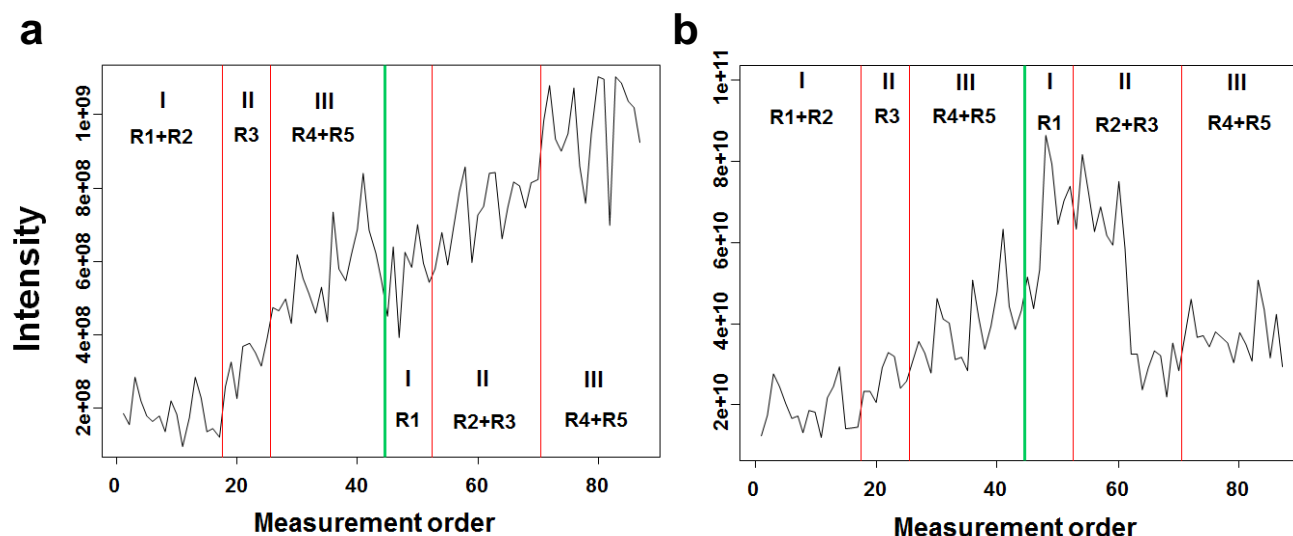


Figure 26 Quality control of FT-ICR-MS measurements (negative mode) by monitoring the variations of di-alanine intensity (a) and total peak intensities (b). Intensities of all samples from two IEs are plotted. The green line in each graph separates IE1-samples from IE2. Red lines indicate that the samples from each IE were measured in three batches (I, II, III). They were split according to replicates as indicated.

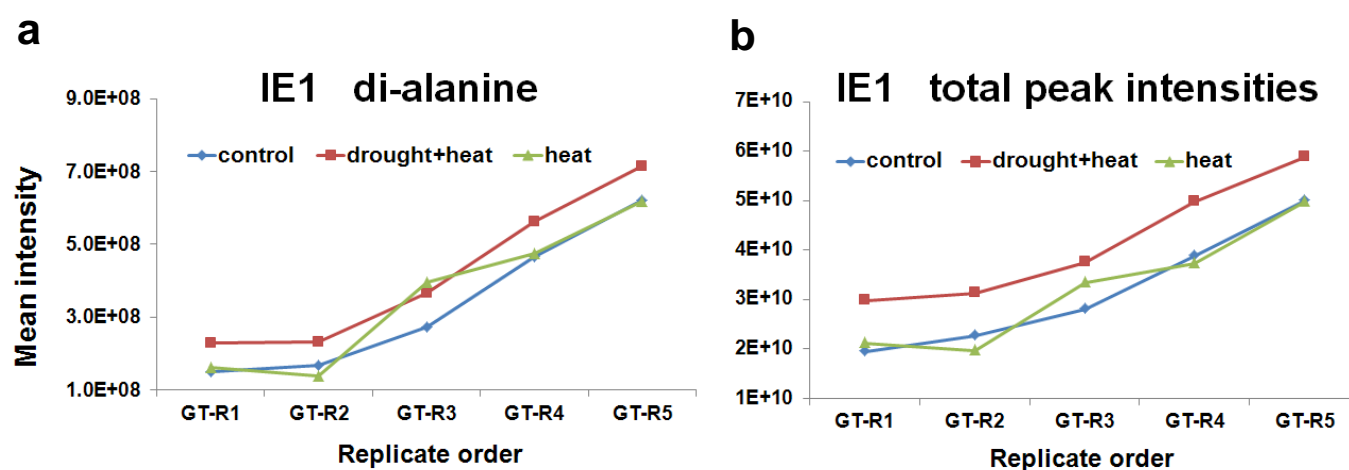


Figure 27 DH-treated samples exhibit higher intensity of di-alanine (a) and total peak intensities (b) than non-drought samples for each replicate in IE1 (negative mode). The mean peak intensity of three genotypes for each replicate under each environmental condition was calculated and plotted. GT represents “combined genotypes” and R1-R5 indicate five replicates.

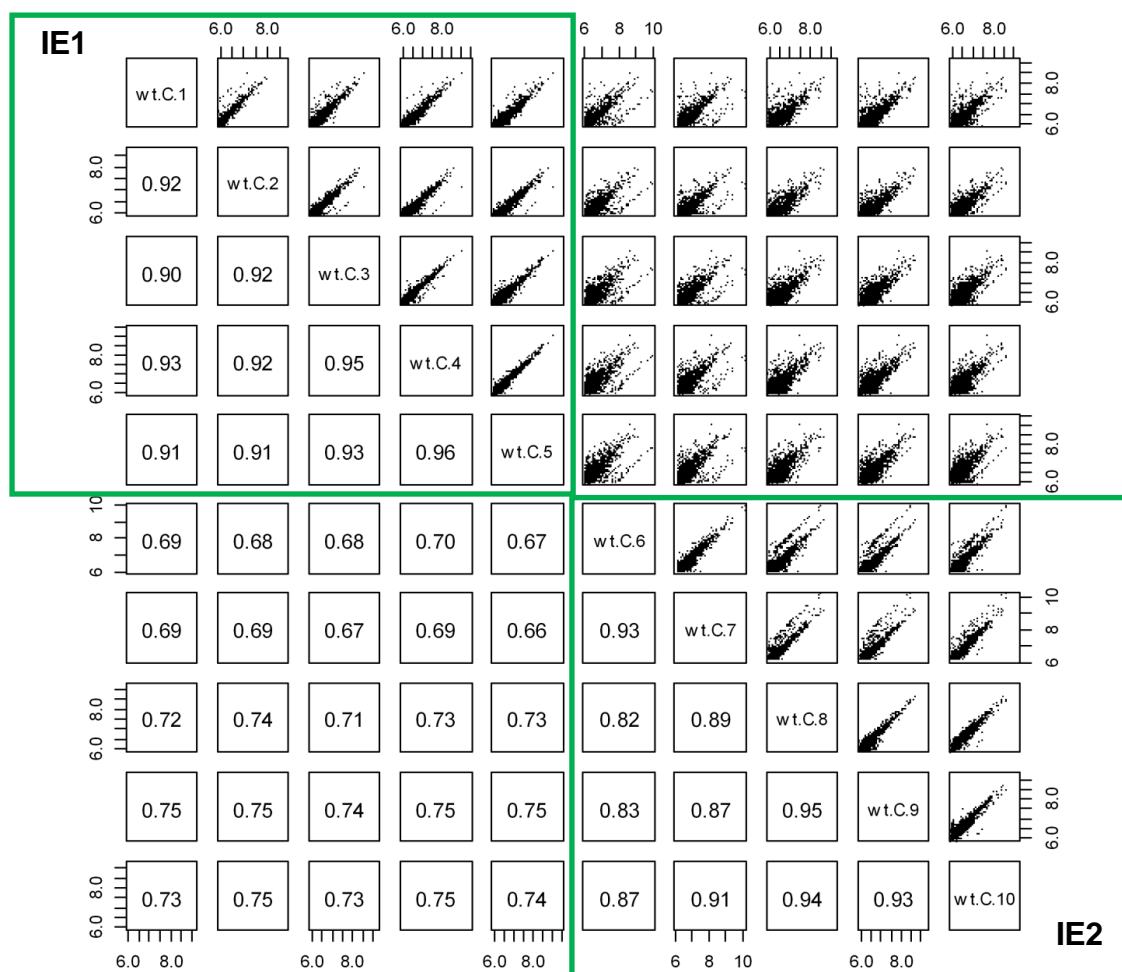


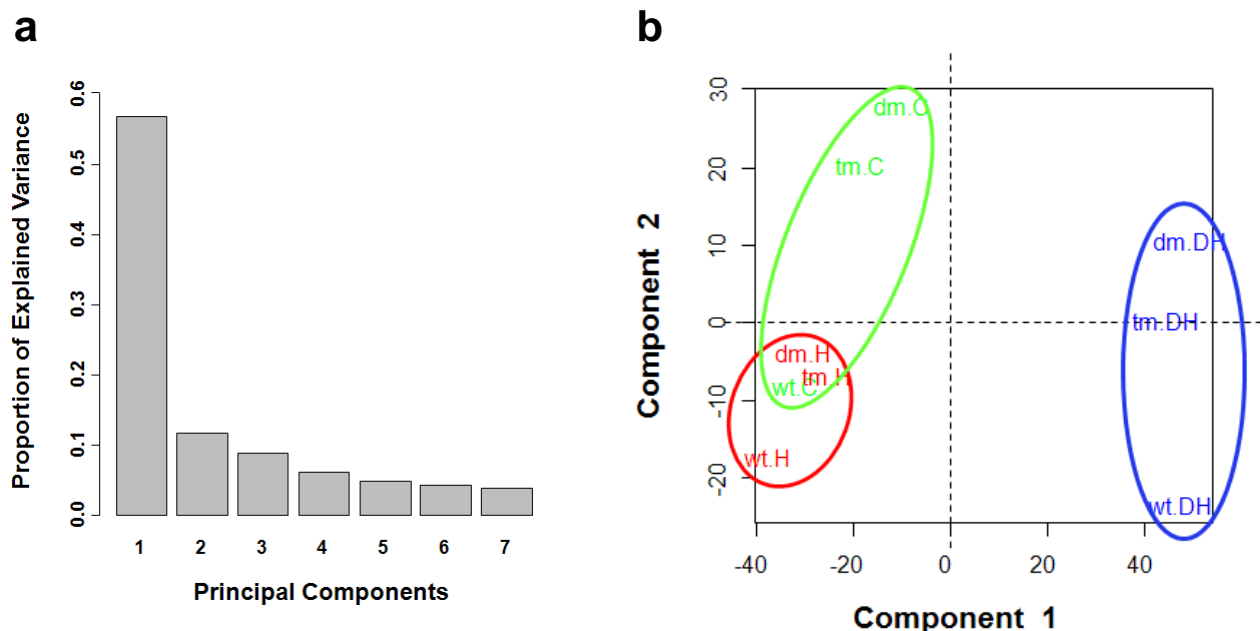
Figure 28 Pairwise xy-plots and Pearson correlation analysis between replicates in the group “wt under control condition” (negative mode). 1-5 represent extracts from IE1, and 6-10 are from IE2. Peak intensities (\log_{10} transformed) between two replicates were compared, and pairwise correlations were calculated as indicated. The results of extract reproducibility in other groups were similar to this group.

3.2.2 Both stress conditions and *PIP* mutations affect metabolic profiles

PCA was performed to visualize the major variances of metabolite profiles between groups. PCA using group means (mean intensity of each peak over all replicates in one group) as loading factors showed that the component 1, accounting for more than 50 % explained variance, separated DH-treated groups from H-treated and control groups in both negative- and positive-mode datasets (Figure 29a, b and S7a, b). The separation by component 1 most likely resulted from the difference in metabolite concentrations between DH-treated and non-drought samples as discussed in 3.2.1. The additional informative variances of metabolite

profiles could be observed in the following principal components. When component 2 and 3 (approximately 10 % explained variance each) were plotted in the negative-mode dataset, separation of groups by conditions and by genotypes was observed (Figure 29c, d). This observation suggested that both stress conditions and genetic modifications triggered the alteration of metabolic responses. In the positive-mode dataset, component 2 and 3 contributed to the separation between stress-treated and control groups (Figure S7c). Furthermore, component 4 separated C and DH-treated *pip* mutants from wild type, whereas H-treated dm, not tm, was discriminated from wild type (Figure S7d).

In addition, PCA using mutant/wt ratios (mean ratio of each peak over all replicates in one group) as loading factors was also performed. The group separation was not affected by the difference in metabolite concentrations in this PCA. The metabolic profiles of *pip* mutants were separated by three environmental conditions in both negative- and positive-mode datasets (Figure 29e, f and S7e, f). H- and DH-treated *pip* mutants were discriminated by both component 1 and 2. Taken together, PCA results revealed that both stresses and *PIP* mutations affected the metabolic profiles, and the metabolic changes associated with *PIP* mutations appeared to be condition-specific.



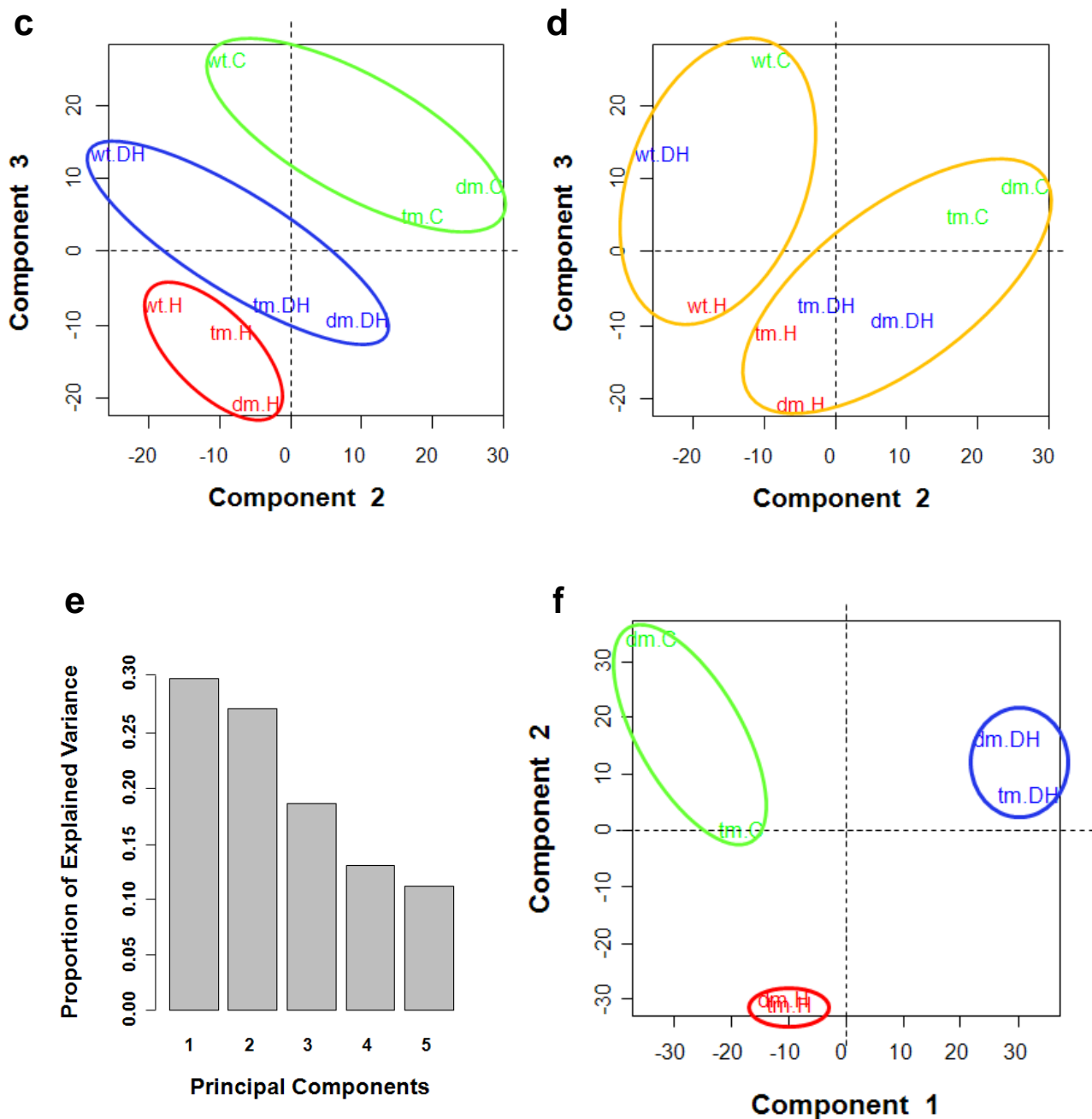


Figure 29 Principal component analysis (PCA) of metabolic profiles (negative mode) using group means (a-d) and mean mutant/wt ratios (e-f) as loading factors demonstrated that differential metabolic responses are caused by both stresses and *PIP* mutations. Principal component 1 and 2 (b and f) and component 2 and 3 (c and d) were plotted. The green, red and blue circles label three (or two) genotypes treated with control (C), heat (H) and combination of drought and heat (DH), respectively (b, c and f). Two orange circles indicate the wild-type groups and mutant groups regardless of conditions (d).

3.2.3 Loss of major PIP isoforms results in specific metabolic changes under different environmental conditions

To further identify significantly changed m/z peaks in *pip* mutants under each environmental condition, ANOVA was performed (comparisons between each mutant and wt) and the m/z peaks showing $p < 0.01$ (without multiple testing correction) were selected.

In both negative- and positive-mode datasets, more significantly changed m/z peaks were identified in dm rather than in tm (which has an additional mutation in *PIP2;4* compared with dm) under each condition (Table 4). Consistent with the PCA result, most of significantly changed m/z peaks were condition-specific in each mutant (Figure 30). In contrast to condition-specific m/z peaks, m/z 338.0882 (negative mode) showed a significant change in dm independent of conditions (Figure 30a). In addition, some m/z peaks were detected in two conditions, either under C and H or C and DH, whereas no common m/z peaks under H and DH were observed. This was also consistent with the PCA result that more variances existed between H- and DH-treated *pip* mutants (separated by both component 1 and 2) than in other comparisons (Figure 29f).

Since dm and tm are highly related mutants, the m/z peaks significantly changed in both mutants were selected (with the ones derived from carbon isotopic peaks and satellite peaks deleted) for downstream analyses. Due to the small number of significantly changed m/z peaks identified in tm, less than ten peaks were commonly found in both *pip* mutants under each condition (Table 4). Again, these m/z peaks were related to a specific condition except for m/z 338.0882 and 575.1526 (Figure 31). In addition, intensity comparisons of significantly changed m/z peaks between *pip* mutants and wild type in original spectra illustrated the ANOVA results (Figure S8 and S9). The replicate-wise spectrum overlays demonstrated clear peak-intensity differences between different genetic backgrounds, which were not observed when the spectra of all genotypes and replicates were overlaid (Figure S8), indicating that inclusion of measurement order during ANOVA suppressed the negative effect of changing ionization efficiency on the identification of significantly changed metabolites (as discussed in 3.2.1).

To further elaborate the metabolic changes in *pip* mutants, conversion of the significantly changed m/z peaks into putative compounds is a crucial step. Twenty-one and 14 m/z peaks identified in both *pip* mutants in negative- and positive-mode datasets, respectively, were subjected to several public metabolite databases (see 4.2.15) to assign possible metabolite identities (mass error less than 1 ppm). Although only putative metabolite identities of the m/z

peaks can be obtained *via* the database search, this information provides important hints towards the real compounds corresponding to the m/z peaks.

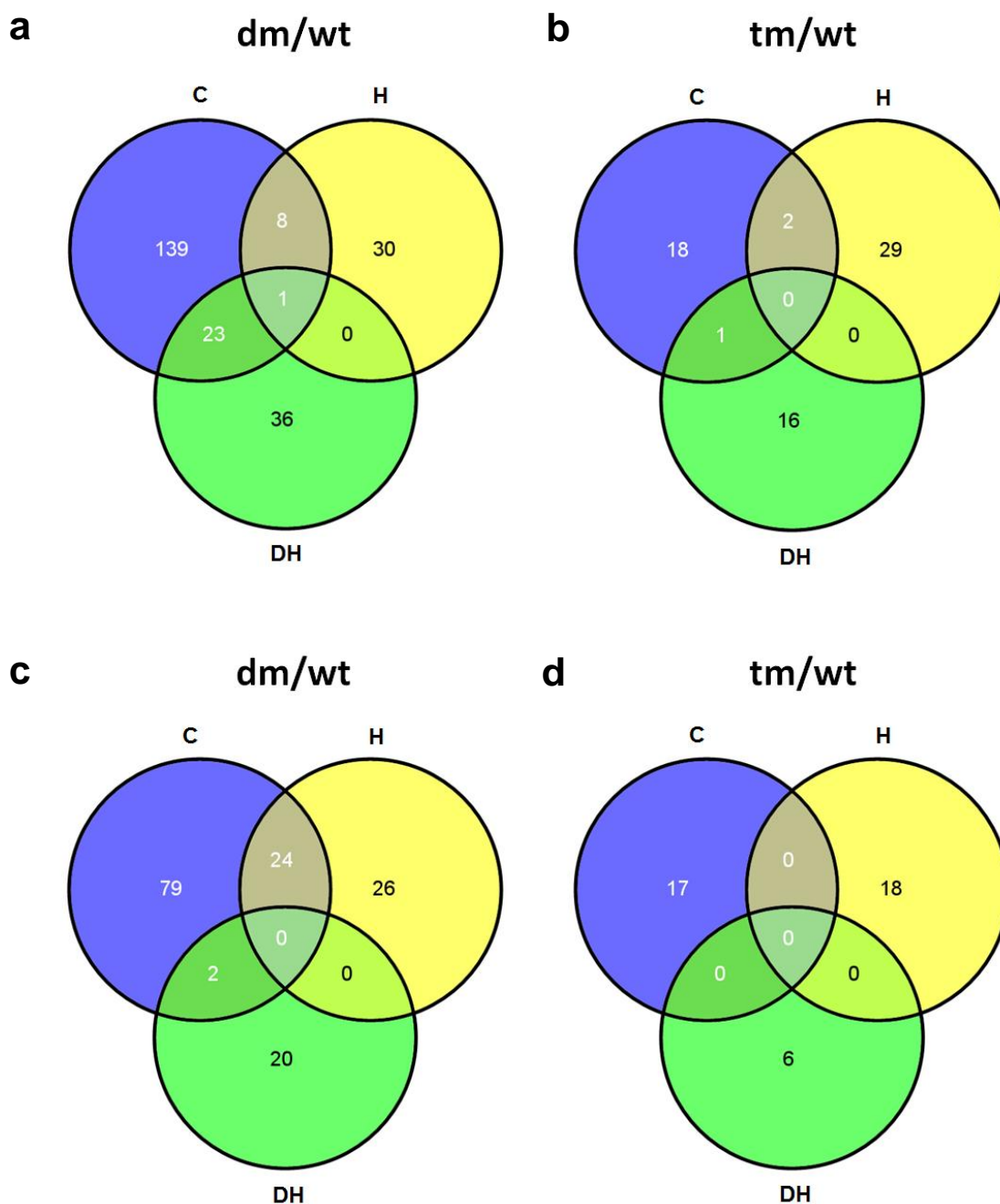


Figure 30 Most of the significantly changed m/z peaks identified in each *pip* mutant (dm or tm) in comparison with wild type (wt) are condition-specific. The Venn diagrams show the numbers of significantly changed m/z peaks specifically present in one condition and commonly detected in two or three conditions. (a, b) Negative-mode dataset. (c, d) Positive-mode dataset. C, H and DH are abbreviated the same as indicated in 3.1.2.

PIP AQUAPORINS – RESPONSES TO ALTERED ENVIRONMENTAL CUES

Table 4 Overview of the number of significantly changed m/z peaks ($p < 0.01$) identified in each *pip* mutant under each condition. The dataset for each ionization mode joining all samples from two independent experiments was used for ANOVA.

Condition	Mutant	Number of significantly changed m/z peaks					
		Negative mode			Positive mode		
Control (C)	dm	171	9	8*	105	9	7*
	tm	21			17		
Heat (H)	dm	39	13	9*	50	5	5*
	tm	31			18		
Drought+Heat (DH)	dm	60	11	6*	22	3	2*
	tm	17			6		

* The number of significantly changed m/z peaks after deletion of carbon isotopic peaks and satellite peaks.

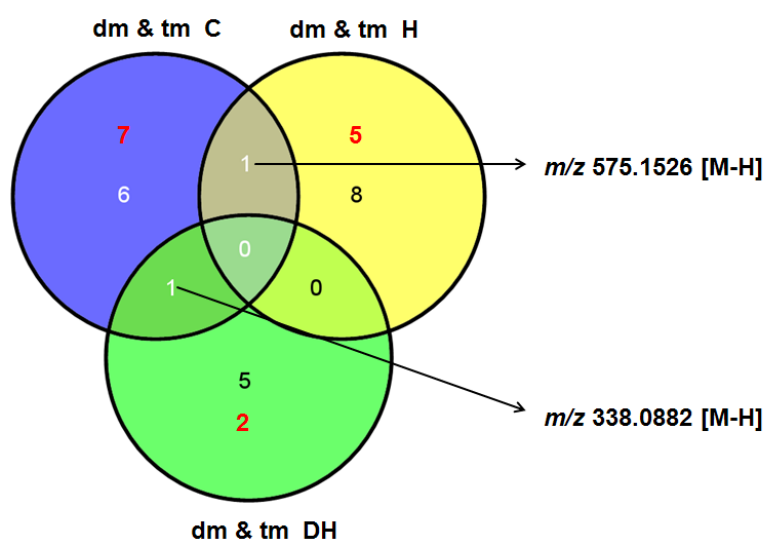


Figure 31 Most of the significantly changed m/z peaks identified in both *pip* mutants are condition-specific. The Venn diagram shows the number of significantly changed m/z peaks specifically present in one condition in negative-mode (number in white or black) and positive-mode (number in red) datasets. The numbers and m/z peaks commonly detected in two conditions are as indicated. C, H and DH are abbreviated the same as indicated in 3.1.2.

Based on the mass accuracy, 10 out of 35 m/z peaks were attributed to putative metabolites (Table 5). Among them, eight peaks (m/z 341.1089, 365.1055, 503.1617, 527.1581, 227.1289, 247.0646, 277.1659 and 338.0882) were found in *Arabidopsis*, whereas the remaining two peaks (m/z 202.0721 and 287.1101) were only identified in other plant species.

PIP AQUAPORINS – RESPONSES TO ALTERED ENVIRONMENTAL CUES

Table 5 The possible predictions of molecular formulas and metabolite identities of significantly changed *m/z* peaks ($p < 0.01$) identified in both *pip* mutants under each environmental condition from both metabolic profile datasets.

<i>m/z</i>	Formula [M]	Error (ppm)	Putative metabolite in plants	Pathway involved	Hits in ChemSpider
dm & tm under C					
<i>negative mode</i> [M-H]					
247.0646	C ₁₀ H ₁₆ O ₅ S	0.004	2-(5'-methylthio) pentylmalate in At ^a	glucosinolate biosynthesis	n.s. ^b
307.0857	C ₁₂ H ₂₀ O ₇ S	0.008	no		12
308.0389	C ₁₇ H ₁₁ NO ₃ S	0.06	no		82
459.1241	C ₂₃ H ₂₈ N ₂ O ₂ S ₃	0.03	no		12
	C ₂₃ H ₂₀ N ₆ O ₃ S	0.07	no		159
503.1617	C ₁₈ H ₃₂ O ₁₆	0.04	trisaccharides in At	carbohydrate metabolism	n.s.
663.2465	C ₂₄ H ₄₄ N ₂ O ₁₉	0.008			1
	C ₃₇ H ₃₆ N ₄ O ₈	0.07	no		12
<i>positive mode</i> [M+H/Na]					
277.1659	C ₁₄ H ₂₀ N ₄ O ₂	0.005	p-coumaroylagmatine in At	amino acid metabolism	n.s.
287.1101	C ₁₁ H ₂₀ O ₇	0.01	two possible metabolites in different plant species ^c		32
365.1055	C ₁₂ H ₂₂ O ₁₁	0.02	disaccharides in At	carbohydrate metabolism	n.s.
458.1397	C ₁₇ H ₂₁ N ₇ O ₇	0.04	no		3
527.1581	C ₁₈ H ₃₂ O ₁₆	0.02	trisaccharides in At	carbohydrate metabolism	n.s.
531.0922	C ₂₈ H ₁₈ O ₁₁	0.05	no		2
557.1551	C ₂₂ H ₂₈ N ₄ O ₁₁ S	0.07	no		3
dm & tm under H					
<i>negative mode</i> [M-H]					
341.1089	C ₁₂ H ₂₂ O ₁₁	0.01	disaccharides in At	carbohydrate metabolism	n.s.
383.0652	C ₁₅ H ₁₇ N ₂ O ₈ P	0.05	no		1
	C ₁₃ H ₂₀ O ₁₁ S	0.05	no		1
395.0830	C ₁₄ H ₂₀ O ₁₃	0.02	no		1
488.1621	C ₂₃ H ₂₃ N ₉ O ₂ S	0.03	no		3
	C ₃₀ H ₂₃ N ₃ O ₄	0.10	no		69

PIP AQUAPORINS – RESPONSES TO ALTERED ENVIRONMENTAL CUES

503.1978	C ₃₂ H ₂₈ N ₂ O ₄	0.04	no	154
511.1034	C ₂₉ H ₂₀ O ₉	0.007	no	2
512.1288	C ₂₈ H ₂₃ N ₃ O ₅ S	0.03	no	165
517.1940	C ₂₄ H ₃₀ N ₄ O ₉	0.002	no	18
————— <i>positive mode</i> [M+H/Na] —————				
381.0794	C ₁₅ H ₁₈ O ₁₀	0.03	no	9
506.1771	C ₂₃ H ₂₇ N ₃ O ₁₀	0.009	no	14
523.2097	C ₂₄ H ₃₂ N ₆ O ₄ S	0.06	no	51
525.1777	C ₂₄ H ₃₀ N ₄ O ₆ S	0.06	no	129
563.1454	C ₂₅ H ₂₂ N ₈ O ₆ S	0.02	no	1
dm & tm under C&H				
————— <i>negative mode</i> [M-H] —————				
575.1526	C ₂₇ H ₃₂ N ₂ O ₈ S ₂	0.03	no	3
dm & tm under DH				
————— <i>negative mode</i> [M-H] —————				
202.0721	C ₈ H ₁₃ NO ₅	0.002	7a-epiallexaflorine in <i>Alexa grandiflora</i>	188
227.1289	C ₁₂ H ₂₀ O ₄	0.09	traumatic acid in At	lipid metabolism n.s.
285.0187	C ₁₀ H ₁₀ N ₂ O ₆ S	0.006	no	34
330.0710	C ₁₉ H ₁₃ N ₃ OS	0.09	no	163
366.0685	C ₁₃ H ₂₁ NO ₇ S ₂	0.04	no	1
	C ₁₅ H ₁₈ N ₃ O ₄ PS	0.06		1
————— <i>positive mode</i> [M+H/Na] —————				
383.1187	C ₁₄ H ₁₆ N ₈ O ₄	0.05	no	13
453.1352	C ₁₆ H ₂₄ N ₂ O ₁₃	0.04	no	2
	C ₁₆ H ₂₆ N ₆ O ₄ S ₂	0.08		5
dm & tm under C&DH				
————— <i>negative mode</i> [M-H] —————				
338.0882	C ₁₅ H ₁₇ NO ₈	0.014	6-hydroxyindole-3- carboxylic acid 6- <i>O</i> -beta-D- glucopyranoside in At	n.s.

a) At is the abbreviation for *Arabidopsis thaliana*.

b) The possible chemical structure(s) of the *m/z* peaks that have been putatively identified in plants have not been searched (n.s.) in ChemSpider.

c) Iridoid in *Eccremocarpus scaber* and ilicifolinoside A in *Maytenus ilicifolia*.

For the remaining 25 m/z peaks that have no putative compounds assigned, the molecular formulas were generated (mass error less than 1 ppm) using the Data Analysis program (Bruker, Germany). One exact molecular formula could be generated for one m/z peak in most cases, whereas some m/z peaks (especially the ones in the higher mass range) corresponded to two possible elemental compositions (Table 5). Interestingly, 12 out of 25 m/z peaks contained sulfur in their molecular formulas. The possible chemical structure(s) of each m/z peak were obtained by searching individual formulas in the public database ChemSpider (<http://www.chemspider.com/>).

To analyze and better visualize the metabolic changes caused by *PIP* mutations under different conditions, hierarchical clustering was performed using all 35 m/z peaks. In general, two major clusters were generated, which were composed of m/z peaks significantly induced and reduced in *pip* mutants compared with the wild type, respectively (Figure 32 and Table S3).

The mutant-induced m/z peaks included putative soluble sugars and condition-specific sulfur-containing metabolites (Figure 32 and Table 5). m/z 341.1089 and 365.1055 from different ionization modes showed the same molecular formula $C_{12}H_{22}O_{11}$ and were predicted as a disaccharide; similarly, m/z 503.1617 and 527.1581 corresponded to a putative trisaccharide with the same formula $C_{18}H_{32}O_{16}$ (Table 5), suggesting that these m/z peaks most likely represent soluble sugars. Interestingly, two m/z peaks of putative disaccharide or trisaccharide detected in negative- and positive-ionization modes, respectively, were grouped together. These putative soluble sugars were accumulated in *pip* mutants under non-drought conditions. The induction of the putative trisaccharide was particularly observed under C. It remained under H, but to a lesser extent. In contrast, the *pip* mutants and wild type exhibited similar contents of the putative disaccharide and trisaccharide under DH. m/z 287.1101, 459.1241 (a sulfur-containing metabolite) and 663.2465, which were grouped together with two m/z peaks of the putative trisaccharide, also showed accumulation under C. m/z 287.1101 fits two possible molecular structures, corresponding to an iridoid in *Eccremocarpus scaber* and ilicifolinoside A (glucoside) in *Maytenus ilicifolia* (Garbarino and Nicoletti, 1989; Zhu *et al.*, 1998). m/z 523.2097 (a sulfur-containing metabolite) was highly and specifically induced under H, and accumulation of three sulfur-containing metabolites (m/z 285.0187, 330.0710 and 336.0685) were specifically observed under DH. In addition to sulfur-containing metabolites, the level of m/z 202.0721 was also high exclusively under DH. m/z 202.0721 ($C_8H_{13}NO_5$) could be a unique pyrrolizidine amino acid, 7a-epialexaflorine in *Alexa grandiflora* (Pereira *et al.*, 1991), or a N2-acetyl-L-aminoadipate as annotated in KEGG

(Kyoto Encyclopedia of Genes and Genomes). Although N2-acetyl-L-amino adipate has not been described in *Arabidopsis*, its related metabolite N2-acetyl-L-amino adipate semialdehyde ($C_8H_{13}NO_4$), which is involved in lysine metabolism, has been identified in *Arabidopsis*.

Among the reduced m/z peaks, the sulfur-containing metabolites m/z 247.0646, 307.0857, 308.0389, 512.1288, 557.1551 and 575.1526 were grouped together. They were repressed in *pip* mutants under non-drought conditions (Figure 32). m/z 247.0646 ($C_{10}H_{16}O_5S$) was predicted as a known sulfur-containing metabolite 2-(5'-methylthio) pentylmalate in *Arabidopsis*, which is involved in aliphatic glucosinolate biosynthesis. In addition, two peaks, m/z 227.1289 and 453.1352, were reduced specifically under DH. m/z 227.1289 ($C_{12}H_{20}O_4$) was identified as putative traumatic acid in *Arabidopsis*, an oxylipin derived from lipoxygenase (9-LOX and 13-LOX) cascade (Berger *et al.*, 2001; Feussner and Wasternack, 2002). Two other peaks, m/z 277.1659 and 338.0882, were diminished under both C and DH. The reduction of these peaks appeared to be independent of conditions when only dm was considered. Both m/z peaks were putatively identified in *Arabidopsis*. m/z 277.1659 ($C_{14}H_{20}N_4O_2$) was found to be a putative p-coumaroylagmatine (Matsuda *et al.*, 2009), which takes part in arginine and proline metabolism. m/z 338.0882 ($C_{15}H_{17}NO_8$) might be 6-hydroxyindole-3-carboxylic acid 6-*O*-beta-D-glucopyranoside, which has previously been identified to be induced by infection in both leaves and roots (Bednarek *et al.*, 2005).

Taken together, the changes of putative soluble sugars, sulfur-containing metabolites and some unknown peaks were associated with the loss of major PIP isoforms. They were significantly induced or reduced in a condition-specific manner. These altered metabolites could reflect the cellular regulations in response to different environmental conditions in the *pip* mutants which reduced the cellular water permeability.

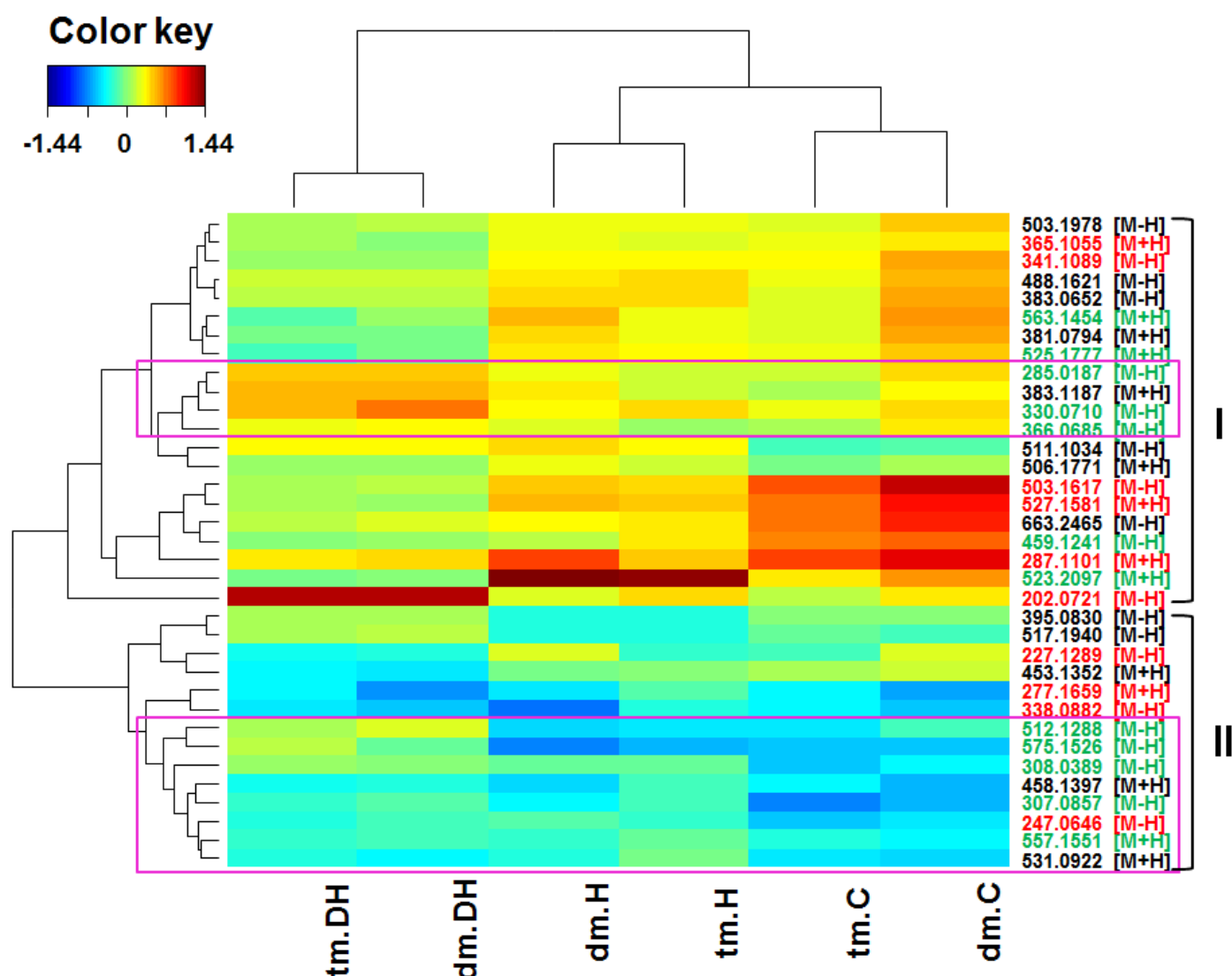


Figure 32 Clustered heat map of significantly changed m/z peaks identified in both *pip* mutants under at least one condition from both metabolic profile datasets by ANOVA (comparisons between mutants and wt under each condition; $p < 0.01$). Plotted values of these m/z peaks are \log_2 -transformed fold change. Two black brackets and Roman number I and II indicate two major clusters composed of the m/z peaks significantly induced and reduced in *pip* mutants compared with wild type, respectively. The m/z peaks in red are putatively known in *Arabidopsis* or other plant species, in green are sulfur-containing metabolites with unknown identities. Two pink frames indicate two main groups of sulfur-containing m/z peaks.

3.3 Discussion

3.3.1 Loss of major PIPs is associated with altered accumulation of putative osmoprotectants and glucosinolate biosynthesis

PIP aquaporins significantly contribute to plant water relations (Da Ines *et al.*, 2010; Javot *et al.*, 2003; Kaldenhoff *et al.*, 1998; Postaire *et al.*, 2010). The maintenance of water homeostasis upon challenging environmental conditions could require the regulation of PIP aquaporins. Heat, drought and their combination represent the climate change scenarios that most frequently occur. Many studies have addressed the regulations and functions of PIPs under drought stress (Alexandersson *et al.*, 2005; Kline *et al.*, 2010; Lee *et al.*, 2009; Martre *et al.*, 2002), however, their roles in response to heat and heat combined with drought remain elusive. To probe this, this study analyzed the altered metabolic responses in *pip* mutants (abundant and root-specific isoforms are affected) under these conditions. The transcriptomic and physiological changes in *pip* mutants are being analyzed by a colleague Ming Jin (Institute of Biochemical Plant Pathology, Helmholtz Zentrum München). Taking advantage of high mass accuracy of the FT-ICR-MS, a non-targeted approach was chosen to assess the metabolic changes in an unbiased manner. Possible metabolite identities of significantly changed m/z peaks related to *PIP* mutations and environmental conditions were unveiled. These results provided important information on PIPs' involvement in coping with the challenging conditions.

An important observation was that most of significantly changed m/z peaks identified in *pip* mutants were condition-specific (Figure 30 and 31). It suggested that the m/z peaks specifically changed under control condition are H/DH-responsive as *pip* mutants and wild type exhibited similar levels of these peaks under stress conditions; in parallel, the m/z peaks specifically changed under H or DH represent novel stress responses caused by the loss of major PIPs. Interestingly, six out of 13 m/z peaks, which were significantly changed under control condition in *pip* mutants in both negative- and positive-mode datasets, were indeed responsive to H in wt in the same manner as observed in *pip* mutants under control condition (Figure S10 and Table S4). For instance, the putative trisaccharide (m/z 503.1617 in the negative mode and m/z 527.1581 in the positive mode) that accumulated in *pip* mutants under control condition was induced by H in wt (Table S4), consistent with the previous observation that raffinose (one trisaccharide) is a heat-inducible metabolite (Kaplan *et al.*, 2004; Panikulangara *et al.*, 2004). Due to the difference in metabolite concentrations between DH-

treated and control samples, the m/z peaks in response to DH identified by ANOVA (comparisons between treatment and control) were not reliable. As a result, it could not be proven whether the remaining seven m/z peaks responded to DH. Nevertheless, the current results support the notion that m/z peaks specifically changed under control condition in *pip* mutants are stress-responsive.

The condition-specific metabolic changes caused by *PIP* mutations included the putative soluble sugars, sulfur-containing metabolites and some unknown m/z peaks. As mentioned above, the *pip* mutants accumulated putative disaccharide and trisaccharide under control condition (Figure 32), indicating that the cells' osmotic potential counters the reduction of membrane water permeability due to *PIP* mutations by enhancing the driving force of water movement into cells.

The putative N2-acetyl-L-aminoadipate (m/z 202.0721, $C_8H_{13}NO_5$), which was highly and specifically induced under DH in *pip* mutants (Figure 32), might function as an osmoprotectant precursor. N2-acetyl-L-aminoadipate is closely related to L-aminoadipate semialdehyde ($C_8H_{13}NO_4$), a metabolite known in *Arabidopsis*. A previous study has shown that osmotic stress induces the production of L-aminoadipate semialdehyde in *Brassica napus* and it could be further converted into L-aminoadipate ($C_8H_{13}NO_5$) and acetyl CoA. L-aminoadipate could behave as a precursor of pipecolic acid, an osmoprotectant in bacteria and is co-accumulated with proline in halophytic plants. Furthermore, the production of L-aminoadipate semialdehyde in *Brassica napus* is catalyzed by lysine-ketoglutarate reductase (LKR) and saccharopine dehydrogenase (SDH) (Moulin *et al.*, 2006). Interestingly, LKR and SDH are encoded by the same gene (AT4G33150) with variant splicing in *Arabidopsis*, and function similarly to these enzymes in *Brassica napus* (Zhu *et al.*, 2000). It is also known that the expression of AT4G33150 is induced by ABA (Fujita *et al.*, 2004), a central hormone responsive to drought stress. These evidences suggest that in *Arabidopsis* the putative N2-acetyl-L-aminoadipate may be involved in osmotic adjustment, like in *Brassica napus*. It has been shown that combination of drought and heat accumulates soluble sugars instead of proline as major osmoprotectant (Rizhsky *et al.*, 2004). *pip* mutants and wild-type plants exhibited similar sugar contents under DH (Figure 32). Accumulation of N2-acetyl-L-aminoadipate suggests that induction of carbohydrates is not sufficient, and an additional osmotic regulation strategy is required in *pip* mutants in response to DH.

Glucosinolate biosynthesis seemed to be inhibited as a consequence of *PIP* mutations. Thirteen out of 35 significantly changed m/z peaks were predicted as sulfur-containing metabolites (Table 5). The putative identities of these metabolites have not been described

except for m/z 247.0646 ($C_{10}H_{16}O_5S$). This m/z peak, which was reduced under control condition (Figure 32), was putatively involved in aliphatic glucosinolate biosynthesis in *Arabidopsis*. The downregulation of m/z 338.0882 (putative 6-hydroxyindole-3-carboxylic acid 6-*O*-beta-D-glucopyranoside) could be another piece of evidence supporting the assumption that glucosinolate biosynthesis was inhibited. Although not a sulfur-containing metabolite, 6-hydroxyindole-3-carboxylic acid 6-*O*-beta-D-glucopyranoside has been shown to accumulate in plants overexpressing genes that regulate the indolic glucosinolate biosynthetic pathways (Malitsky *et al.*, 2008), suggesting a correlation between production of this metabolite and glucosinolate biosynthesis. The reduction of m/z 338.0882 could therefore be indicative for the inhibition of glucosinolate biosynthesis. This inhibition seems to be independent of conditions in *pip* mutants since the reduction of m/z 338.0882 occurred under each condition (Figure 32).

The potentially reduced content of glucosinolates together with the accumulation of condition-specific sulfur-containing metabolites (i.e. m/z 459.1241 under C, m/z 523.2097 under H, m/z 285.0187, 330.0710 and 336.0685 under DH) (Figure 32) suggest the differential regulation of sulfur metabolism in *pip* mutants compared with wild type. It is known that the primary and secondary sulfur metabolism compete for the common substrate adenosine 5'-phosphosulfate (APS) (Chan *et al.*, 2012; Davidian and Kopriva, 2010; Kopriva, 2006; Mugford *et al.*, 2011; Mugford *et al.*, 2009). The wild-type plants represent a balance in sulfur partitioning between primary and secondary sulfur metabolism. Experimental evidences have shown that such a balance could be regulated by the oxidative stress, i.e. the primary sulfur metabolism is enhanced (accumulation of glutathione) while the secondary sulfur metabolism is inhibited (reduction of glucosinolates) (Mugford *et al.*, 2011; Mugford *et al.*, 2009; Ravilious *et al.*, 2012). Mutations in *PIPs* appear to disrupt the balance of primary and secondary sulfur metabolism under control condition as well as the regular sulfur-partitioning regulation under stress conditions.

The metabolic changes discussed in this study were observed in the double and triple *pip* mutants. It could be interesting to examine whether a single mutation (e.g. *pip2;1* or *pip2;2* single mutant) is sufficient to induce the metabolic changes, such as the accumulation of putative soluble sugars. With respect to the further identification of the metabolite identities, the annotation of significantly changed m/z peaks via the *in silico* routine (database search) should be further combined with experimental routines. On the one hand, a targeted metabolomics approach will be used to determine predefined group of metabolites. One limitation of the non-targeted FT-ICR-MS approach is that metabolites with the same mass

(e.g. isomers) cannot be distinguished. The putative trisaccharide, with the molecular formula $C_{18}H_{32}O_{16}$, could be raffinose, fructan or other polymers of monosaccharide molecules. An analysis of individual soluble sugars will help to identify which sugar molecule(s) contribute to the accumulation of trisaccharide(s) observed in *pip* mutants under control condition. On the other hand, fragmentation of significantly changed m/z peaks with unknown identities will help to identify their possible structures. This strategy has been successfully used to identify the substrate of UDP-dependent glucosyltransferase UGT76B1 in *Arabidopsis* (von Saint Paul *et al.*, 2011). Therefore, more hints of metabolite identities will be obtained through fragmentation, e.g. whether m/z 202.0721 corresponds to N2-acetyl-L-aminoadipate in *Arabidopsis* as predicted.

3.3.2 Heat stress in combination with high air humidity seems to trigger specific metabolic responses

Temperature increase lowers the relative air humidity if no water is added to the ambient atmosphere. As a consequence, plants suffer from not only heat stress, but also an additional drought stress from the ambient air. This scenario has been used in all studies on heat stress in plants (Bennett *et al.*, 2005; Kaplan *et al.*, 2004; Panikulangara *et al.*, 2004; Rizhsky *et al.*, 2004). In contrast, this study has taken the reduction of air humidity upon high temperature into account, analyzing the plants' responses to heat stress (33 °C) with increased, adjusted relative air humidity to maintain the same vapour pressure deficit (VPD) as observed at control temperature (22 °C). Investigation of the combination of high temperature and high air humidity is meaningful as this is an environmental condition frequently occurring in the summer of some regions, such as Southeast Asia.

To identify whether heat stress in combination with high air humidity (H) triggers differential metabolic responses, the metabolome data obtained in this study was compared with the published data on the metabolic changes induced by classical heat stress (without air-humidity adjustment) in *Arabidopsis*. Forty-three m/z peaks, which were significantly changed under H in wt (comparisons between H and C in wt *via* ANOVA, $p < 0.01$), have been identified in this study. The putative metabolite identities of nine m/z peaks were assigned in *Arabidopsis* and other plant species, and they appeared to be involved in diverse metabolic pathways, including carbohydrate metabolism, glucosinolate biosynthesis, flavonoid metabolism and monoterpene biosynthesis (Table S5). Previous studies have been shown that raffinose is induced and glucose 6-phosphate is reduced by the classical heat stress (Kaplan *et al.*, 2004;

Panikulangara *et al.*, 2004). The m/z peaks putatively corresponding to raffinose (m/z 503.1617 and 527.1581) and glucose 6-phosphate (m/z 259.0225) exhibited similar changes in response to H (Table S5). In addition, the accumulation of some glucosinolates and anthocyanins in response to classical heat stress has been reported (Bennett *et al.*, 2005). The induction of m/z 221.0491, which was predicted as a metabolite involved in glucosinolate biosynthesis (Table S5), suggests that H also upregulates the glucosinolate content. In addition, the reduced level of m/z 411.0688 gives a hint of anthocyanin accumulation (Table S5). This peak was predicted as two different flavonols in *Gutierrezia texana* and *Melicope triphylla*, respectively. Since flavonols and anthocyanins are derived from common precursors and their accumulations have been shown antagonistic in *Arabidopsis* (Gou *et al.*, 2011), the reduction of the putative flavonols (m/z 411.0688) could therefore be suggestive for the accumulation of anthocyanins. In contrast to the metabolites responsive to heat stress independent of the air humidity, the changes of some metabolites seem to be specific to each heat stress condition. Most of the m/z peaks showing significant changes under H have no putative metabolites identified in *Arabidopsis*, therefore, it is not clear whether these m/z peaks are altered exclusively under this heat stress condition. Nevertheless, they could be good candidates as metabolites differentially reacting to heat stress with different air humidity. The H-reduced putative syringin (m/z 395.1312, $C_{17}H_{24}O_9$) (Table S5), which has not been reported to respond to classical heat stress, could represent a specific change under H. In addition, the putative metabolites sucrose (m/z 341.1089 and 365.1055, $C_{12}H_{22}O_{11}$), glycerol 3-phosphate (m/z 171.0064, $C_3H_9O_6P$), ribonic acid (m/z 165.0405, $C_5H_{10}O_6$), citric acid (m/z 191.0197, $C_6H_8O_7$), quinic acid (m/z 191.0561, $C_7H_{12}O_6$) and galactonic acid (m/z 195.0510, $C_6H_{12}O_7$) are induced under classical heat stress (Kaplan *et al.*, 2004), but not changed under H (Table S6). In fact, the contents of some amino acids (e.g. alanine and valine) are also affected by classical heat stress (Kaplan *et al.*, 2004; Rizhsky *et al.*, 2004). However, the changes of amino acids cannot be compared because such small molecules are not detectable in FT-ICR-MS measurements (which detect masses ranging from m/z 148 to m/z 1999). Nevertheless, these data suggest that heat stress in combination with high air humidity appears to cause specific metabolic responses.

One should be aware that the published data on metabolic changes in response to classical heat stress were not fully comparable with the data obtained in this study as different temperatures and treatment durations were used and, more importantly, the metabolite identities of detected m/z peaks could be different from current predictions. The future study focusing on a direct comparison of metabolic responses to heat stress with different air

humidity using both targeted and non-targeted metabolomics approaches could overcome these problems and provide more insights into the plants' responses to the combinational conditions.

It has been demonstrated that the major *PIPs* are upregulated under classical heat stress (Rae *et al.*, 2011). A previous study has also shown that increased relative air humidity (45 % to 85 %) enhances the osmotic water permeability of isolated mesophyll protoplasts, suggesting the regulation of PIP aquaporins in response to high air humidity (Morillon and Chrispeels, 2001). Therefore, the role of major PIP isoforms in response to heat stress with different air humidity could be interesting to characterize.

3.3.3 Integration of metabolome and transcriptome data helps to better understand the metabolic responses caused by *PIP* mutations

In addition to analyses of altered responses in *pip* mutants under different conditions at the metabolome level, the transcriptome level has also been examined (done by Ming Jin from the Institute of Biochemical Plant Pathology, Helmholtz Zentrum München). Similar to the metabolic responses, the differential gene expressions are caused by both environmental conditions and loss of major PIP isoforms. In addition, the significantly up- and down-regulated genes in *pip* mutants under each condition have been identified. Currently, PIP-dependent changes determined using two experimental platforms are being integrated (by Theresa Faus-Kessler from the Institute of Developmental Genetics, Helmholtz Zentrum München). An important part of this integration is to cluster the significantly changed metabolites and genes, which show similar behaviours. This could lead to the confirmation of observed responses and, more importantly, the prediction of metabolite identities and gene functions. For example, the putatively accumulated trisaccharide grouping together with carbohydrate biosynthesis-related genes would confirm the changes in both datasets; a well-annotated gene showing similar behaviour to an unknown *m/z* peak would provide the possibility that this metabolite is highly associated with the gene function. The integration will therefore improve the information content of each single dataset, better understanding the altered cellular/molecular regulations upon the reduction of water permeability due to the loss of major PIPs.

4. MATERIALS AND METHODS

4.1 Materials

4.1.1 Plant materials

Insertion lines and wild-type plants used in this study are *Arabidopsis thaliana* ecotype Columbia (Col-0 or Col-4), except for *pip2;7*, which is ecotype Landsberg (*Ler*). Col-0 background *pip2;7* mutant was generated by backcross. Most of the seeds were obtained from the Nottingham *Arabidopsis* Stock Center (NASC) or from the *Arabidopsis* Biological Resource Center (ABRC, Ohio State University, USA). GABI lines were purchased from GABI-Kat (MPI, Köln, Germany). *arf7* seeds were provided by Professor Malcolm Bennett (University of Nottingham). Double or quadruple mutants were generated by crossing and verified by PCR-based genotyping at the DNA level and by RT-PCR at the RNA level. The single, double and multiple mutants used in this work are listed in Table 6 and 7. In addition, the seeds of *pip2;1-2* complementing with *proPIP2;1:PIP2;1-mCHERRY* construct were provided by Professor Christophe Maurel (CNRS Montpellier).

proPIP:GUS or *proPIP:GFP-GUS* constructs transformed plants (C24 or Col-0 ecotype), were used for expression studies. The expression pattern of each *PIP* gene during LR development was confirmed by observation of the same expression pattern in two transgenic lines (Table 8).

4.1.2 Media and solutions

Typical media, buffers and solutions were prepared according to common protocols used in molecular biology. The preparation of special media and solutions is described in the corresponding methods section below.

4.1.3 Restriction enzymes and modifying enzymes

The restriction enzymes and their buffers were purchased from New England Biolabs (Frankfurt, Germany) or MBI Fermentas Life Sciences (St. Leon-Rot, Germany). Other enzymes, including *Taq* DNA polymerase, high fidelity DNA polymerase, DNase, RNase A and H, Reverse Transcriptase SuperScript II were purchased from Amersham Pharmacia, MBI Fermentas, Gibco-BRL, Promega, Q-Biogene, Stratagene, Roche and Sigma.

MATERIALS AND METHODS

Table 6 Single mutants used in this work.

These mutants are derived from collections including AMAZE (ZIGIA project, MPI, Köln, Germany), JIC SM (Tissier *et al.*, 1999), GABI (Rosso *et al.*, 2003), SAIL (Sessions *et al.*, 2002), SALK (Alonso *et al.*, 2003), CSHL (Martienssen, 1998) and SK (Robinson *et al.*, 2009).

Mutant type	AGI code	Name	Line	Ecotype
<i>pip</i> mutant	AT3G61430	<i>pip1;1-1</i>	GABI_437b11	Col-0
	AT2G45960	<i>pip1;2-1</i>	SALK_145347	Col-0
		<i>pip1;2-2</i>	SALK_019794	Col-0
	AT3G53420	<i>pip2;1-1</i>	AMAZE_6AAS98	Col-0
		<i>pip2;1-2</i>	SM_3_35928	Col-0
	AT2G37170	<i>pip2;2-3</i>	SAIL_169A03	Col-0
		<i>pip2;2-4</i>	GABI_098D07	Col-0
	AT5G60660	<i>pip2;4-1</i>	SM_3_20853	Col-0
	AT4G35100	<i>pip2;7-1</i>	CSHL_GT19652	Ler*
	AT2G16850	<i>pip2;8-1</i>	SALK_099098	Col-0
		<i>pip2;8-2</i>	SK_16840	Col-4
Other mutant	AT5G20730	<i>arf7</i>	SALK_040394	Col-0

* Col-0 background *pip2;7* mutant, which was generated by backcross, was used in this work.

Table 7 Double and multiple mutants used in this work.

Mutant type	Name	Source	Generation
Double mutant	<i>arf7 pip2;1</i>	this work	<i>arf7</i> × <i>pip2;1-2</i>
	<i>pip1;1 pip2;4</i>	this work	<i>pip1;1-1</i> × <i>pip2;4-1</i>
	<i>pip1;2 pip2;7</i>	this work	<i>pip1;2-2</i> × <i>pip2;7-1</i>
	<i>pip2;1 pip2;2</i>	lab stock	—
Triple mutant	<i>pip2;1 pip2;2 pip2;4</i>	lab stock	—
Quadruple mutant	<i>pip1;2 pip2;1 pip2;2 pip2;7</i>	this work	<i>pip1;2-2 pip2;1-2 pip2;2-3*</i> × <i>pip2;7-1</i>

* Seeds were provided by Chen Liu (Institute of Biochemical Plant Pathology, Helmholtz Zentrum München).

MATERIALS AND METHODS

Table 8 *proPIP:GUS* and *proPIP:GFP-GUS* reporter lines.

<i>PIP</i> Gene	Independent line (lab name)	Ecotype	Source / Reference	Reporter
<i>PIP1;1</i>	1a-15a 1a-6			
<i>PIP1;2</i>	4 5			
<i>PIP2;1</i>	2a-3/2 2a-6a	C24	(Franck, 1999)	GUS
<i>PIP2;2</i>	26/3-1 26/1			
<i>PIP2;3</i>	4-1 7-1			
<i>PIP2;4</i>	1-1 2-1			
<i>PIP2;5</i>	8 28	Col-0	Dr. Ulrich Hammes (University of Regensburg)	
<i>PIP2;6</i>	4 5			GFP-GUS
<i>PIP2;7</i>	2 5	C24	(Da Ines, 2008)	
<i>PIP2;8</i>	2 4			

4.1.4 Bacterial strains

Species	Strain
<i>Escherichia coli</i>	DH 5α
<i>Agrobacterium tumefaciens</i>	GV3101 (pMP90)

4.1.5 Vectors

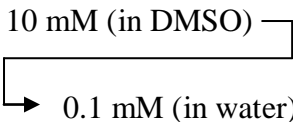
Name	Source / Reference
pGEM-T easy	Promega, Germany
pDONR221	Invitrogen, Germany
pBGW pKGW	(Karimi <i>et al.</i> , 2002)

4.1.6 Antibiotics

Name	Stock solution* (mg/ml)	Working concentration (µg/ml)	Source
Ampicillin	100 (in water)	100	Roche, Mannheim, Germany
Gentamicin	50 (in water)	25	
Rifampicin	50 (in methanol)	100	Sigma, Deisenhofen, Germany
Kanamycin	50 (in water)	50	
Spectinomycin	100 (in water)	100	

* All stock solutions were stored at -20 °C before use.

4.1.7 Plant hormones and hormone response inhibitor

Name*	Stock solution	Working concentration	Source
Kinetin	10 mM (in water)	0.5 µM	Serva, Heidelberg, Germany
PCIB	10 mM (in ethanol)	10 µM	VWR, Darmstadt, Germany
IAA	10 mM (in ethanol)	1 µM	Sigma, Deisenhofen, Germany
6-BA	10 mM (in DMSO) 	0.1 µM	
ACC	10 mM (in water)	0.1 µM	
BL	1 mM (in DMSO)	10 nM	
ABA	5 mM (in methanol)	0.1 µM	

* The chemical abbreviations are used (except for kinetin). PCIB, IAA, 6-BA, ACC, BL and ABA are the abbreviations for p-chlorophenoxy-isobutyric acid, indole-3-acetic acid, 6-benzylaminopurine, 1-aminocyclopropane-1-carboxylic-acid, brassinolide and abscisic acid, respectively.

4.2 Methods

4.2.1 Plant growth conditions

For plant growth, soil (Floragard) was mixed with silica sand in a ratio of 5:1 and poured into six-well packs. The soil-sand mixture was first wetted with water, and then seeds were placed on the surface of the soil with a toothpick and stratified for two days at 4 °C to synchronize germination before transfer into the plant chamber.

For hormone treatments and determination of the LRE phenotype, seeds were first surface-sterilized twice with 90 % (v/v) ethanol spread on a filter paper and dried under a sterile hood. After complete dryness, seeds were then sown on squared petri dishes (120 mm × 120 mm × 17 mm Greiner Bio-One Germany) containing 75 ml half-strength MS (Murashige and Skoog) medium. Plates were sealed with parafilm and kept for two days at 4 °C for stratification. After transfer into the plant chamber, plates were placed vertically to ensure roots grow along the medium.

Half-strength MS medium

2.2 g/l MS medium powder (M5519, Sigma)

0.5 % (w/v) Gelrite (Duchefa)

pH 5.8 adjusted with KOH

Arabidopsis thaliana plants grown on soil or MS medium in a growth chamber were under the following environmental parameters (or otherwise mentioned): 16 h light / 8 h dark cycle, 200 $\mu\text{E m}^{-2}\text{s}^{-1}$ light intensity, 22 °C temperature and 60 % relative humidity.

4.2.2 Hormone treatments

For expression analysis (qPCR), seven-day-old seedlings were transferred to vertical half-strength MS plates supplemented with 1 μM IAA for 0.5 h, 3 h, 6 h, 12 h, 18 h, 24 h and 36 h as indicated in Figure 5.

To investigate the effects of different hormones on the expression patterns of *proPIP:GUS* fusion lines during LR development, seven-day-old seedlings were transferred to half-strength MS plates supplemented with 1 μM IAA, 10 μM PCIB, 0.1 μM 6-benzylaminopurine, 0.5 μM kinetin, 0.1 μM ACC, 10 nM BL and 0.1 μM ABA and grown for 24 h or 48 h as indicated in Figure 10, 16 and 17. Seedlings transferred to normal MS plates were used as control.

4.2.3 qPCR (quantitative Polymerase Chain Reaction)

qPCR was performed to investigate the expression of *PIP* genes in response to exogenous auxin (1 μ M IAA) in Col-0 and *arf7* mutant backgrounds (done together with Benjamin Péret in the University of Nottingham). Total RNA and cDNA have already been prepared (by the colleague in the University of Nottingham). qPCR was performed in 384-well optical reaction plates using SYBR Green Sensimix (Quantace) on a Roche LightCycler 480 apparatus.

PCR program

95 °C	1 min	} 40 cycles
95 °C	5 s	
62 °C (annealing)	8 s	
72 °C	30 s	

Expression levels were normalized to the ubiquitin-associated gene *UBA* (AT1G04850). All qPCR experiments were performed in triplicate and the values represent means \pm sem (standard error of the mean) (Péret *et al.*, 2012).

4.2.4 Generation of double/quadruple mutants

4.2.4.1 Crossing

The double and quadruple mutants used for LRE phenotype analysis were generated by crossing the parent lines indicated in Table 7. Take *arf7 pip2;1* double mutant as an example. Two single mutant plants were grown under long light conditions until mature flowers were present. Two to three inflorescences from the *arf7* mutant were chosen, and mature siliques, open flowers with visible white petals and flower buds that were too small were removed. Three flower buds from each inflorescence normally remained and were used for crossing. To prepare the recipient flower (ovary), all flower parts except the pistil were carefully removed without touching the stigma. A mature flower was taken with forceps from a *pip2;1* plant, and anthers were dabbed onto the exposed stigma of the emasculated plant. This step was repeated at least twice to ensure the pollination. When several crosses were done in a row, forceps should be cleaned in between by dipping them in 95 % ethanol (v/v) followed by rinsing with distilled water. A successful cross was indicated by obvious elongation of stigma after 1-2 days to generate a silique.

4.2.4.2 Verification of homozygous double/quadruple mutants

4.2.4.2.1 PCR-based genotyping

To identify homozygous mutants at the genomic DNA level, PCR-based genotyping was employed in F₂ generation plants using Extract-N-AmpTM Plant PCR Kit (Sigma). A small piece of leaf was used for genomic DNA extraction according to the manufacturer's instructions. One cotyledon from a young seedling was also sufficient to isolate genomic DNA when the volume of extraction and dilution buffers was reduced to 25 µl. PCR reactions were performed immediately after genomic DNA extraction using a Multicycler PTC-200 (Biozym, Germany). Two reactions suffice to determine the genotype of one sample: one reaction amplifies a fragment of the target gene with primers flanking the putative insertion site in wild-type genomic DNA, whereas the other reaction uses a primer from the T-DNA insertion and one from the genomic DNA, respectively. The judgment of a plant genotype is based on the presence or absence of DNA fragments amplified by specific primer combinations (Figure 33). The plants showing the presence of only insertion band (like "Plant 2" in Figure 33) of each gene were selected as homozygous double or quadruple mutants.

	Plant 1	Plant 2	Plant 3
Genomic DNA primer 1 and 2	—		—
Genomic DNA primer 1 or 2 Insertion primer		—	—
	wild type	homozygous	heterozygous

Figure 33 Scheme for judgment of a plant genotype by PCR-based genotyping after electrophoresis.

4.2.4.2.2 Reverse Transcription Polymerase Chain Reaction (RT-PCR)

Further confirmation of the homozygous mutants at the RNA level was performed using RT-PCR. Total RNA was extracted using RNeasy Plant Mini Kit (Qiagen, Hilden, Germany). The leaf material was disrupted with a dismembrator (micro-dismembrator S; 2500 rpm, 1 min). 50-100 mg powder was used for RNA extraction according to the manufacturer's instructions. DNase treatment was performed on the column as recommended. One µg total RNA was reverse transcribed into cDNA using the SuperScript II First Strand synthesis system (Invitrogen) according to the manufacturer's instructions. For each sample, a negative RT reaction without reverse transcriptase (-RT) was prepared in parallel to control contaminations.

MATERIALS AND METHODS

with genomic DNA. To ensure RT was successful and examine whether genomic DNA was present in RNA samples, PCR reactions with *TUBULIN* primers were performed using a Multicycler PTC-200 (Biozym, Germany). A successful RNA isolation and cDNA synthesis yielded a positive band for the +RT reaction and no band in the -RT reaction. By using the cDNA samples without contamination, no amplification of target fragments in the mutants were observed. The seeds of these confirmed homozygous mutants were harvested and the seedlings were used for LRE phenotype analysis.

4.2.5 Complementation of *pip2;1* mutants

The mutant complementation was performed using GatewayTM cloning system (Invitrogen, Germany). A 4.6 kb genomic *PIP2;1* fragment was amplified by PCR using primers 5'- GGG GACAAGTTTGTACAAAAAAGCAGGCTGGAGTGACTAAAAAGGACAA -3' (forward) and 5'- GGGGACCACTTTGTACAAGAAAGCTGGGTTCGAGCATTTTCCTATATGATT -3' (reverse) with high fidelity DNA polymerase. This fragment was first cloned into the pDONR221 vector and transformed into *E. coli* (see 4.2.6). After verification by sequencing, the fragment was further recombined and cloned into pBGW and pKGW vectors and transformed into *Agrobacterium tumefaciens* (see 4.2.7). The *Agrobacterium tumefaciens*-mediated transformation into two alleles of *pip2;1* mutants was performed using floral dip (Clough and Bent, 1998). The *pip2;1* mutants were grown in big pots to the flowering stage. Siliques and open flowers were removed before transformation to increase the transformation rate. The inflorescences were dipped into the bacterial suspension for several seconds. Dipped plants were dried, covered with a transparent plastic bag to maintain humidity and kept in a low light condition for one day. After being returned to the growth chamber, plants continued growing until seed harvest.

The transformants were selected either on soil on the basis of BASTA resistance or *in vitro* on MS solid medium supplemented with Kanamycin. The BASTA/Kanamycin-resistant T1 generation plants were individually harvested and used for segregation in the next generation. The line showing 3 (resistant):1 (non-resistant) segregation ratio in T2 generation and no segregation (all resistant) in T3 generation was considered as a homozygous transformant with single insertion. Two to three independent homozygous transformants with single insertion of each allele were confirmed at mRNA level by RT-PCR (see 4.2.4.2.2). A restored *PIP2;1* expression in complementation samples was observed. The seeds of these successfully complemented lines were harvested and the seedlings were used for LRE phenotype analysis.

4.2.6 *E. coli* transformation and preparation of plasmid DNA

The genomic *PIP2;1* fragment was cloned into the pDONR221 vector and transformed into *E. coli*. An aliquot of competent *E. coli* cells was thawed on ice and mixed with 100-200 ng plasmid DNA. After incubation on ice for 30 min, the mixture in an Eppendorf tube was treated at 42 °C (water bath) for 30 sec, and immediately cooled on ice for 2 min. 500 µl of SOC medium was added, and then the sample was incubated at 37 °C for 30 min with agitation (1400 rpm). Transformed bacterial suspensions were centrifuged, resuspended with 50 µl SOC medium, and plated on selective LB solid medium.

Plasmid DNA from *E. coli* was extracted using the QIAprep Spin Miniprep Kit (Qiagen, Hilden, Germany) according to the manufacturer's instructions. After verification of the target fragment being correctly inserted by restriction digests, plasmid DNA was prepared for sequencing according to the manufacturer's instructions (plasmid DNA/water mixture 15 µl and 0.5 µl 10 µM primer) and processed by Eurofins MWG GmbH (Ebersberg, Germany).

4.2.7 *Agrobacterium* transformation

For plant transformation, the plasmid DNA (pBGW or pKGW vector with the *PIP2;1* fragment) was transformed into *Agrobacterium tumefaciens* by electroporation. An aliquot of competent *Agrobacterium tumefaciens* strain GV3101 containing a Ti plasmid (pMP90) was thawed on ice. Less than 50 ng of plasmid DNA was added and incubated for 2 min on ice. The mixture was then transferred into a dry, pre-chilled 0.2 cm cuvette for electroporation. Pulsing was done using the following conditions: resistance 400 Ω, capacitance 25 µF and voltage 2.5 kV, and the time constant should be larger than 9.1 (optimal would be 9.4 to 9.6) to give a relevant number of transformants. Immediately after the pulse, 1 ml of SOC medium was added into the cuvette and the suspension was transferred into a 1.5 ml Eppendorf tube. After incubation at 28 °C for 60-90 min (with gentle agitation), the bacterial cells were centrifuged and resuspended. A quarter of total cells was spread onto a selective LB solid medium (Rifampicin and Gentamicin for *agrobacteria* and appropriate antibiotics for the vectors) and incubated at 28 °C for two to three days. A single colony of *Agrobacterium tumefaciens* strain GV3101 carrying the *PIP2;1* genomic fragment was used to prepare a 2 ml preculture (28 °C, overnight). 1 ml of the preculture was then diluted 1:300 in selective LB medium on the next day (Rifampicin and Gentamicin for *agrobacteria* and an appropriate antibiotic for the vector). The *agrobacterial* cells were collected by centrifugation and then resuspended in a 5 % (w/v) sucrose solution to a final OD₆₀₀ of approximately 0.8.

4.2.8 Histochemical GUS assay

To study the expression pattern of individual *PIP* isoforms during LR development, in the stele and in response to different plant hormones, the histochemical localization of β -glucuronidase gene (GUS) was determined in transgenic plants expressing this reporter under the control of native *PIP* promoters (Deruère *et al.*, 1999). Treated or untreated seedlings were harvested and transferred to the fixation solution, vacuum-infiltrated for 10 times, and then incubated for 30 min at room temperature. Seedlings were washed three times with phosphate buffer (Na-phosphate, pH 7.0) and then the GUS-staining solution was added. After 10-times vacuum infiltration, seedlings were incubated for several minutes to overnight at 37 °C in the GUS-staining solution (depending on the expression level of corresponding *PIP* genes). Staining solution was replaced by 70 % (v/v) ethanol to terminate the reaction. Destaining was done by keeping seedlings in the ethanol at room temperature overnight or at 80 °C (water bath) for 10 min. The seedlings were then submerged and stored in fresh 70 % (v/v) ethanol at room temperature before microscopic pictures were taken.

Fixation solution

0.5 % Formaldehyde
0.05 % Triton X 100
50 mM Na-phosphate, pH7.0

GUS-staining solution

1 mM X-Gluc in DMSO
1 mM Potassiumhexacyanoferrat II
1 mM Potassiumhexacyanoferrat III
0.1 % Triton X 100
50 mM Na-phosphate, pH7.0

4.2.9 Vibratome sectioning

To observe the expression patterns of *PIPs* in the stele, GUS stained roots were cross-sectioned using a vibratome (Series 1000, Ted Pella). 5 % low melting agarose (Biozym Plaque GP Agarose) was prepared and kept in a water bath at 60 °C before use. The upper part of blue pipette tips was cut into approximately 0.5 cm segments, which were used for root embedment. 1-1.5 cm root segment was first cut from the whole root (lower cutting site positioned at 5 mm from the root tip), and further dissected into 2-2.5 mm segments. One minute after addition of agarose into a blue tip segment, one root segment was introduced to the middle position of semi-liquid agarose by a toothpick. The one minute interval was optimal for agarose to cool down a bit, avoiding the embedded root segment swimming to the agarose surface. The embedding blocks were then kept at 4 °C for at least one hour to fully

MATERIALS AND METHODS

strengthen the agarose. Before sectioning, the agarose block was taken out of the blue tip, cut into a trapeze shape. Importantly, the root segment to be sectioned should be vertical to the bottom of agarose block. The trapeze shaped agarose block was fixed to a petri dish with instant glue, and the petri dish afterwards was installed in the middle of sectioning station of the vibratome. The whole area of sectioning station was filled with ice-water mixture until it covered the front part of the razor blade. Section thickness was set to 30 μm . Moving speed of the razor blade was set to 7 and its amplitude to 4. After each cut, the section was gently caught by a small paint brush, and immediately transferred to a petri dish with cold water. When all sections from one agarose block were collected, they were mounted with water and observed under the microscope.

4.2.10 Application of gravitropic stimulus and sampling

For determination of LRE phenotype, three-day-old seedlings were given a gravitropic stimulus by turning the MS plates to 90° for 18 and 42 h pgi, respectively. Seedlings were harvested and cleared in the chloral hydrate solution for 24 h. Before microscopy, the bending site of each root should be mounted horizontally with the slide using 50 % glycerol to avoid the twisting of primordia, of which the following observation of developmental stages would be inaccurate.

Chloral hydrate solution

200 g chloral hydrate (Sigma)

25 ml glycerol

50 ml H₂O

4.2.11 Microscopy

The expression patterns of *proPIP:GUS* fusion lines during LR development and the hormone effects were observed with a Olympus BX61 microscope, and LR developmental stages at root bending sites in wild-type and *pip2;1* seedlings (Figure 4 and 14) were observed with a Leica DMRB microscope (University of Nottingham) using Differential Interference Contrast (DIC) setting. For examining the expression pattern of *PIP2;1* during LR development in the *proPIP2;1:PIP2;1-mCHERRY* complementing *pip2;1-2* mutant, confocal microscopy was performed using a Zeiss LSM 510 META microscope with a 40× water immersion objective. The emitted fluorescence signal was captured by alternately switching the 488 nm (autofluorescence) and 543 nm (mCHERRY) excitation lines.

4.2.12 SOM (self-organizing map) analysis

SOM analysis implemented in the “som” package of the statistical software R, which is suitable for clustering of expression data (Tamayo *et al.*, 1999), was performed for identification of genes correlated with the expression profile of *PIP2;8* during LR development from a time-course microarray dataset with 14 time-points (done by Dietrich Trümbach from the Institute of Developmental Genetics, Helmholtz Zentrum München). The x-, y-dimensions of the map were set to 8 and 2, respectively. A hexagonal topology of the grid was chosen with a Gaussian neighborhood function for the distance measure. To eliminate genes that did not change much across samples a variation filter was used. Genes were excluded with a fold change < 2 and an absolute expression difference < 50. Furthermore, only genes which have their maximum expression level not at the last time-point (42 h pgi) were considered. As a result, 224 genes were obtained and subjected to SOM analysis together with *PIP2;8*. The genes with similar expression profiles and expression levels along LR induction were grouped. The overlay graph and gene list of each cluster were obtained.

4.2.13 Metabolite extraction and FT-ICR-MS measurements

Pooled material from eight plants was ground with a dismembrator (micro-dismembrator S; 2500 rpm, 2.5 min), and 100 mg powder of each sample was used for metabolite extraction, which was performed as described previously (Weckwerth *et al.*, 2004) with slight modifications (Figure 34). Forty-four µg/ml loganin and 3 µg/ml nitrophenol were added to the extraction buffer 1 (methanol/chloroform/H₂O 2.5:1:1 v/v/v) as internal standards. Two ml pre-cooled extraction buffer 1 (-20 °C) was added to 100 mg plant material and mixed at 4 °C for 30 min. After centrifugation (10 min, 14000 rpm, 4 °C), 1 ml of the supernatant (supernatant A) was transferred into a fresh 2 ml Eppendorf tube and the remaining pellet was extracted in a second step with 1 ml pre-cooled (4 °C) extraction buffer 2 (methanol/chloroform 1:1 v/v). After a second centrifugation, 500 µl of the supernatant (supernatant B) were mixed with supernatant A. The chloroform phase was then separated from the water/methanol phase by addition of 250 µl of HPLC grade water (4 °C, Merck). The aqueous phase was divided into several 200 µl aliquots and dried completely using a Speed-Vac.

Measurements were performed in both negative and positive ionization modes. One dried aliquot of each sample was redissolved in 200 µl 70 % methanol and diluted 1:100 (or

MATERIALS AND METHODS

otherwise mentioned) in 70 % methanol containing 35 (for negative mode) or 100 (for positive mode) pmol/ml di-alanine. High-resolution mass spectra were acquired on a Bruker APEX Fourier transform ion cyclotron resonance mass spectrometer (FT-ICR-MS; Bruker, Germany) equipped with a 12 Tesla superconducting magnet and an Apollo II Electrospray ionization source. Sample measurement order of each independent experiment was organized as shown in Figure 35. In general, 45 samples from one independent experiment were sorted and measured according to the replicate order. Within each replicate, three genotypes under control condition were first determined, followed by DH- and H-treated samples. Extracts were introduced automatically into the electrospray source under control of an autosampling program. Spectra were externally calibrated based on arginine cluster ions (5 ppm). 385 (for negative mode) or 415 (for positive mode) scans were accumulated for each spectrum. Prior to the acquisition of the first sample, methanol was measured several times until its signal intensity of all peaks was lower than 1×10^7 after 20 scans.

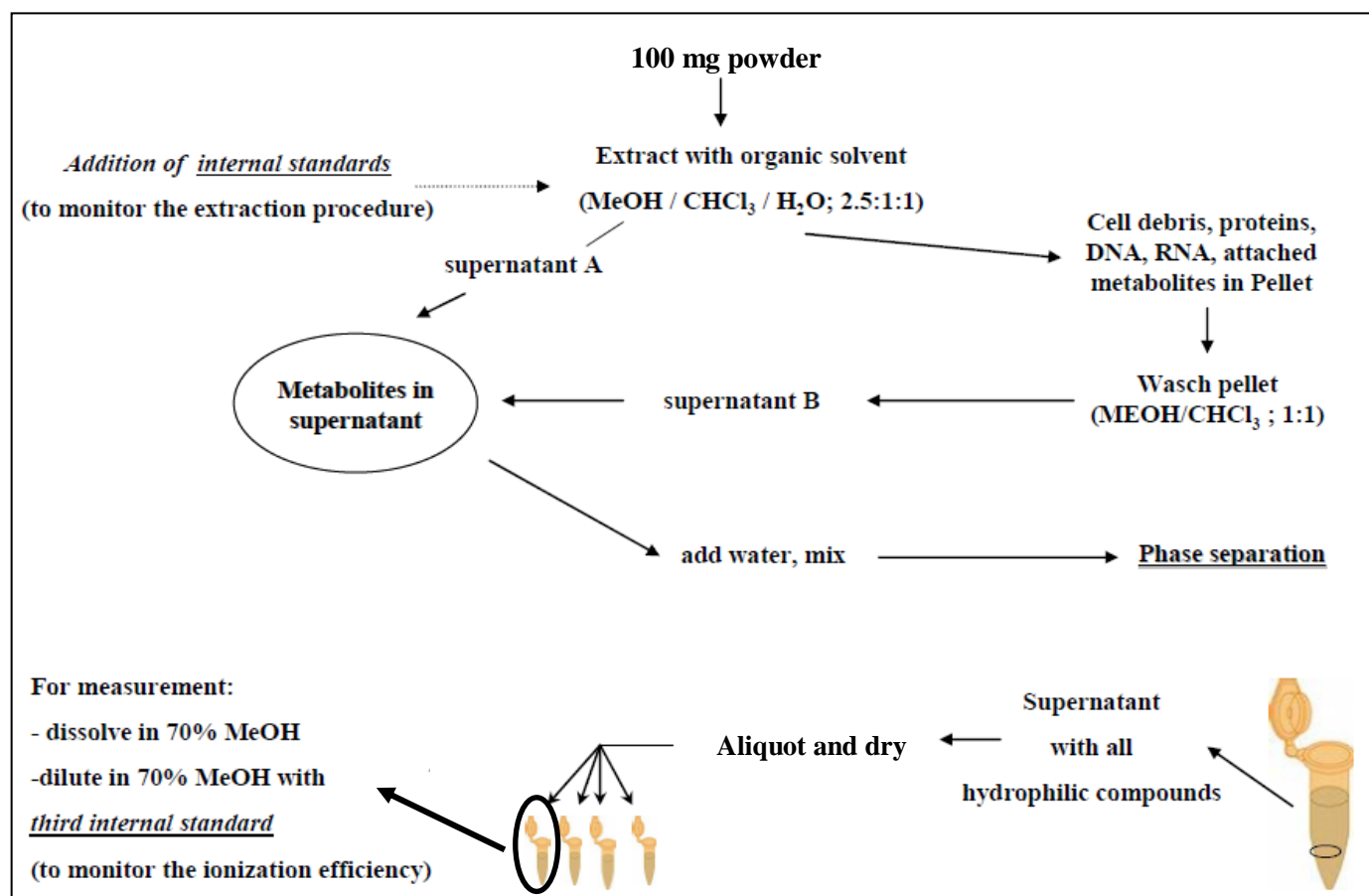


Figure 34 Work flow of metabolite extraction.

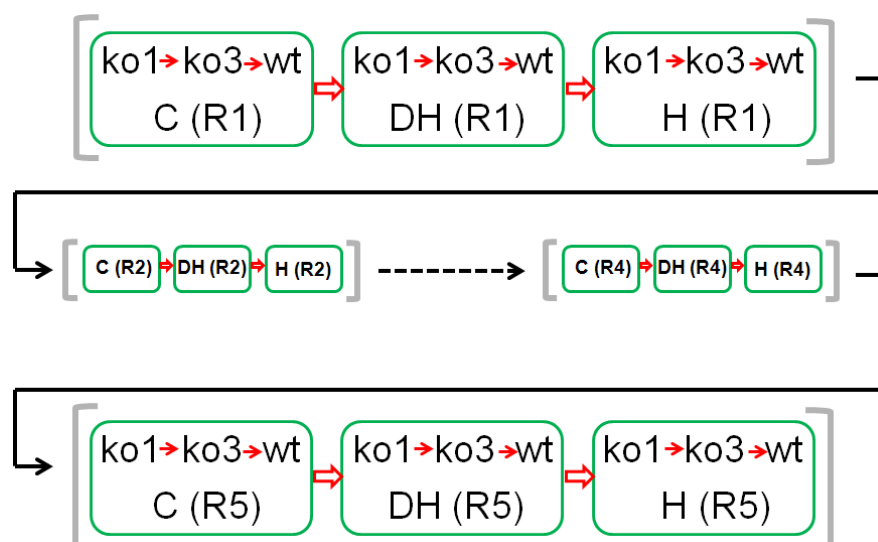


Figure 35 Arrangement of the sample measurement order in one independent experiment. Each bracket pair (in grey) contains all samples of each replicate. Within each replicate, three genotypes under control condition were first analyzed with the order as indicated, followed by DH- and H-treated samples. C, DH and H represent the same abbreviations as described in 3.1.2. R1-R5 indicate five replicates.

4.2.14 FT-ICR-MS data processing

The spectrum of each sample obtained from FT-ICR-MS measurement was calibrated using the Data Analysis program (Bruker, Germany). This internal mass calibration was performed using internal standards (loganin and di-alanine) in addition to endogenous plant metabolites with calibration accuracy smaller than 0.05 ppm (Table 9 and 10). Calibrated mass list of each sample was exported to an .asc file, which contains a m/z column and a peak-intensity column. The signal to noise ratio (S/N value) was set to 4, and mass precision was set to 4 decimal places. For each ionization mode, two spectra were problematic so that no mass lists could be extracted from these samples, therefore, 88 mass lists were obtained from two independent experiments.

The raw mass lists from each ionization mode were joined into a matrix using a custom-made program with a window width of 1 ppm (M. Frommberger, Helmholtz Zentrum München). Each matrix consisted of accurate masses of peaks and their peak intensity values obtained from each sample. Initial matrices, each of which combined all 88 samples, contained 184808 (for negative mode) and 162248 (for positive mode) m/z peaks, respectively. However, most of the m/z peaks were detected only in one or a few samples, but not in the remaining ones, in which zeroes were generated as missing values. These m/z peaks normally have no statistical

MATERIALS AND METHODS

significance. Thus, size reduction of matrices by deleting m/z peaks with many missing values was required. In detail, only m/z peaks, signals of which were detected in seven or more replicates in at least one group, were kept (in most cases, a group contained ten replicates, only two groups had nine replicates). This dramatically reduced the size of matrices, resulting in 2434 and 1430 m/z peaks for negative and positive modes, respectively. By using these final matrices, the quality control and statistical analyses (PCA and ANOVA) were performed in R (R-Development-Core-Team, 2009; R scripts were written by Theresa Faus-Kessler from the Institute of Developmental Genetics and the program was run by Veronica von Saint Paul from the Institute of Biochemical Plant Pathology, Helmholtz Zentrum München).

4.2.15 Assignment of possible metabolite identities

The putative metabolite identities of m/z peaks that were significantly changed in *pip* mutants in comparison with the wild type under each environmental condition were identified using following metabolite databases:

KNAPSAcK (<http://kanaya.naist.jp/KNAPSAcK/>)

PMN (Plant Metabolic Network) (<http://plantcyc.org/>)

KEGG (<http://www.genome.jp/kegg/ligand.html>)

METLIN (<http://metlin.scripps.edu/>)

For the significantly changed m/z peaks which are not present in the metabolite databases above, the putative molecular formulas were generated and then searched in the public database ChemSpider (<http://www.chemspider.com/>) to obtain the possible chemical structures.

Table 9 Mass list used for internal mass calibration of spectra measured in negative ionization mode.

Compound	Formula [M-H]	m/z [M-H]
Di-alanine	C ₆ H ₁₁ N ₂ O ₃ -	159.07752
Dehydroascorbate	C ₆ H ₅ O ₆ -	173.0091599
Ascorbate	C ₆ H ₇ O ₆ -	175.0248108
Glucose	C ₆ H ₁₁ O ₆ -	179.056114
2-Methylcitrate	C ₇ H ₉ O ₇ -	205.0353666
Hexadecanoic acid	C ₁₆ H ₃₁ O ₂ -	255.2329409
Octadecanoic acid	C ₁₈ H ₃₅ O ₂ -	283.2642483
SA-Glucoside	C ₁₃ H ₁₅ O ₈ -	299.077244

MATERIALS AND METHODS

Glutathione	C ₁₀ H ₁₆ N ₃ O ₆ S -	306.0765244
Di-alanine Clusterion	C ₁₂ H ₂₃ N ₄ O ₆ -	319.162308
Ascorbic acid glucoside	C ₁₂ H ₁₇ O ₁₁ -	337.077639
Sucrose	C ₁₂ H ₂₁ O ₁₁ -	341.108939
1- <i>O</i> -Sinapoyl-beta-D-glucose	C ₁₇ H ₂₁ O ₁₀ -	385.114024
Loganin	C ₁₇ H ₂₅ O ₁₀ -	389.145324
Glucoraphanin	C ₁₂ H ₂₂ NO ₁₀ S ₃ -	436.041135
Glucobrassicin	C ₁₆ H ₁₉ N ₂ O ₉ S ₂ -	447.053743
Neoglucobrassicin	C ₁₇ H ₂₁ N ₂ O ₁₀ S ₂ -	477.064308
Raffinose	C ₁₈ H ₃₁ O ₁₆ -	503.1618002
Kaempferol di-rhamnoside	C ₂₇ H ₂₉ O ₁₄ -	577.156284
Kaempferol glucoside-rhamnoside	C ₂₇ H ₂₉ O ₁₅ -	593.151199
Kaempferol di-glucoside-rhamnoside	C ₃₃ H ₃₉ O ₂₀ -	755.204024

Table10 Mass list used for internal mass calibration of spectra measured in positive ionization mode.

Compound	Formula [M+H/Na]	<i>m/z</i> [M+H/Na]
Di-alanine	C ₆ H ₁₃ N ₂ O ₃ +	161.092069
Arginine	C ₆ H ₁₅ N ₄ O ₂ +	175.118952
Coniferyl aldehyde	C ₁₀ H ₁₁ O ₃ +	179.07027
Glucose	C ₆ H ₁₂ O ₆ Na+	203.052609
2-Methylcitrate	C ₇ H ₁₀ O ₇ Na+	229.031874
Sinapyl alcohol	C ₁₁ H ₁₄ O ₄ Na+	233.07843
Slaframine	C ₁₂ H ₂₁ N ₂ O ₃ +	241.154669
3-Deoxy-D-manno-octulosonate	C ₈ H ₁₄ O ₈ Na+	261.058089
Kaempferol	C ₁₅ H ₁₀ O ₆ +	287.055015
Acetylmuramate	C ₁₁ H ₂₀ NO ₈ +	294.118343
Dibutyl phthalate	C ₁₆ H ₂₂ O ₄ Na+	301.14103
Myricetin	C ₁₅ H ₁₁ O ₈ +	319.044844
Di-alanine Clusterion	C ₁₂ H ₂₅ N ₄ O ₆ +	321.176861
Sucrose	C ₁₂ H ₂₂ O ₁₁ Na+	365.105433
Gibberellin A29	C ₂₀ H ₂₆ O ₅ Na+	369.167245
Gibberellin A34	C ₁₉ H ₂₄ O ₆ Na+	371.14651
Cortisone	C ₂₁ H ₂₈ O ₅ Na+	383.182895
Hydroxygibberellin 1	C ₁₉ H ₂₄ O ₇ Na+	387.141424
Loganin	C ₁₇ H ₂₆ O ₁₀ Na+	413.141818
Kaempferol di-rhamnoside	C ₂₇ H ₃₁ O ₁₄ +	579.170836
Kaempferol glucoside-rhamnoside	C ₂₇ H ₃₁ O ₁₅ +	595.165751
Kaempferol di-glucoside-rhamnoside	C ₃₃ H ₄₁ O ₂₀ +	757.218576

5. REFERENCES

- Alexandersson E, Danielson JA, Råde J, Moparathi VK, Fontes M, Kjellbom P, Johanson U.** Transcriptional regulation of aquaporins in accessions of *Arabidopsis* in response to drought stress. *Plant J.* (2010) 61(4):650-660.
- Alexandersson E, Frayse L, Sjövall-Larsen S, Gustavsson S, Fellert M, Karlsson M, Johanson U, Kjellbom P.** Whole gene family expression and drought stress regulation of aquaporins. *Plant Mol. Biol.* (2005) 59(3):469-484.
- Allan WL, Simpson JP, Clark SM, Shelp BJ.** γ -Hydroxybutyrate accumulation in *Arabidopsis* and tobacco plants is a general response to abiotic stress: putative regulation by redox balance and glyoxylate reductase isoforms. *J. Exp. Bot.* (2008) 59(9):2555-2564.
- Alonso JM, Stepanova AN, Leisse TJ, Kim CJ, Chen H, Shinn P, Stevenson DK, Zimmerman J, Barajas P, Cheuk R, Gadrinab C, Heller C, Jeske A, Koesema E, Meyers CC, Parker H, Prednis L, Ansari Y, Choy N, Deen H, Geralt M, Hazari N, Hom E, Karnes M, Mulholland C, Ndubaku R, Schmidt I, Guzman P, Aguilar-Henonin L, Schmid M, Weigel D, Carter DE, Marchand T, Risseuw E, Brogden D, Zeko A, Crosby WL, Berry CC, Ecker JR.** Genome-wide insertional mutagenesis of *Arabidopsis thaliana*. *Science* (2003) 301(5633):653-657.
- Bao F, Shen J, Brady SR, Muday GK, Asami T, Yang Z.** Brassinosteroids interact with auxin to promote lateral root development in *Arabidopsis*. *Plant Physiol.* (2004) 134(4):1624-1631.
- Bednarek P, Schneider B, Svatos A, Oldham NJ, Hahlbrock K.** Structural complexity, differential response to infection, and tissue specificity of indolic and phenylpropanoid secondary metabolism in *Arabidopsis* roots. *Plant Physiol.* (2005) 138(2):1058-1070.
- Beeckman T, Burssens S, Inzé D.** The peri-cell-cycle in *Arabidopsis*. *J. Exp. Bot.* (2001) 52(Spec Issue):403-411.
- Benková E, Michniewicz M, Sauer M, Teichmann T, Seifertová D, Jürgens G, Friml J.** Local, efflux-dependent auxin gradients as a common module for plant organ formation. *Cell* (2003) 115(5):591-602.
- Bennett RN, Wenke T, Freudenberg B, Mellon FA, Ludwig-Müller J.** The tu8 mutation of *Arabidopsis thaliana* encoding a heterochromatin protein 1 homolog causes defects in the induction of secondary metabolite biosynthesis. *Plant Biol. (Stuttg)* (2005) 7(4):348-357.
- Berger S, Weichert H, Porzel A, Wasternack C, Kühn H, Feussner I.** Enzymatic and non-enzymatic lipid peroxidation in leaf development. *Biochim. Biophys. Acta* (2001) 1533(3):266-276.
- Bhalerao RP, Eklöf J, Ljung K, Marchant A, Bennett M, Sandberg G.** Shoot-derived auxin is essential for early lateral root emergence in *Arabidopsis* seedlings. *Plant J.* (2002) 29(3):325-332.
- Biela A, Grote K, Otto B, Hoth S, Hedrich R, Kaldenhoff R.** The *Nicotiana tabacum* plasma membrane aquaporin NtAQP1 is mercury-insensitive and permeable for glycerol. *Plant J.* (1999) 18(5):565-570.
- Bienert GP, Møller AL, Kristiansen KA, Schulz A, Møller IM, Schjoerring JK, Jahn TP.** Specific aquaporins facilitate the diffusion of hydrogen peroxide across membranes. *J. Biol. Chem.* (2007) 282(2):1183-1192.

REFERENCES

- Bittner F, Oreb M, Mendel RR.** ABA3 is a molybdenum cofactor sulfurase required for activation of aldehyde oxidase and xanthine dehydrogenase in *Arabidopsis thaliana*. *J. Biol. Chem.* (2001) 276(44):40381-40384.
- Boursiac Y, Chen S, Luu DT, Sorieul M, van den Dries N, Maurel C.** Early effects of salinity on water transport in *Arabidopsis* roots. Molecular and cellular features of aquaporin expression. *Plant Physiol.* (2005) 139(2):790-805.
- Boursiac Y, Prak S, Boudet J, Postaire O, Luu DT, Tournaire-Roux C, Santoni V, Maurel C.** The response of *Arabidopsis* root water transport to a challenging environment implicates reactive oxygen species- and phosphorylation-dependent internalization of aquaporins. *Plant Signal Behav.* (2008) 3(12):1096-1098.
- Boyer J, Wu G.** Auxin increases the hydraulic conductivity of auxin-sensitive hypocotyl tissue. *Planta* (1978) 139(3):227-237.
- Boyer JS.** Plant productivity and environment. *Science* (1982) 218(4571):443-448.
- Boyer JS, Silk WK.** Hydraulics of plant growth. *Funct. Plant Biol.* (2004) 31(8):761-773.
- Brady SM, Zhang L, Megraw M, Martinez NJ, Jiang E, Yi CS, Liu W, Zeng A, Taylor-Teeples M, Kim D, Ahnert S, Ohler U, Ware D, Walhout AJ, Benfey PN.** A stele-enriched gene regulatory network in the *Arabidopsis* root. *Mol. Syst. Biol.* (2011) 7:459.
- Casimiro I, Beeckman T, Graham N, Bhalerao R, Zhang H, Casero P, Sandberg G, Bennett MJ.** Dissecting *Arabidopsis* lateral root development. *Trends Plant Sci.* (2003) 8(4):165-171.
- Casimiro I, Marchant A, Bhalerao RP, Beeckman T, Dhooge S, Swarup R, Graham N, Inzé D, Sandberg G, Casero PJ, Bennett M.** Auxin transport promotes *Arabidopsis* lateral root initiation. *Plant Cell* (2001) 13(4):843-852.
- Chan KX, Wirtz M, Phua SY, Estavillo GM, Pogson BJ.** Balancing metabolites in drought: the sulfur assimilation conundrum. *Trends Plant Sci.* (2013) 18(1):18-29.
- Clarkson DT, Carvajal M, Henzler T, Waterhouse RN, Smyth AJ, Cooke DT, Steudle E.** Root hydraulic conductance: diurnal aquaporin expression and the effects of nutrient stress. *J. Exp. Bot.* (2000) 51(342):61-70.
- Clough SJ, Bent AF.** Floral dip: a simplified method for *Agrobacterium*-mediated transformation of *Arabidopsis thaliana*. *Plant J.* (1998) 16(6):735-743.
- Cosgrove DJ.** Water uptake by growing cells: an assessment of the controlling roles of wall relaxation, solute uptake, and hydraulic conductance. *Int. J. Plant Sci.* (1993) 154(1):10-21.
- Da Ines O.** Functional analysis of PIP2 aquaporins in *Arabidopsis thaliana*. *Ludwig-Maximilians-Universität, München* (2008).
- Da Ines O, Graf W, Franck KI, Albert A, Winkler JB, Scherb H, Stichler W, Schäffner AR.** Kinetic analyses of plant water relocation using deuterium as tracer - reduced water flux of *Arabidopsis pip2* aquaporin knockout mutants. *Plant Biol. (Stuttg)* (2010) 12 Suppl 1:129-139.
- Daniels MJ, Chaumont F, Mirkov TE, Chrispeels MJ.** Characterization of a new vacuolar membrane aquaporin sensitive to mercury at a unique site. *Plant Cell* (1996) 8(4):587-599.
- Daniels MJ, Mirkov TE, Chrispeels MJ.** The plasma membrane of *Arabidopsis thaliana* contains a mercury-insensitive aquaporin that is a homolog of the tonoplast water channel protein TIP. *Plant Physiol.* (1994) 106(4):1325-1333.
- Davidian JC, Kopriva S.** Regulation of sulfate uptake and assimilation—the same or not the same? *Mol. Plant* (2010) 3(2):314-325.

REFERENCES

- De Smet I, Tetsumura T, De Rybel B, dit Frey NF, Laplaze L, Casimiro I, Swarup R, Naudts M, Vanneste S, Audenaert D, Inzé D, Bennett MJ, Beeckman T.** Auxin-dependent regulation of lateral root positioning in the basal meristem of *Arabidopsis*. *Development* (2007) 134(4):681-690.
- De Smet I, Vassileva V, De Rybel B, Levesque MP, Grunewald W, Van Damme D, Van Noorden G, Naudts M, Van Isterdael G, De Clercq R, Wang JY, Meuli N, Vanneste S, Friml J, Hilson P, Jürgens G, Ingram GC, Inzé D, Benfey PN, Beeckman T.** Receptor-like kinase ACR4 restricts formative cell divisions in the *Arabidopsis* root. *Science* (2008) 322(5901):594-597.
- De Smet I, Zhang H, Inzé D, Beeckman T.** A novel role for abscisic acid emerges from underground. *Trends Plant Sci.* (2006) 11(9):434-439.
- Deruère J, Jackson K, Garbers C, Söll D, Delong A.** The RCN1-encoded A subunit of protein phosphatase 2A increases phosphatase activity *in vivo*. *Plant J.* (1999) 20(4):389-399.
- Dharmasiri N, Dharmasiri S, Estelle M.** The F-box protein TIR1 is an auxin receptor. *Nature* (2005a) 435(7041):441-445.
- Dharmasiri N, Dharmasiri S, Weijers D, Lechner E, Yamada M, Hobbie L, Ehrismann JS, Jürgens G, Estelle M.** Plant development is regulated by a family of auxin receptor F box proteins. *Dev. Cell* (2005b) 9(1):109-119.
- DiDonato RJ, Arbuckle E, Buker S, Sheets J, Tobar J, Totong R, Grisafi P, Fink GR, Celenza JL.** *Arabidopsis* ALF4 encodes a nuclear localized protein required for lateral root formation. *Plant J.* (2004) 37(3):340-353.
- Ditengou FA, Teale WD, Kochersperger P, Flittner KA, Kneuper I, van der Graaff E, Nziengui H, Pinosa F, Li X, Nitschke R, Laux T, Palme K.** Mechanical induction of lateral root initiation in *Arabidopsis thaliana*. *Proc. Natl. Acad. Sci. U S A.* (2008) 105(48):18818-18823.
- Dubrovsky JG, Rost TL, Colón-Carmona A, Doerner P.** Early primordium morphogenesis during lateral root initiation in *Arabidopsis thaliana*. *Planta* (2001) 214(1):30-36.
- Feng ZH, Sun XD, Wang GC, Liu HL, Zhu J.** LBD29 regulates the cell cycle progression in response to auxin during lateral root formation in *Arabidopsis thaliana*. *Ann. Bot.* (2012) 110(1):1-10.
- Fernandez A, Drozdzecki A, Hoogewijs K, Nguyen A, Beeckman T, Madder A, Hilson P.** Transcriptional and functional classification of the GOLVEN/ROOT GROWTH FACTOR/CLE-like signaling peptides reveals their role in lateral root and hair formation. *Plant Physiol.* (2013) 161(2):954-970.
- Feussner I, Wasternack C.** The lipoxygenase pathway. *Annu. Rev. Plant Biol.* (2002) 53:275-297.
- Finkelstein RR, Somerville CR.** Three Classes of Abscisic Acid (ABA)-Insensitive Mutations of *Arabidopsis* Define Genes that Control Overlapping Subsets of ABA Responses. *Plant Physiol.* (1990) 94(3):1172-1179.
- Fortin MG, Morrison NA, Verma DP.** Nodulin-26, a peribacteroid membrane nodulin is expressed independently of the development of the peribacteroid compartment. *Nucleic Acids Res.* (1987) 15(2):813-824.
- Franck KI.** Untersuchungen zur Lokalisation, Genexpression und physiologischen Rolle der Plasmamembran-Aquaporine aus *Arabidopsis thaliana*. *Ludwig-Maximilians-Universität, München* (1999).
- Friml J, Vieten A, Sauer M, Weijers D, Schwarz H, Hamann T, Offringa R, Jürgens G.** Efflux-dependent auxin gradients establish the apical-basal axis of *Arabidopsis*. *Nature* (2003) 426(6963):147-153.

REFERENCES

- Fujita M, Fujita Y, Maruyama K, Seki M, Hiratsu K, Ohme-Takagi M, Tran LSP, Yamaguchi-Shinozaki K, Shinozaki K.** A dehydration-induced NAC protein, RD26, is involved in a novel ABA-dependent stress-signaling pathway. *Plant J.* (2004) 39(6):863-876.
- Fujiyoshi Y, Mitsuoka K, de Groot BL, Philippsen A, Grubmüller H, Agre P, Engel A.** Structure and function of water channels. *Curr. Opin. Struct. Biol.* (2002) 12(4):509-515.
- Fukaki H, Nakao Y, Okushima Y, Theologis A, Tasaka M.** Tissue-specific expression of stabilized SOLITARY-ROOT/IAA14 alters lateral root development in *Arabidopsis*. *Plant J.* (2005) 44(3):382-395.
- Fukaki H, Tameda S, Masuda H, Tasaka M.** Lateral root formation is blocked by a gain-of-function mutation in the SOLITARY-ROOT/IAA14 gene of *Arabidopsis*. *Plant J.* (2002) 29(2):153-168.
- Garbarino J, Nicoletti M.** Iridoids from endemic Chilean bignoniaceae. *Heterocycles* (1989) 28(2):697-702.
- Gerbeau P, Güçlü J, Ripoché P, Maurel C.** Aquaporin Nt-TIPa can account for the high permeability of tobacco cell vacuolar membrane to small neutral solutes. *Plant J.* (1999) 18(6):577-587.
- Goh T, Joi S, Mimura T, Fukaki H.** The establishment of asymmetry in *Arabidopsis* lateral root founder cells is regulated by LBD16/ASL18 and related LBD/ASL proteins. *Development* (2012) 139(5):883-893.
- Gomes D, Agasse A, Thiébaud P, Delrot S, Gerós H, Chaumont F.** Aquaporins are multifunctional water and solute transporters highly divergent in living organisms. *Biochim. Biophys. Acta* (2009) 1788(6):1213-1228.
- González-Guzmán M, Apostolova N, Bellés JM, Barrero JM, Piqueras P, Ponce MR, Micol JL, Serrano R, Rodríguez PL.** The short-chain alcohol dehydrogenase ABA2 catalyzes the conversion of xanthoxin to abscisic aldehyde. *Plant Cell* (2002) 14(8):1833-1846.
- Gou J, Strauss SH, Tsai CJ, Fang K, Chen Y, Jiang X, Busov VB.** Gibberellins regulate lateral root formation in *Populus* through interactions with auxin and other hormones. *Plant Cell* (2010) 22(3):623-639.
- Gou JY, Felippes FF, Liu CJ, Weigel D, Wang JW.** Negative regulation of anthocyanin biosynthesis in *Arabidopsis* by a miR156-targeted SPL transcription factor. *Plant Cell* (2011) 23(4):1512-1522.
- Gougeon RD, Lucio M, De Boel A, Frommberger M, Hertkorn N, Peyron D, Chassagne D, Feuillat F, Cayot P, Voilley A, Gebefügi I, Schmitt-Kopplin P.** Expressing Forest Origins in the Chemical Composition of Cooperage Oak Woods and Corresponding Wines by Using FTICR-MS. *Chemistry* (2009) 15(3):600-611.
- Greenham K, Santner A, Castillejo C, Mooney S, Sairanen I, Ljung K, Estelle M.** The AFB4 Auxin Receptor Is a Negative Regulator of Auxin Signaling in Seedlings. *Curr. Biol.* (2011) 21(6):520-525.
- Guilfoyle TJ, Hagen G.** Auxin response factors. *Curr. Opin. Plant Biol.* (2007) 10(5):453-460.
- Han J, Danell RM, Patel JR, Gumerov DR, Scarlett CO, Speir JP, Parker CE, Rusyn I, Zeisel S, Borchers CH.** Towards high-throughput metabolomics using ultrahigh-field Fourier transform ion cyclotron resonance mass spectrometry. *Metabolomics* (2008) 4(2):128-140.

REFERENCES

- Himanen K, Boucheron E, Vanneste S, de Almeida Engler J, Inzé D, Beeckman T.** Auxin-mediated cell cycle activation during early lateral root initiation. *Plant Cell* (2002) 14(10):2339-2351.
- Holm LM, Jahn TP, Møller AL, Schjoerring JK, Ferri D, Klaerke DA, Zeuthen T.** NH_3 and NH_4^+ permeability in aquaporin-expressing *Xenopus* oocytes. *Pflügers Arch.* (2005) 450(6):415-428.
- Hummel I, Pantin F, Sulpice R, Piques M, Rolland G, Dauzat M, Christophe A, Pervert M, Bouteillé M, Stitt M, Gibon Y, Muller B.** *Arabidopsis* plants acclimate to water deficit at low cost through changes of carbon usage: an integrated perspective using growth, metabolite, enzyme, and gene expression analysis. *Plant Physiol.* (2010) 154(1):357-372.
- Ishikawa F, Suga S, Uemura T, Sato MH, Maeshima M.** Novel type aquaporin SIPs are mainly localized to the ER membrane and show cell-specific expression in *Arabidopsis thaliana*. *FEBS Lett.* (2005) 579(25):5814-5820.
- Iuchi S, Kobayashi M, Taji T, Naramoto M, Seki M, Kato T, Tabata S, Kakubari Y, Yamaguchi-Shinozaki K, Shinozaki K.** Regulation of drought tolerance by gene manipulation of 9-cis-epoxycarotenoid dioxygenase, a key enzyme in abscisic acid biosynthesis in *Arabidopsis*. *Plant J.* (2001) 27(4):325-333.
- Ivanchenko MG, Muday GK, Dubrovsky JG.** Ethylene-auxin interactions regulate lateral root initiation and emergence in *Arabidopsis thaliana*. *Plant J.* (2008) 55(2):335-347.
- Jang JY, Kim DG, Kim YO, Kim JS, Kang H.** An expression analysis of a gene family encoding plasma membrane aquaporins in response to abiotic stresses in *Arabidopsis thaliana*. *Plant Mol. Biol.* (2004) 54(5):713-725.
- Javot H, Lauvergeat V, Santoni V, Martin-Laurent F, Güçlü J, Vinh J, Heyes J, Franck KI, Schäffner AR, Bouchez D, Maurel C.** Role of a single aquaporin isoform in root water uptake. *Plant Cell* (2003) 15(2):509-522.
- Johanson U, Karlsson M, Johansson I, Gustavsson S, Sjövall S, Fraysse L, Weig AR, Kjellbom P.** The complete set of genes encoding major intrinsic proteins in *Arabidopsis* provides a framework for a new nomenclature for major intrinsic proteins in plants. *Plant Physiol.* (2001) 126(4):1358-1369.
- Jung JS, Preston GM, Smith BL, Guggino WB, Agre P.** Molecular structure of the water channel through aquaporin CHIP. The hourglass model. *J. Biol. Chem.* (1994) 269(20):14648-14654.
- Kaldenhoff R, Grote K, Zhu JJ, Zimmermann U.** Significance of plasmalemma aquaporins for water-transport in *Arabidopsis thaliana*. *Plant J.* (1998) 14(1):121-128.
- Kammerloher W, Fischer U, Piechottka GP, Schäffner AR.** Water channels in the plant plasma membrane cloned by immunoselection from a mammalian expression system. *Plant J.* (1994) 6(2):187-199.
- Kang JY, Choi HI, Im MY, Kim SY.** *Arabidopsis* basic leucine zipper proteins that mediate stress-responsive abscisic acid signaling. *Plant Cell* (2002) 14(2):343-357.
- Kaplan F, Kopka J, Haskell DW, Zhao W, Schiller KC, Gatzke N, Sung DY, Guy CL.** Exploring the temperature-stress metabolome of *Arabidopsis*. *Plant Physiol.* (2004) 136(4):4159-4168.
- Karimi M, Inzé D, Depicker A.** GATEWAY vectors for *Agrobacterium*-mediated plant transformation. *Trends Plant Sci.* (2002) 7(5):193-195.
- Kepinski S, Leyser O.** The *Arabidopsis* F-box protein TIR1 is an auxin receptor. *Nature* (2005) 435(7041):446-451.

REFERENCES

- Kline KG, Barrett-Wilt GA, Sussman MR.** *In planta* changes in protein phosphorylation induced by the plant hormone abscisic acid. *Proc. Natl. Acad. Sci. U S A.* (2010) 107(36):15986-15991.
- Kopriva S.** Regulation of sulfate assimilation in *Arabidopsis* and beyond. *Ann. Bot.* (2006) 97(4):479-495.
- Koussevitzky S, Suzuki N, Huntington S, Armijo L, Sha W, Cortes D, Shulaev V, Mittler R.** Ascorbate peroxidase 1 plays a key role in the response of *Arabidopsis thaliana* to stress combination. *J. Biol. Chem.* (2008) 283(49):34197-34203.
- Kumpf RP, Shi CL, Larrieu A, Stø IM, Butenko MA, Péret B, Riiser ES, Bennett MJ, Aalen RB.** Floral organ abscission peptide IDA and its HAE/HSL2 receptors control cell separation during lateral root emergence. *Proc. Natl. Acad. Sci. U S A.* (2013) 110(13):5235-5240.
- Kurup S, Runions J, Köhler U, Laplace L, Hodge S, Haseloff J.** Marking cell lineages in living tissues. *Plant J.* (2005) 42(3):444-453.
- Laplace L, Benková E, Casimiro I, Maes L, Vanneste S, Swarup R, Weijers D, Calvo V, Parizot B, Herrera-Rodriguez MB, Offringa R, Graham N, Doumas P, Friml J, Bogusz D, Beeckman T, Bennett M.** Cytokinins act directly on lateral root founder cells to inhibit root initiation. *Plant Cell* (2007) 19(12):3889-3900.
- Laskowski M, Grieneisen VA, Hofhuis H, Hove CA, Hogeweg P, Marée AF, Scheres B.** Root system architecture from coupling cell shape to auxin transport. *PLoS Biol.* (2008) 6(12):e307.
- Lee HK, Cho SK, Son O, Xu Z, Hwang I, Kim WT.** Drought stress-induced Rma1H1, a RING membrane-anchor E3 ubiquitin ligase homolog, regulates aquaporin levels via ubiquitination in transgenic *Arabidopsis* plants. *Plant Cell* (2009) 21(2):622-641.
- Lee SH, Chung GC, Jang JY, Ahn SJ, Zwiazek JJ.** Overexpression of PIP2;5 aquaporin alleviates effects of low root temperature on cell hydraulic conductivity and growth in *Arabidopsis*. *Plant Physiol.* (2012) 159(1):479-488.
- Lei Z, Huhman DV, Sumner LW.** Mass spectrometry strategies in metabolomics. *J. Biol. Chem.* (2011) 286(29):25435-25442.
- Lin W-D, Liao Y-Y, Yang TJ, Pan C-Y, Buckhout TJ, Schmidt W.** Coexpression-based clustering of *Arabidopsis* root genes predicts functional modules in early phosphate deficiency signaling. *Plant Physiol.* (2011) 155(3):1383-1402.
- Liu FL, VanToai T, Moy LP, Bock G, Linford LD, Quackenbush J.** Global transcription profiling reveals comprehensive insights into hypoxic response in *Arabidopsis*. *Plant Physiol.* (2005) 137(3):1115-1129.
- Lucas M, Godin C, Jay-Allemand C, Laplace L.** Auxin fluxes in the root apex co-regulate gravitropism and lateral root initiation. *J. Exp. Bot.* (2008) 59(1):55-66.
- Ma JF, Tamai K, Yamaji N, Mitani N, Konishi S, Katsuhara M, Ishiguro M, Murata Y, Yano M.** A silicon transporter in rice. *Nature* (2006) 440(7084):688-691.
- Macková H, Hronková M, Dobrá J, Turecková V, Novák O, Lubovská Z, Motyka V, Haisel D, Hájek T, Prášil IT, Gaudinová A, Storchová H, Ge E, Werner T, Schmülling T, Vanková R.** Enhanced drought and heat stress tolerance of tobacco plants with ectopically enhanced cytokinin oxidase/dehydrogenase gene expression. *J. Exp. Bot.* (2013) 64(10):2805-2815.
- Malamy JE, Benfey PN.** Organization and cell differentiation in lateral roots of *Arabidopsis thaliana*. *Development* (1997) 124(1):33-44.
- Malitsky S, Blum E, Less H, Venger I, Elbaz M, Morin S, Eshed Y, Aharoni A.** The transcript and metabolite networks affected by the two clades of *Arabidopsis* glucosinolate biosynthesis regulators. *Plant Physiol.* (2008) 148(4):2021-2049.

REFERENCES

- Marin E, Nussaume L, Quesada A, Gonneau M, Sotta B, Hugueney P, Frey A, Marion-Poll A.** Molecular identification of zeaxanthin epoxidase of *Nicotiana plumbaginifolia*, a gene involved in abscisic acid biosynthesis and corresponding to the ABA locus of *Arabidopsis thaliana*. *EMBO J.* (1996) 15(10):2331-2342.
- Markakis MN, De Cnodder T, Lewandowski M, Simon D, Boron A, Balcerowicz D, Doubbo T, Taconnat L, Renou JP, Höfte H, Verbelen JP, Vissenberg K.** Identification of genes involved in the ACC-mediated control of root cell elongation in *Arabidopsis thaliana*. *BMC Plant Biol.* (2012) 12:208.
- Martienssen RA.** Functional genomics: probing plant gene function and expression with transposons. *Proc. Natl. Acad. Sci. U S A.* (1998) 95(5):2021-2026.
- Martínez-Ballesta MC, Aparicio F, Pallás V, Martínez V, Carvajal M.** Influence of saline stress on root hydraulic conductance and PIP expression in *Arabidopsis*. *J. Plant Physiol.* (2003) 160(6):689-697.
- Martinière A, Li X, Runions J, Lin J, Maurel C, Luu DT.** Salt stress triggers enhanced cycling of *Arabidopsis* root plasma-membrane aquaporins. *Plant Signal Behav.* (2012) 7(4):529-532.
- Martre P, Morillon R, Barrieu F, North GB, Nobel PS, Chrispeels MJ.** Plasma membrane aquaporins play a significant role during recovery from water deficit. *Plant Physiol.* (2002) 130(4):2101-2110.
- Matsuda F, Yonekura-Sakakibara K, Niida R, Kuromori T, Shinozaki K, Saito K.** MS/MS spectral tag-based annotation of non-targeted profile of plant secondary metabolites. *Plant J.* (2009) 57(3):555-577.
- Méndez-Bravo A, Raya-González J, Herrera-Estrella L, López-Bucio J.** Nitric oxide is involved in alkamide-induced lateral root development in *Arabidopsis*. *Plant Cell Physiol.* (2010) 51(10):1612-1626.
- Meng L, Buchanan BB, Feldman LJ, Luan S.** CLE-like (CLEL) peptides control the pattern of root growth and lateral root development in *Arabidopsis*. *Proc. Natl. Acad. Sci. U S A.* (2012) 109(5):1760-1765.
- Monneuse JM, Sugano M, Becue T, Santoni V, Hem S, Rossignol M.** Towards the profiling of the *Arabidopsis thaliana* plasma membrane transportome by targeted proteomics. *Proteomics* (2011) 11(9):1789-1797.
- Moon C, Preston GM, Griffin CA, Jabs EW, Agre P.** The human aquaporin-CHIP gene. Structure, organization, and chromosomal localization. *J. Biol. Chem.* (1993) 268(21):15772-15778.
- Morales D, Rodríguez P, Dell'Amico J, Nicolás E, Torrecillas A, Sánchez-Blanco MJ.** High-temperature preconditioning and thermal shock imposition affects water relations, gas exchange and root hydraulic conductivity in tomato. *Biol. Plantarum* (2003) 47(2):203-208.
- Morillon R, Chrispeels MJ.** The role of ABA and the transpiration stream in the regulation of the osmotic water permeability of leaf cells. *Proc. Natl. Acad. Sci. U S A.* (2001) 98(24):14138-14143.
- Moulin M, Deleu C, Larher F, Bouchereau A.** The lysine-ketoglutarate reductase-saccharopine dehydrogenase is involved in the osmo-induced synthesis of pipecolic acid in rapeseed leaf tissues. *Plant Physiol. Biochem.* (2006) 44(7):474-482.
- Mugford SG, Lee BR, Koprivova A, Matthewman C, Kopriva S.** Control of sulfur partitioning between primary and secondary metabolism. *Plant J.* (2011) 65(1):96-105.
- Mugford SG, Yoshimoto N, Reichelt M, Wirtz M, Hill L, Mugford ST, Nakazato Y, Noji M, Takahashi H, Kramell R, Gigolashvili T, Flügge UI, Wasternack C,**

REFERENCES

- Gershenzon J, Hell R, Saito K, Kopriva S.** Disruption of adenosine-5'-phosphosulfate kinase in *Arabidopsis* reduces levels of sulfated secondary metabolites. *Plant Cell* (2009) 21(3):910-927.
- Mustilli AC, Merlot S, Vavasseur A, Fenzi F, Giraudat J.** *Arabidopsis* OST1 protein kinase mediates the regulation of stomatal aperture by abscisic acid and acts upstream of reactive oxygen species production. *Plant Cell* (2002) 14(12):3089-3099.
- Nambara E, Marion-Poll A.** Absciscic acid biosynthesis and catabolism. *Annu. Rev. Plant Biol.* (2005) 56:165-185.
- Nieuwland J, Maughan S, Dewitte W, Scofield S, Sanz L, Murray JA.** The D-type cyclin CYCD4;1 modulates lateral root density in *Arabidopsis* by affecting the basal meristem region. *Proc. Natl. Acad. Sci. U S A.* (2009) 106(52):22528-22533.
- Okushima Y, Fukaki H, Onoda M, Theologis A, Tasaka M.** ARF7 and ARF19 regulate lateral root formation via direct activation of LBD/ASL genes in *Arabidopsis*. *Plant Cell* (2007) 19(1):118-130.
- Okushima Y, Overvoorde PJ, Arima K, Alonso JM, Chan A, Chang C, Ecker JR, Hughes B, Lui A, Nguyen D, Onodera C, Quach H, Smith A, Yu GX, Theologis A.** Functional genomic analysis of the AUXIN RESPONSE FACTOR gene family members in *Arabidopsis thaliana*: Unique and overlapping functions of ARF7 and ARF19. *Plant Cell* (2005) 17(2):444-463.
- Oparka KJ, Prior DA, Wright KM.** Symplastic communication between primary and developing lateral roots of *Arabidopsis thaliana*. *J. Exp. Bot.* (1995) 46(2):187-197.
- Overvoorde P, Fukaki H, Beeckman T.** Auxin control of root development. *Cold Spring Harb. Perspect. Biol.* (2010) 2(6):a001537.
- Panikulangara TJ, Eggers-Schumacher G, Wunderlich M, Stransky H, Schöffl F.** Galactinol synthase1. A novel heat shock factor target gene responsible for heat-induced synthesis of raffinose family oligosaccharides in *Arabidopsis*. *Plant Physiol.* (2004) 136(2):3148-3158.
- Pei ZM, Murata Y, Benning G, Thomine S, Klusener B, Allen GJ, Grill E, Schroeder JI.** Calcium channels activated by hydrogen peroxide mediate abscisic acid signaling in guard cells. *Nature* (2000) 406(6797):731-734.
- Pereira AdS, Kaplan M, Maia J, Gottlieb O, Nash R, Fleet G, Pearce L, Watkin D, Scofield A.** Isolation of 7a-epialexaflorine from leaves of *Alexia grandiflora* a unique pyrrolizidine amino acid with a carboxylic acid substituent at C-3. *Tetrahedron* (1991) 47(29):5637-5640.
- Péret B, De Rybel B, Casimiro I, Benková E, Swarup R, Laplace L, Beeckman T, Bennett MJ.** *Arabidopsis* lateral root development: an emerging story. *Trends Plant Sci.* (2009a) 14(7):399-408.
- Péret B, Larrieu A, Bennett MJ.** Lateral root emergence: a difficult birth. *J. Exp. Bot.* (2009b) 60(13):3637-3643.
- Péret B, Li G, Zhao J, Band LR, Voss U, Postaire O, Luu DT, Da Ines O, Casimiro I, Lucas M, Wells DM, Lazzerini L, Nacry P, King JR, Jensen OE, Schäffner AR, Maurel C, Bennett MJ.** Auxin regulates aquaporin function to facilitate lateral root emergence. *Nat. Cell Biol.* (2012) 14(10):991-998.
- Pérez-Torres CA, López-Bucio J, Cruz-Ramírez A, Ibarra-Laclette E, Dharmasiri S, Estelle M, Herrera-Estrella L.** Phosphate availability alters lateral root development in *Arabidopsis* by modulating auxin sensitivity via a mechanism involving the TIR1 auxin receptor. *Plant Cell* (2008) 20(12):3258-3272.
- Postaire O, Tournaire-Roux C, Grondin A, Boursiac Y, Morillon R, Schäffner AR, Maurel C.** A PIP1 Aquaporin Contributes to Hydrostatic Pressure-Induced Water

REFERENCES

- Transport in Both the Root and Rosette of *Arabidopsis*. *Plant Physiol.* (2010) 152(3):1418-1430.
- Prado K, Boursiac Y, Tournaire-Roux C, Monneuse JM, Postaire O, Da Ines O, Schäffner AR, Hem S, Santoni V, Maurel C.** Regulation of *Arabidopsis* Leaf Hydraulics Involves Light-Dependent Phosphorylation of Aquaporins in Veins. *Plant Cell* (2013) 25(3):1029-1039.
- Prak S, Hem S, Boudet J, Viennois G, Sommerer N, Rossignol M, Maurel C, Santoni V.** Multiple phosphorylations in the C-terminal tail of plant plasma membrane aquaporins: role in subcellular trafficking of AtPIP2;1 in response to salt stress. *Mol. Cell Proteomics* (2008) 7(6):1019-1030.
- Preston GM, Agre P.** Isolation of the cDNA for erythrocyte integral membrane protein of 28 kilodaltons: member of an ancient channel family. *Proc. Natl. Acad. Sci. U S A.* (1991) 88(24):11110-11114.
- Prosser IM, Massonneau A, Smyth AJ, Waterhouse RN, Forde BG, Clarkson DT.** Nitrate assimilation in the forage legume *Lotus japonicus* L. *Planta* (2006) 223(4):821-834.
- Quigley F, Rosenberg JM, Shachar-Hill Y, Bohnert HJ.** From genome to function: the *Arabidopsis* aquaporins. *Genome Biol.* (2002) 3(1):RESEARCH0001.
- Rae L, Lao NT, Kavanagh TA.** Regulation of multiple aquaporin genes in *Arabidopsis* by a pair of recently duplicated DREB transcription factors. *Planta* (2011) 234(3):429-444.
- Ravilious GE, Nguyen A, Francois JA, Jez JM.** Structural basis and evolution of redox regulation in plant adenosine-5'-phosphosulfate kinase. *Proc. Natl. Acad. Sci. U S A.* (2012) 109(1):309-314.
- Rivers RL, Dean RM, Chandy G, Hall JE, Roberts DM, Zeidel ML.** Functional analysis of nodulin 26, an aquaporin in soybean root nodule symbiosomes. *J. Biol. Chem.* (1997) 272(26):16256-16261.
- Rizhsky L, Liang HJ, Shuman J, Shulaev V, Davletova S, Mittler R.** When Defense pathways collide. The response of *Arabidopsis* to a combination of drought and heat stress. *Plant Physiol.* (2004) 134(4):1683-1696.
- Robinson SJ, Tang LH, Mooney BA, McKay SJ, Clarke WE, Links MG, Karcz S, Regan S, Wu YY, Gruber MY, Cui D, Yu M, Parkin IA.** An archived activation tagged population of *Arabidopsis thaliana* to facilitate forward genetics approaches. *BMC Plant Biol.* (2009) 9:101.
- Rosso MG, Li Y, Strizhov N, Reiss B, Dekker K, Weisshaar B.** An *Arabidopsis thaliana* T-DNA mutagenized population (GABI-Kat) for flanking sequence tag-based reverse genetics. *Plant Mol. Biol.* (2003) 53(1-2):247-259.
- Ruggiero B, Koiwa H, Manabe Y, Quist TM, Inan G, Saccardo F, Joly RJ, Hasegawa PM, Bressan RA, Maggio A.** Uncoupling the effects of abscisic acid on plant growth and water relations. Analysis of *sto1/nced3*, an abscisic acid-deficient but salt stress-tolerant mutant in *Arabidopsis*. *Plant Physiol.* (2004) 136(2):3134-3147.
- Ruyter-Spira C, Kohlen W, Charnikhova T, van Zeijl A, van Bezouwen L, de Ruijter N, Cardoso C, Lopez-Raez JA, Matusova R, Bours R, Verstappen F, Bouwmeester H.** Physiological effects of the synthetic strigolactone analog GR24 on root system architecture in *Arabidopsis*: another belowground role for strigolactones? *Plant Physiol.* (2011) 155(2):721-734.
- Seckmeyer G, Payer H-D.** A new sunlight simulator for ecological research on plants. *J. Photoch. Photobio. B* (1993) 21(2):175-181.

REFERENCES

- Seo M, Aoki H, Koiwai H, Kamiya Y, Nambara E, Koshiba T.** Comparative studies on the *Arabidopsis* aldehyde oxidase (AAO) gene family revealed a major role of AAO3 in ABA biosynthesis in seeds. *Plant Cell Physiol.* (2004) 45(11):1694-1703.
- Sessions A, Burke E, Presting G, Aux G, McElver J, Patton D, Dietrich B, Ho P, Bacwaden J, Ko C, Clarke JD, Cotton D, Bullis D, Snell J, Miguel T, Hutchison D, Kimmerly B, Mitzel T, Katagiri F, Glazebrook J, Law M, Goff SA.** A high-throughput *Arabidopsis* reverse genetics system. *Plant Cell* (2002) 14(12):2985-2994.
- Shatil-Cohen A, Attia Z, Moshelion M.** Bundle-sheath cell regulation of xylem-mesophyll water transport via aquaporins under drought stress: a target of xylem-borne ABA? *Plant J.* (2011) 67(1):72-80.
- Signarbieux C, Feller U.** Effects of an extended drought period on physiological properties of grassland species in the field. *J. Plant Res.* (2012) 125(2):251-261.
- Singh TN, Aspinall D, Paleg LG.** Proline accumulation and varietal adaptability to drought in barley: a potential metabolic measure of drought resistance. *Nat. New Biol.* (1972) 236(67):188-190.
- Sperdouli I, Moustakas M.** Interaction of proline, sugars, and anthocyanins during photosynthetic acclimation of *Arabidopsis thaliana* to drought stress. *J. Plant Physiol.* (2012) 169(6):577-585.
- Stenson AC, Marshall AG, Cooper WT.** Exact masses and chemical formulas of individual Suwannee River fulvic acids from ultrahigh resolution electrospray ionization Fourier transform ion cyclotron resonance mass spectra. *Anal. Chem.* (2003) 75(6):1275-1284.
- Steudle E.** The Cohesion-Tension Mechanism and the Acquisition of Water by Plant Roots. *Annu. Rev. Plant Physiol. Plant Mol. Biol.* (2001) 52:847-875.
- Sutka M, Li G, Boudet J, Boursiac Y, Doumas P, Maurel C.** Natural variation of root hydraulics in *Arabidopsis* grown in normal and salt-stressed conditions. *Plant Physiol.* (2011) 155(3):1264-1276.
- Swarup K, Benková E, Swarup R, Casimiro I, Péret B, Yang Y, Parry G, Nielsen E, De Smet I, Vanneste S, Levesque MP, Carrier D, James N, Calvo V, Ljung K, Kramer E, Roberts R, Graham N, Marillonnet S, Patel K, Jones JD, Taylor CG, Schachtman DP, May S, Sandberg G, Benfey P, Friml J, Kerr I, Beeckman T, Laplace L, Bennett MJ.** The auxin influx carrier LAX3 promotes lateral root emergence. *Nat. Cell Biol.* (2008) 10(8):946-954.
- Takano J, Wada M, Ludewig U, Schaaf G, von Wirén N, Fujiwara T.** The *Arabidopsis* major intrinsic protein NIP5;1 is essential for efficient boron uptake and plant development under boron limitation. *Plant Cell* (2006) 18(6):1498-1509.
- Takei K, Ueda N, Aoki K, Kuromori T, Hirayama T, Shinozaki K, Yamaya T, Sakakibara H.** AtIPT3 is a key determinant of nitrate-dependent cytokinin biosynthesis in *Arabidopsis*. *Plant Cell Physiol.* (2004) 45(8):1053-1062.
- Tamayo P, Slonim D, Mesirov J, Zhu Q, Kitareewan S, Dmitrovsky E, Lander ES, Golub TR.** Interpreting patterns of gene expression with self-organizing maps: methods and application to hematopoietic differentiation. *Proc. Natl. Acad. Sci. U S A.* (1999) 96(6):2907-2912.
- Tan BC, Joseph LM, Deng WT, Liu L, Li QB, Cline K, McCarty DR.** Molecular characterization of the *Arabidopsis* 9-cis epoxycarotenoid dioxygenase gene family. *Plant J.* (2003) 35(1):44-56.
- Tan X, Calderon-Villalobos LI, Sharon M, Zheng C, Robinson CV, Estelle M, Zheng N.** Mechanism of auxin perception by the TIR1 ubiquitin ligase. *Nature* (2007) 446(7136):640-645.

REFERENCES

- Thiel S, Döhning T, Köfferlein M, Kosak A, Martin P, Seidlitz HK.** A phytotron for plant stress research: how far can artificial lighting compare to natural sunlight? *J. Plant Physiol.* (1996) 148(3):456-463.
- Tian QY, Sun P, Zhang WH.** Ethylene is involved in nitrate-dependent root growth and branching in *Arabidopsis thaliana*. *New Phytol.* (2009) 184(4):918-931.
- Tissier AF, Marillonnet S, Klimyuk V, Patel K, Torres MA, Murphy G, Jones JD.** Multiple independent defective suppressor-mutator transposon insertions in *Arabidopsis*: a tool for functional genomics. *Plant Cell* (1999) 11(10):1841-1852.
- Tiwari SB, Hagen G, Guilfoyle T.** The roles of auxin response factor domains in auxin-responsive transcription. *Plant Cell* (2003) 15(2):533-543.
- Törnroth-Horsefield S, Wang Y, Hedfalk K, Johanson U, Karlsson M, Tajkhorshid E, Neutze R, Kjellbom P.** Structural mechanism of plant aquaporin gating. *Nature* (2006) 439(7077):688-694.
- Tournaire-Roux C, Sutka M, Javot H, Gout E, Gerbeau P, Luu DT, Bligny R, Maurel C.** Cytosolic pH regulates root water transport during anoxic stress through gating of aquaporins. *Nature* (2003) 425(6956):393-397.
- Tziotis D, Hertkorn N, Schmitt-Kopplin P.** Kendrick-analogous network visualisation of ion cyclotron resonance Fourier transform mass spectra: improved options for the assignment of elemental compositions and the classification of organic molecular complexity. *Eur. J. Mass Spectrom (Chichester, Eng).* (2011) 17(4):415-421.
- Uehlein N, Lovisolo C, Siefritz F, Kaldenhoff R.** The tobacco aquaporin NtAQP1 is a membrane CO₂ pore with physiological functions. *Nature* (2003) 425(6959):734-737.
- Urano K, Maruyama K, Ogata Y, Morishita Y, Takeda M, Sakurai N, Suzuki H, Saito K, Shibata D, Kobayashi M, Yamaguchi-Shinozaki K, Shinozaki K.** Characterization of the ABA-regulated global responses to dehydration in *Arabidopsis* by metabolomics. *Plant J.* (2009) 57(6):1065-1078.
- Vander Willigen C, Postaire O, Tournaire-Roux C, Boursiac Y, Maurel C.** Expression and inhibition of aquaporins in germinating *Arabidopsis* seeds. *Plant Cell Physiol.* (2006) 47(9):1241-1250.
- von Saint Paul V, Zhang W, Kanawati B, Geist B, Faus-Keßler T, Schmitt-Kopplin P, Schäffner AR.** The *Arabidopsis* glucosyltransferase UGT76B1 conjugates isoleucic acid and modulates plant defense and senescence. *Plant Cell* (2011) 23(11):4124-4145.
- Walch-Liu P, Ivanov II, Filleur S, Gan YB, Remans T, Forde BG.** Nitrogen regulation of root branching. *Ann. Bot.* (2006) 97(5):875-881.
- Wallace IS, Choi WG, Roberts DM.** The structure, function and regulation of the nodulin 26-like intrinsic protein family of plant aquaglyceroporins. *Biochim. Biophys. Acta* (2006) 1758(8):1165-1175.
- Wang W, Zhou H, Lin H, Roy S, Shaler TA, Hill LR, Norton S, Kumar P, Anderle M, Becker CH.** Quantification of proteins and metabolites by mass spectrometry without isotopic labeling or spiked standards. *Anal. Chem.* (2003) 75(18):4818-4826.
- Wang YH, Garvin DF, Kochian LV.** Nitrate-induced genes in tomato roots. Array analysis reveals novel genes that may play a role in nitrogen nutrition. *Plant Physiol.* (2001) 127(1):345-359.
- Wasilewska A, Vlad F, Sirichandra C, Redko Y, Jammes F, Valon C, Frei dit Frey N, Leung J.** An update on abscisic acid signaling in plants and more. *Mol. Plant* (2008) 1(2):198-217.

REFERENCES

- Weckwerth W, Wenzel K, Fiehn O.** Process for the integrated extraction, identification and quantification of metabolites, proteins and RNA to reveal their co-regulation in biochemical networks. *Proteomics* (2004) 4(1):78-83.
- Weig A, Deswarte C, Chrispeels MJ.** The major intrinsic protein family of *Arabidopsis* has 23 members that form three distinct groups with functional aquaporins in each group. *Plant Physiol.* (1997) 114(4):1347-1357.
- Wilmoth JC, Wang S, Tiwari SB, Joshi AD, Hagen G, Guilfoyle TJ, Alonso JM, Ecker JR, Reed JW.** NPH4/ARF7 and ARF19 promote leaf expansion and auxin-induced lateral root formation. *Plant J.* (2005) 43(1):118-130.
- Wu G, Lewis DR, Spalding EP.** Mutations in *Arabidopsis* multidrug resistance-like ABC transporters separate the roles of acropetal and basipetal auxin transport in lateral root development. *Plant Cell* (2007) 19(6):1826-1837.
- Zhang WH, Tyerman SD.** Inhibition of water channels by HgCl₂ in intact wheat root cells. *Plant Physiol.* (1999) 120(3):849-858.
- Zhu N, Sharapin N, Zhang J.** Three glucosides from *Maytenus ilicifolia*. *Phytochemistry* (1998) 47(2):265-268.
- Zhu X, Tang G, Galili G.** Characterization of the two saccharopine dehydrogenase isozymes of lysine catabolism encoded by the single composite AtLKR/SDH locus of *Arabidopsis*. *Plant Physiol.* (2000) 124(3):1363-1372.

6. SUPPLEMENTARY MATERIALS

6.1 Regulation of PIP aquaporins is required to facilitate lateral root emergence

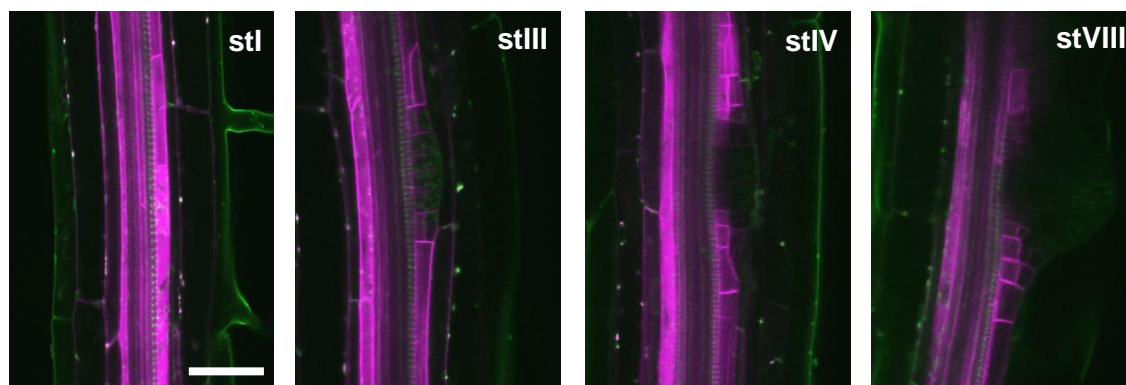


Figure S1 Expression pattern of PIP2;1 during LR development determined with the translational *proPIP2;1:PIP2;1-mCHERRY* construct complementing *pip2;1* mutant. The LR developmental stages are as indicated. Scale bar represents 50 μ m.

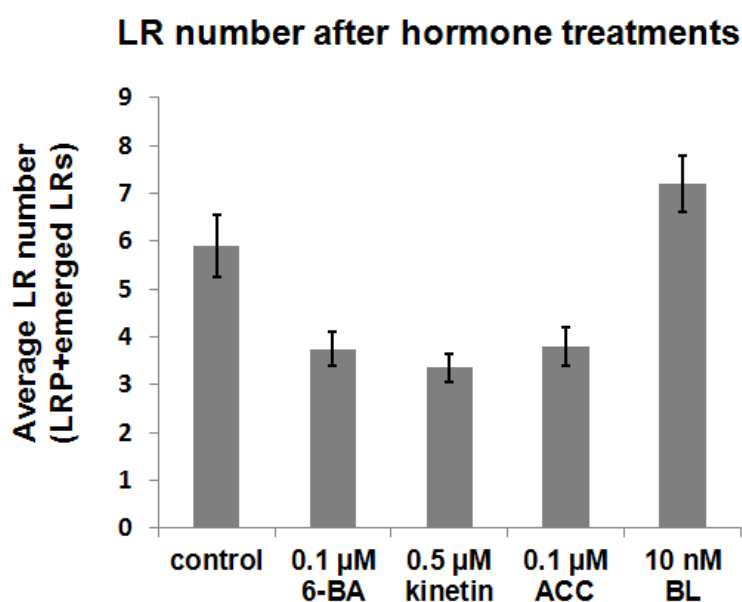


Figure S2 Cytokinin and ethylene inhibit LR formation whereas BR promotes LR formation. The hormone treatments of *proPIP2;8:GUS* fusion line (48 h) were the same as indicated in Figure 17. Average LR number and sem (standard error of the mean) values are shown (n=30-35).

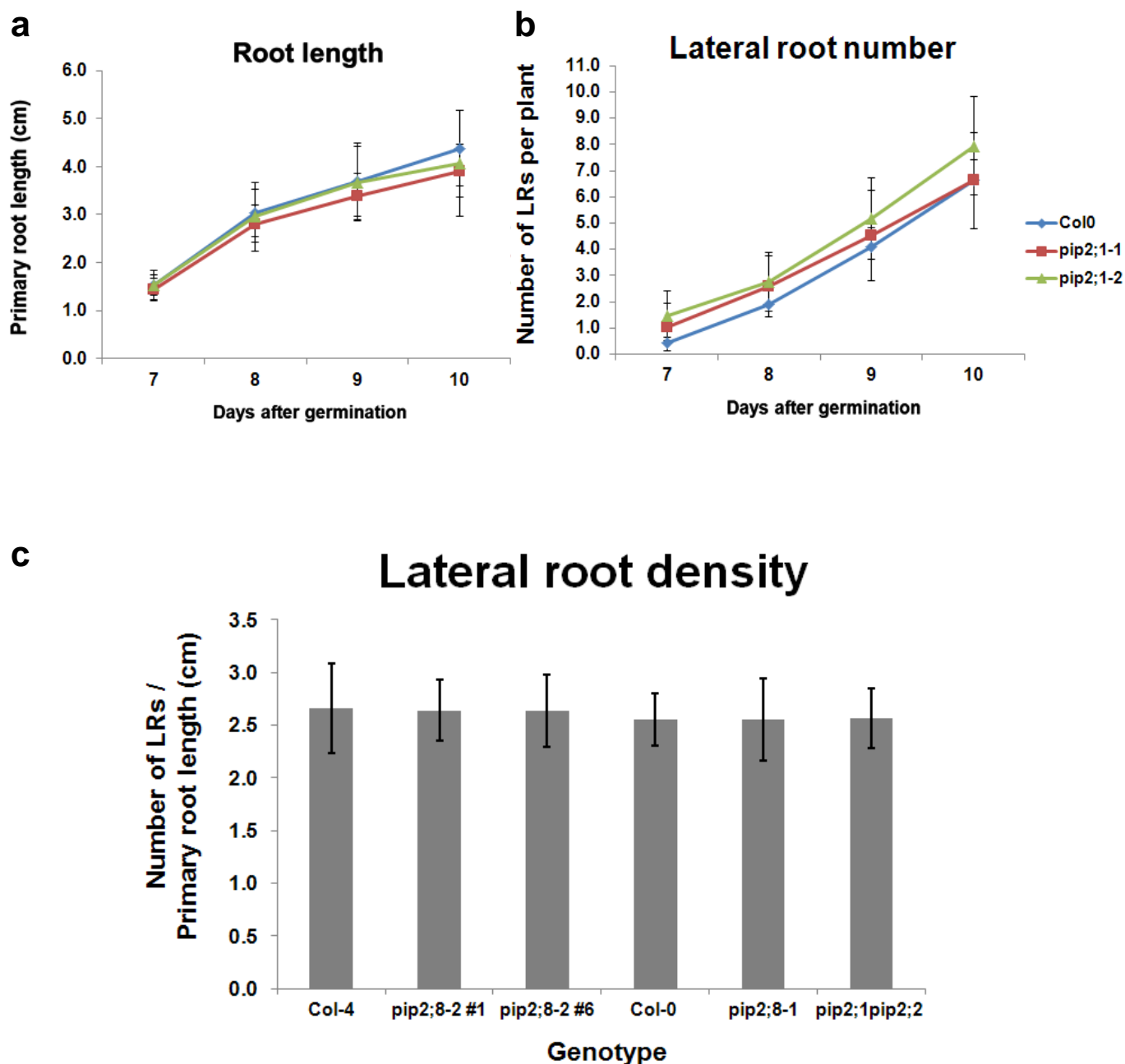


Figure S3 The primary root length and number of emerged LRs in *pip2;1* mutants (a, b) and lateral root density (LR number / primary root length) in two alleles of *pip2;8* mutants and *pip2;1 pip2;2* double mutant (c) are not altered compared with wild-type seedlings under normal growth condition. (a, b) The primary root length and emerged LR number of seven to ten-day-old seedlings were examined. Average root length and LR number and sem (standard error of the mean) values are shown (n=25). (c) The number of emerged LRs of nine-day-old seedlings was counted and their primary root lengths were measured by Image J (Version 1.46). Average LR density and sem (standard error of the mean) values are shown (n=30-35).

SUPPLEMENTARY MATERIALS

Table S1 The details of 29 TF genes selected from initial SOM analysis as candidates for controlling *PIP2;8* expression during LR development, which are ABA-inducible and/or not expressed in the stele.

AGI code	SOM cluster	Stele expression	Regulation of transcription	Response to hormones tested in this work		Response to other factors (hormones or stresses)
				ABA	other hormones	
AT1G02150	(0,0)	no	unknown	reduced		
AT1G10480	(0,0)	yes	unknown	induced		gibberellin
AT1G16530	(0,0)	no	unknown	no		
AT1G19050	(0,0)	no	unknown	no	cytokinin	chitin
AT1G70810	(0,0)	no	unknown	no		
AT2G37120	(0,0)	no	unknown	no		
AT2G46680	(0,0)	yes	positive	induced		
AT3G04570	(0,0)	no	unknown	no	auxin	
AT3G12720	(0,0)	no	unknown	no		
AT3G15790	(0,0)	no	unknown	induced		
AT3G18490	(0,0)	no	unknown	induced		
AT3G19380	(0,0)	no	unknown	no	auxin	chitin
AT4G30080	(0,0)	no	unknown	no	auxin	
AT4G34990	(0,0)	yes	unknown	induced	ethylene	jasmonic acid, salicylic acid, Ca ²⁺
AT4G36730	(0,0)	yes	negative	no		
AT4G36740	(0,0)	yes	unknown	induced	auxin	
AT5G07030	(0,0)	no	unknown	reduced		
AT5G66700	(0,0)	no	unknown	no	auxin, cytokinin	
AT1G10470	(0,1)	no	unknown	reduced	cytokinin	
AT1G13300	(0,1)	no	unknown	reduced		phosphate starvation
AT1G17950	(0,1)	yes	unknown	induced		
AT1G34670	(0,1)	no	unknown	induced	auxin	salicylic acid
AT1G73410	(0,1)	yes	unknown	induced		
AT1G77930	(0,1)	no	unknown	no		
AT3G01770	(0,1)	no	positive	no		
AT3G04070	(0,1)	yes	unknown	induced		
AT4G16780	(0,1)	yes	negative	no	auxin, cytokinin	
AT5G15830	(0,1)	no	unknown	reduced		
AT3G50700	(1,0)	no	positive	reduced		bacterium, systemic acquired resistance

6.2 Involvement of PIP aquaporins in response to altered environmental cues

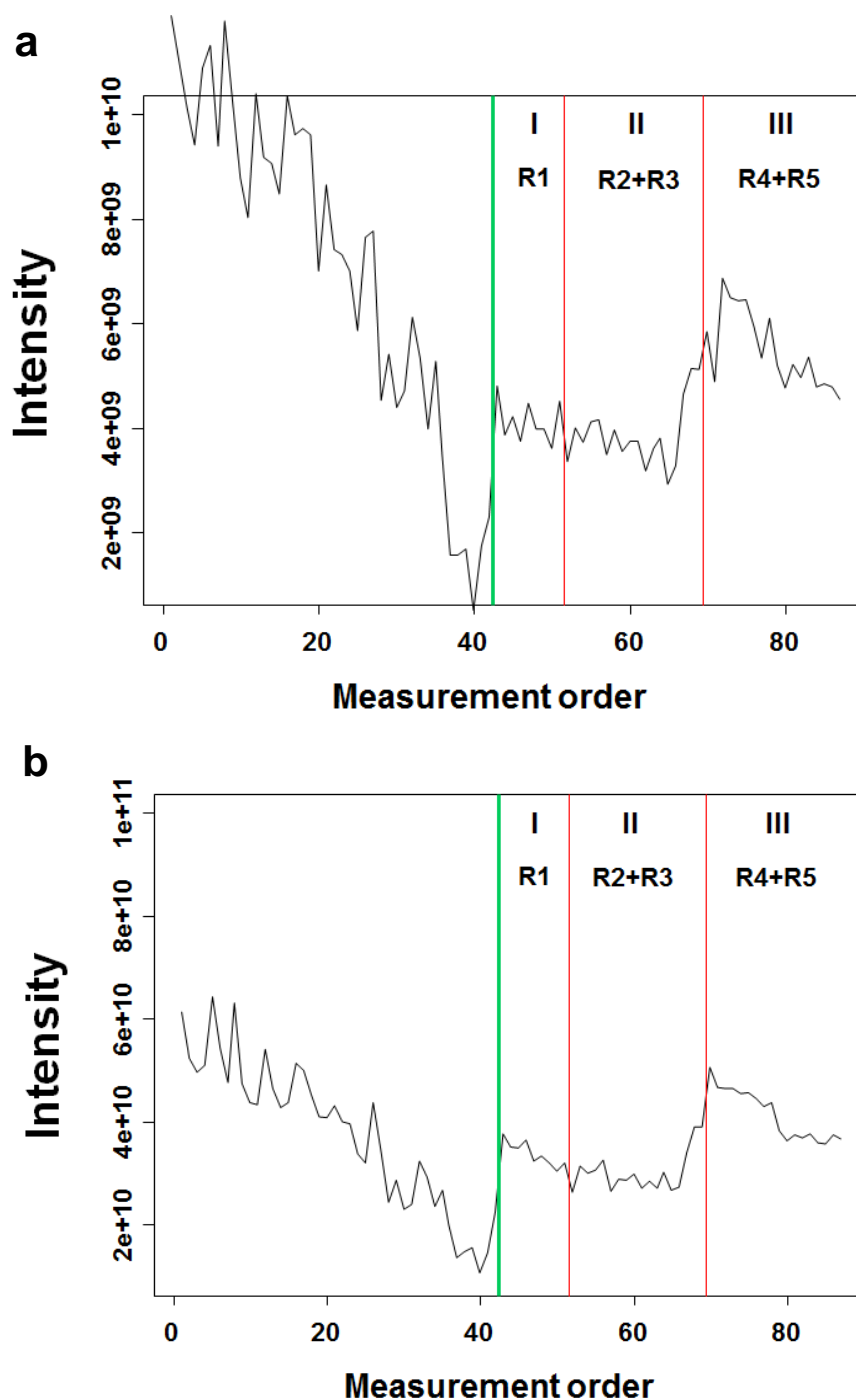


Figure S4 Quality control of FT-ICR-MS measurements (positive mode) by monitoring the variations of di-alanine intensity (a) and total peak intensities (b). Intensities of all samples from two IEs are plotted. Green line in each graph separates IE1-samples from IE2. Red lines indicate that the samples in IE2 were measured in three batches (I, II, III). They were split according to replicates as indicated.

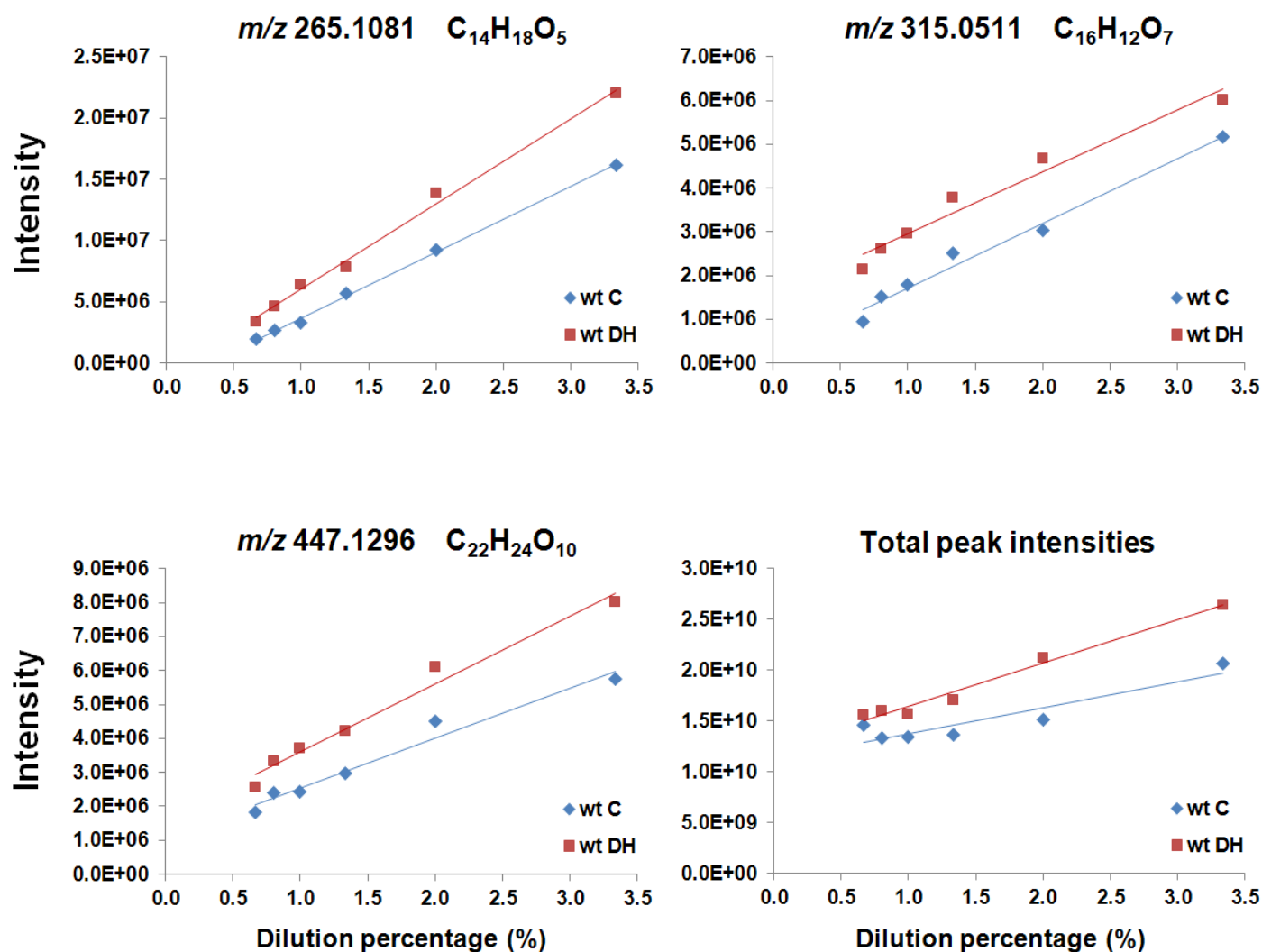


Figure S5 Dilution series assay using two wild-type samples under C and DH, respectively, demonstrated that the intensities of some endogenous metabolites (not drought inducible) and total peak intensities are higher in the DH-treated sample than those in the control sample regardless of dilution ratios. Six dilution ratios were performed: 1:150, 1:125, 1:100, 1:75, 1:50 and 1:30, and they correspond to 0.67 %, 0.8 %, 1 %, 1.33 %, 2 % and 3.33 % dilutions, respectively.

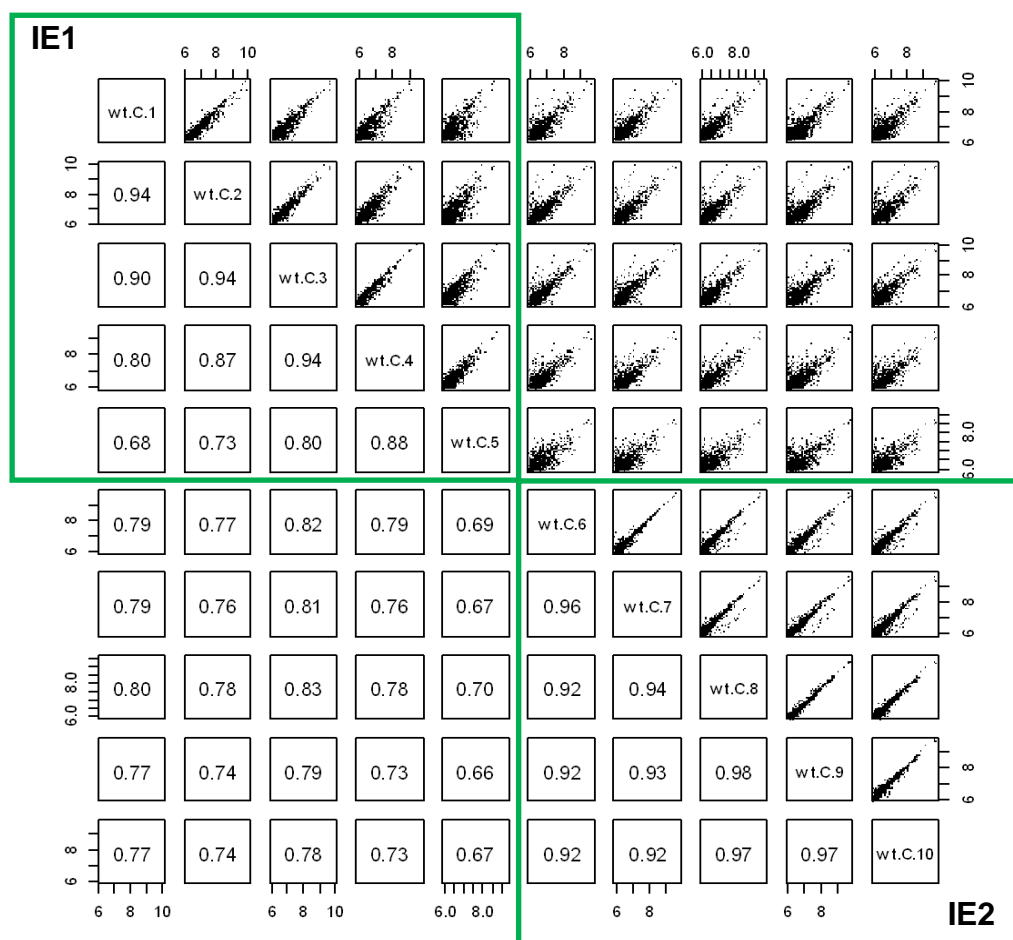
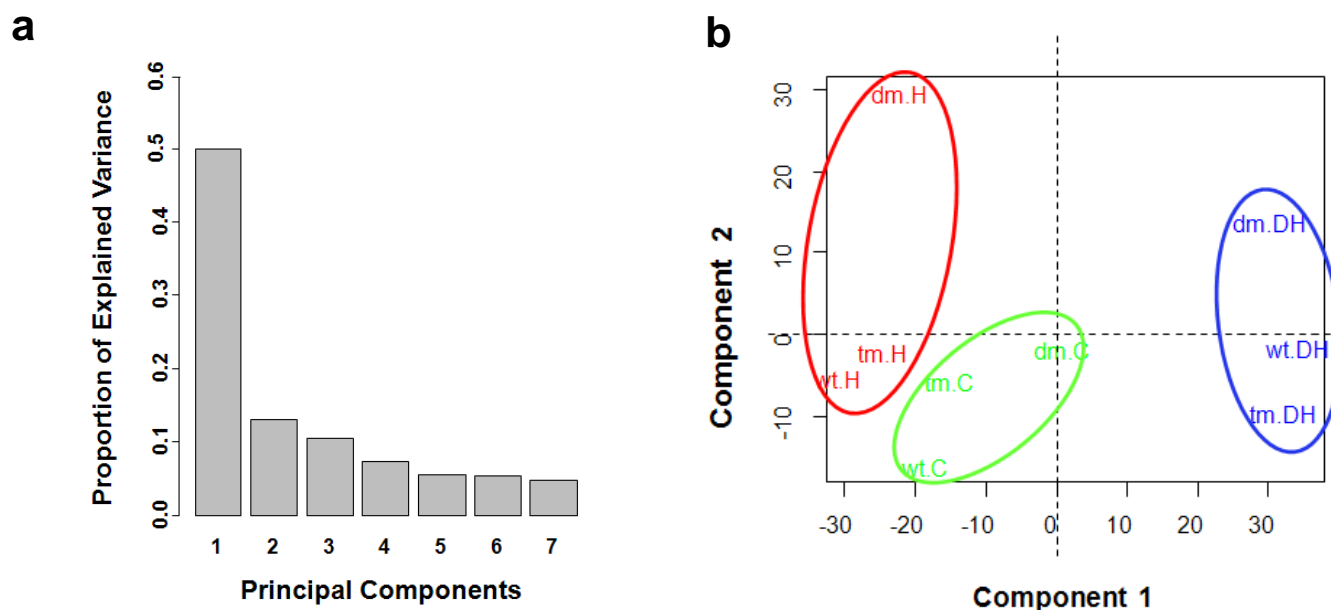


Figure S6 Pairwise xy-plots and Pearson correlation analysis between replicates in the group “wt under control condition” (positive mode). 1-5 represent extracts from IE1, and 6-10 are from IE2. Peak intensities (\log_{10} transformed) between two replicates were compared, and pairwise correlations were calculated as indicated. The results of extract reproducibility in other groups were similar to this group.



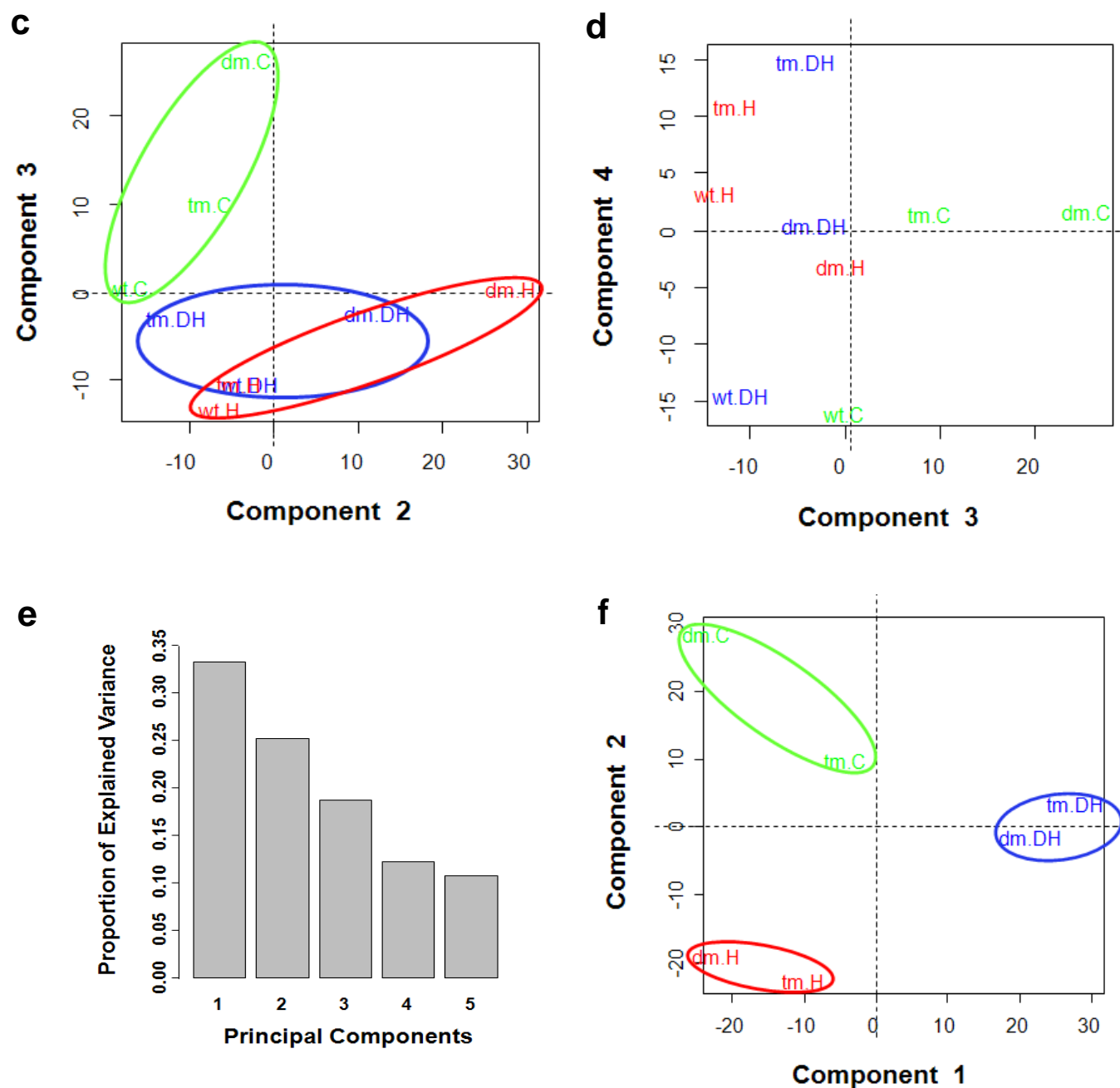


Figure S7 Principal component analysis (PCA) of metabolic profiles (positive mode) using group means (a-d) and mean mutant/wt ratios (e-f) as loading factors demonstrated that differential metabolic responses are caused by both stresses and *PIP* mutations. Principal component 1 and 2 (b and f), component 2 and 3 (c) and component 3 and 4 (d) are plotted. The green, red and blue circles label three (or two) genotypes treated with C, H and DH, respectively (b, c and f).

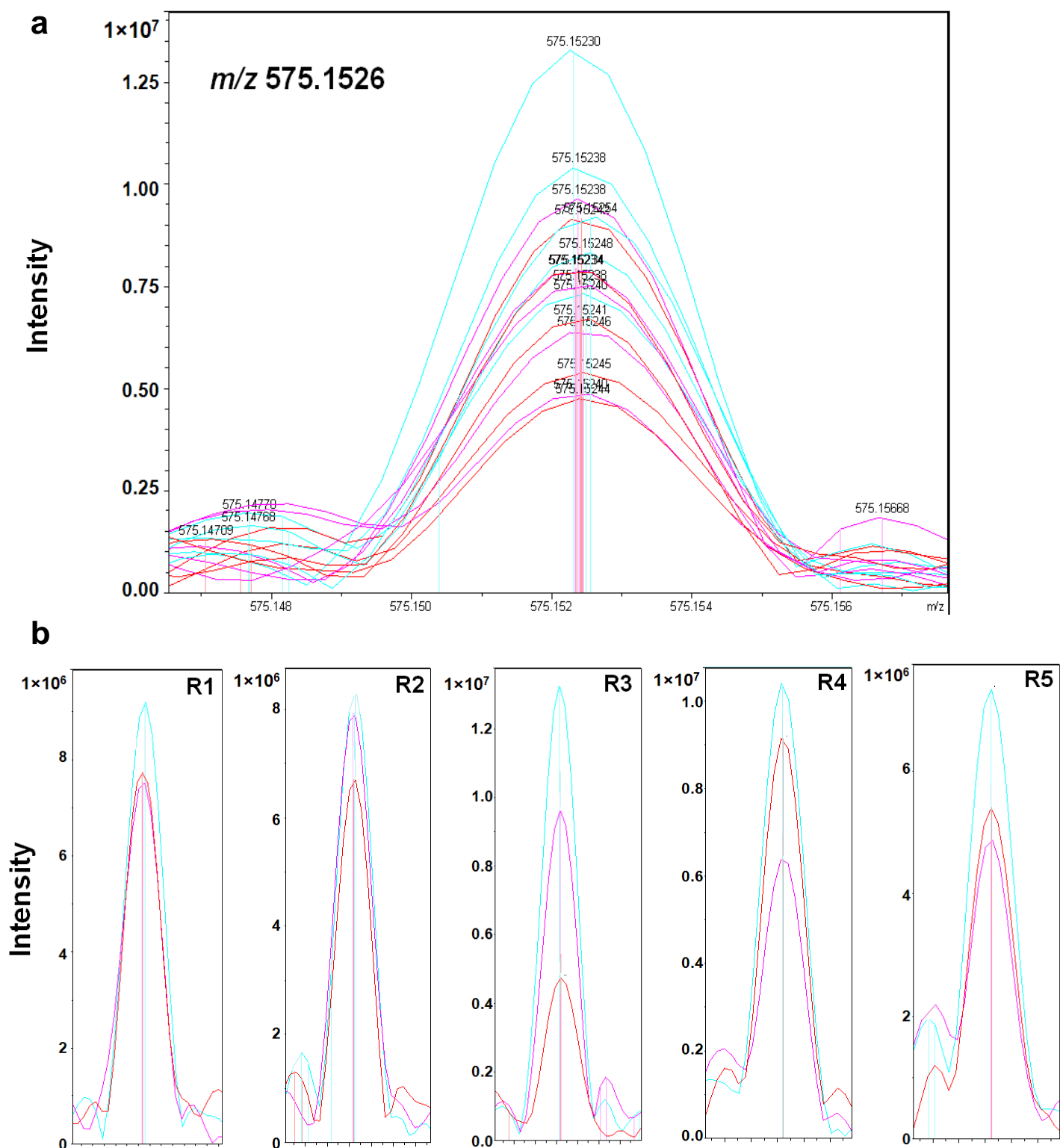


Figure S8 Original mass spectra of a selected peak m/z 575.1526 (significantly changed in *pip* mutants under C and H) overlaying all genotypes and replicates in IE1 (a) and overlaying all genotypes for each replicate (b). R1-R5 represent replicates 1 to 5. Spectra highlighted in light blue correspond to wild type and the ones in red and pink indicate two *pip* mutants.

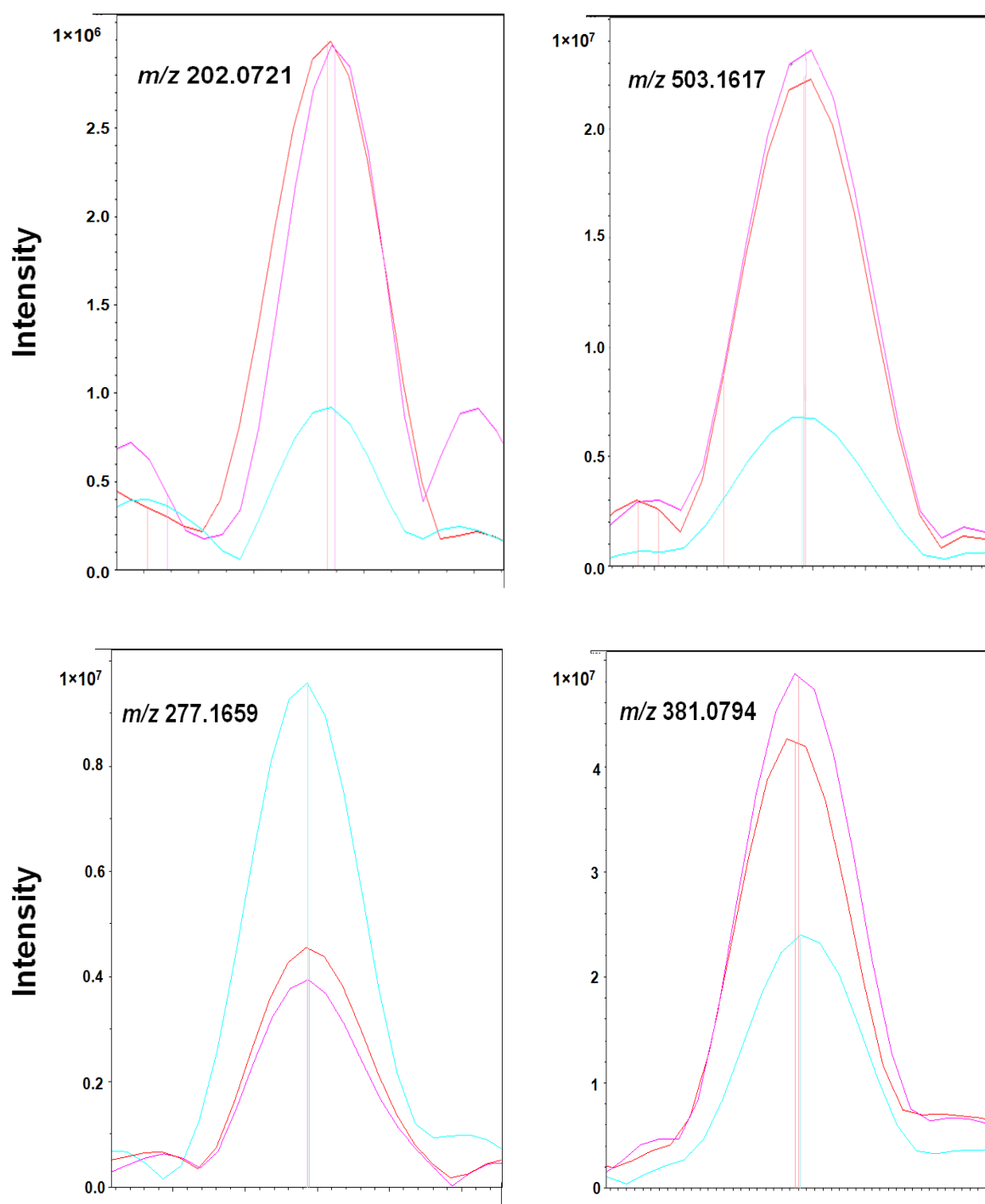


Figure S9 Original mass spectra of selected m/z peaks that were significantly changed in both *pip* mutants. For each m/z peak, the spectra from one replicate of three genotypes were overlaid. Spectrum highlighted in light blue in each graph corresponds to wild type and the ones in red and pink indicate two *pip* mutants. The spectrum overlays of these m/z peaks illustrate the ANOVA results.

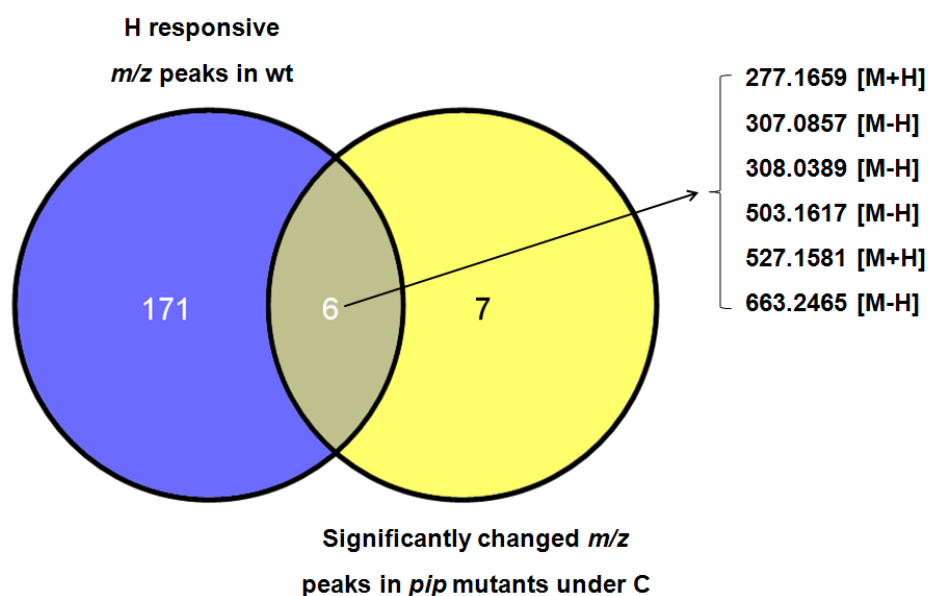


Figure S10 Six out of 13 *m/z* peaks, which were significantly changed in *pip* mutants under C in both negative- and positive-mode datasets, were responsive to heat stress (H) in wt (see Table S4). The H responsive *m/z* peaks in wt ($p < 0.05$) in both datasets were obtained *via* ANOVA (comparisons between H and C).

Table S2 The mean fresh weight in each group (a) and the corresponding ratio referring to the group “wt under C” (b) in each IE.

a		IE1			IE2		
	Genotype	Condition			Condition		
		C	DH	H	C	DH	H
	wt	4.38 g	2.80 g	4.43 g	4.97 g	3.53 g	5.18 g
	dm	4.48 g	2.99 g	4.65 g	4.91 g	3.57 g	5.17 g
	tm	4.53 g	3.03 g	4.69 g	4.87 g	3.61 g	5.20 g

b		IE1			IE2		
	Genotype	Condition			Condition		
		C	DH	H	C	DH	H
	wt	1.00	0.64	1.01	1.00	0.71	1.04
	dm	1.02	0.68	1.06	0.99	0.72	1.04
	tm	1.03	0.69	1.07	0.98	0.73	1.05

SUPPLEMENTARY MATERIALS

Table S3 Details of the significantly changed m/z peaks ($p < 0.01$) identified in both *pip* mutants under each environmental condition. The values of fold change showing > 1 and < 1 indicate “induced” and “reduced”, respectively.

<i>m/z</i>	log₁₀ transformed peak intensity	Fold change		<i>p</i> value	
		tm/wt	dm/wt	tm/wt	dm/wt
dm & tm under C					
<i>negative mode</i> [M-H]					
247.0646	6.05	0.70	0.75	0.0033	0.0097
307.0857	6.05	0.61	0.67	0.0011	0.0043
308.0389	6.11	0.68	0.76	0.0007	0.0058
338.0882	6.23	0.76	0.69	0.0065	0.0005
459.1241	6.14	1.61	1.74	0.0059	0.0014
503.1617	6.87	1.81	2.30	0.0063	0.0003
575.1526	6.93	0.69	0.70	0.0072	0.0074
663.2465	6.74	1.65	1.97	0.0058	0.0004
<i>positive mode</i> [M+H/Na]					
277.1659	6.82	0.76	0.65	0.0079	0.0002
287.1101	6.64	1.86	2.16	0.0057	0.0010
365.1055	8.20	1.23	1.31	0.0094	0.0013
458.1397	7.02	0.77	0.67	0.0055	0.0001
527.1581	6.91	1.68	2.06	0.0063	0.0004
531.0922	6.49	0.73	0.71	0.0085	0.0064
557.1551	8.04	0.82	0.77	0.0027	0.0002
dm & tm under H					
<i>negative mode</i> [M-H]					
341.1089	8.06	1.25	1.28	0.0091	0.0069
383.0652	6.17	1.35	1.36	0.0056	0.0064
395.0830	6.81	0.82	0.82	0.0018	0.0038
488.1621	6.55	1.35	1.33	0.0026	0.0048
503.1978	6.51	1.23	1.23	0.0047	0.0061
511.1034	6.35	1.25	1.34	0.0073	0.0013
512.1288	6.33	0.75	0.71	0.0005	0.0001
517.1940	7.76	0.83	0.82	0.0015	0.0015
575.1526	6.93	0.67	0.61	0.0029	0.0008
<i>positive mode</i> [M+H/Na]					
381.0794	7.98	1.24	1.36	0.0087	0.0006
506.1771	6.77	1.16	1.24	0.0067	0.0003

SUPPLEMENTARY MATERIALS

523.2097	6.96	2.60	2.72	0.0042	0.0030
525.1777	7.54	1.26	1.31	0.0020	0.0005
563.1454	6.91	1.23	1.47	0.0087	3.55e-05
dm & tm under DH					
<i>negative mode</i> [M-H]					
202.0721	5.92	2.42	2.38	3.22e-09	4.15e-09
227.1289	6.05	0.80	0.81	0.00709	0.00817
285.0187	6.00	1.43	1.41	0.00573	0.00751
330.0710	6.04	1.43	1.67	0.00949	0.00064
338.0882	6.23	0.74	0.70	0.00795	0.00241
366.0685	6.60	1.24	1.28	0.00399	0.00162
<i>positive mode</i> [M+H/Na]					
383.1187	6.50	1.43	1.46	0.0045	0.0032
453.1352	6.06	0.76	0.74	0.0071	0.0039

Table S4 Six out of 13 *m/z* peaks that were significantly changed in *pip* mutants under C ($p < 0.01$) were responsive to H in wt ($p < 0.05$). The rows of these six *m/z* peaks are highlighted. The values of fold change showing > 1 and < 1 indicate “induced” and “reduced”, respectively.

<i>m/z</i>	Fold change H/C in wt	<i>p</i> value H/C in wt	Fold change		<i>p</i> value	
			tm/wt under C	dm/wt under C	tm/wt under C	dm/wt under C
<i>negative mode</i> [M-H]						
247.0646	0.89	0.4182	0.70	0.75	0.0033	0.0097
307.0857	0.76	0.0361	0.61	0.67	0.0011	0.0043
308.0389	0.79	0.0484	0.68	0.76	0.0007	0.0058
459.1241	1.05	0.8256	1.61	1.74	0.0059	0.0014
503.1617	2.60	0.0035	1.81	2.30	0.0063	0.0003
663.2465	2.51	0.0016	1.65	1.97	0.0058	0.0004
<i>positive mode</i> [M+H/Na]						
277.1659	0.76	0.0106	0.76	0.65	0.0079	0.0002
287.1101	1.05	0.8923	1.86	2.16	0.0057	0.0010
365.1055	0.88	0.3646	1.23	1.31	0.0094	0.0013
458.1397	1.00	0.9988	0.77	0.67	0.0055	0.0001
527.1581	2.44	0.0027	1.68	2.06	0.0063	0.0004
531.0922	0.95	0.6174	0.73	0.71	0.0085	0.0064
557.1551	0.97	0.7754	0.82	0.77	0.0027	0.0002

SUPPLEMENTARY MATERIALS

Table S5 The predictions of molecular formulas and metabolite identities of m/z peaks significantly changed under heat stress with high air humidity (H) in wt ($p < 0.01$) in both negative- and positive-mode datasets. Forty-three significantly changed m/z peaks were identified, and only the ones attributed to putative metabolites in plants (*via* database search) are shown. The values of fold change showing > 1 and < 1 indicate “induced” and “reduced”, respectively.

m/z	Formula [M]	Putative metabolite in plants/annotated in KEGG	Pathway involved	Fold change ^a (p value)
<i>negative mode</i> [M-H]				
221.0491	C ₈ H ₁₄ O ₅ S	2-(3'-Methylthio) propylmalic acid in At ^b	glucosinolate biosynthesis	1.36 (0.0035)
259.0225	C ₆ H ₁₃ O ₉ P	glucose 6-phosphate etc. in At	carbohydrate metabolism	0.65 (0.0001)
503.1617	C ₁₈ H ₃₂ O ₁₆	trisaccharides in At	carbohydrate metabolism	2.60 (0.0035)
<i>positive mode</i> [M+H/Na]				
207.0992	C ₁₀ H ₁₆ O ₃	different metabolites in different plant species	monoterpenoid biosynthesis	1.43 (0.0017)
229.0496	C ₁₃ H ₈ O ₄	dihydroxyxanthone in many plant species	polyketide metabolism	0.57 (0.0028)
280.0921	C ₈ H ₂₀ NO ₆ P	glycerophosphocholine in KEGG	lipid metabolism	1.76 (0.0006)
395.1312	C ₁₇ H ₂₄ O ₉	syringin in At	phenylpropanoid biosynthesis	0.65 (0.0091)
411.0688	C ₁₉ H ₁₆ O ₉	different flavonols in different plant species	flavonoid metabolism	0.58 (0.0018)
527.1581	C ₁₈ H ₃₂ O ₁₆	trisaccharides in At	carbohydrate metabolism	2.44 (0.0027)

a) Fold change: H/C in wt.

b) At is the abbreviation for *Arabidopsis thaliana*.

SUPPLEMENTARY MATERIALS

Table S6 The putative metabolites showing induction upon classical heat stress have no response to heat stress with high air humidity (H). The formulas of the metabolites that have been shown to be induced by classical heat stress were obtained in KEGG. The m/z peaks with the same formulas were predicted as the corresponding putative metabolites detected in this work.

m/z	Formula [M]	Putative metabolite in <i>Arabidopsis</i>	Pathway involved	Fold change ^a (p value)	Response to classical heat ^b
165.0405 [M-H]	C ₅ H ₁₀ O ₆	ribonic acid		1.04 (0.6805)	induced
171.0064 [M-H]	C ₃ H ₉ O ₆ P	glycerol 3-phosphate	lipid metabolism	1.00 (0.9472)	induced
191.0197 [M-H]	C ₆ H ₈ O ₇	citric acid	citrate cycle etc.	1.04 (0.5595)	induced
191.0561 [M-H]	C ₇ H ₁₂ O ₆	quinic acid	amino acid metabolism	0.79 (0.1427)	induced
195.0510 [M-H]	C ₆ H ₁₂ O ₇	galactonic acid	carbohydrate metabolism	0.78 (0.2874)	induced
341.1089 [M-H]	C ₁₂ H ₂₂ O ₁₁	sucrose	carbohydrate metabolism	0.93 (0.6767)	induced
365.1055 [M+Na]	C ₁₂ H ₂₂ O ₁₁	sucrose	carbohydrate metabolism	0.88 (0.3646)	induced

a) Fold change: H/C in wt.

b) The response of each putative metabolite to classical heat stress is based on the published data (Kaplan *et al.*, 2004).

ACKNOWLEDGEMENTS

First of all, I would like to thank my supervisor PD Dr. Anton Schäffner for providing me an opportunity to pursue my scientific career and for his excellent guidance and support throughout my PhD study. His encouragement, advices and constructive criticism helped me all the time to solve the confusions and break the difficulties. In addition, his broad knowledge, scientific enthusiasm and stringency have deeply influenced me and set an example for my future work.

I would like to especially acknowledge Prof. Dr. Jörg Durner and the members of the examination committee for their willingness to review this work. I am also indebted to Prof. Dr. Jörg Durner for his ideas and advices to improve my projects during three thesis committee meetings and institute seminars.

I am very much grateful to all collaborators of two projects during my PhD study. First, I would like to give my sincere thanks to Prof. Malcolm Bennett from the University of Nottingham for his brilliant ideas and overall insights of the lateral root project. My thanks also go to other scientists in Prof. Bennett's lab, Dr. Benjamin Péret for teaching me the key experimental approaches and knowledge for lateral root research, Dr. Ute Voß for her kindness to provide the lateral root transcriptomic dataset, and Dr. Leah Band for her help on simulations of lateral root emergence phenotypes of *pip* mutants. Second, I am indebted to PD Dr. Philippe Schmitt-Kopplin and Dr. Basem Kanawati from the Research unit of Analytical BioGeoChemistry for their help with FT-ICR-MS measurements. Third, I wish to express my warm thanks to Dr. Andreas Albert, Dr. Barbro Winkler, Peter Bader and Andreas Glaser from the Research unit of Environmental Simulation for their strong support during the stress response experiments in the climate simulation chambers.

I am also very thankful to some Helmholtz colleagues who kindly provided help. I would like to especially acknowledge Theresa Faus-Kessler from the Institute of Developmental Genetics for her great contributions to the statistical analyses of metabolome data. My thanks also go to Dr. Peter Hutzler for introducing me the confocal laser scanning microscope, Dr. Ruben Ispiryan for his help on collecting photographic data and Dr. Hagen Scherb from the Institute of Biomathematics and Biometry for the statistical analysis of lateral root emergence phenotyping data.

I would like to express my gratitude to Dr. Veronica von Saint Paul for her valuable advices and support with regard to FT-ICR-MS measurements and data analysis, to Ming Jin and

ACKNOWLEDGEMENTS

Chen Liu for nice cooperation throughout the stress response experiments and for providing aquaporin mutant seeds, respectively. I am also very grateful to Dr. Günther Bahnweg for important advice for language corrections. In addition, I would like to express my gratitude to Birgit Geist and Susanne Stich for their help and technical assistance, also to Karoline Stoll and Antonie Bernhard for helping me fill-in many German forms. Special thanks go to other current and former members of Dr. Schäffner's group and my office mates, including Dr. Stephan Dräxl, Dr. Ruohé Yin, Wei Zhang, Dr. Malay Das, Kerstin Schuster, Rafał Maksym and Christian Holzmeister, for many interesting discussions. I also would like to give my thanks to all other BIOP colleagues.

Finally, I want to say "thank you" to my family and friends in China. My parents and parents in law, grandmother, aunt and uncle gave me a lot of support and love since I started my PhD study. My deepest gratitude also goes to my husband Guangzhe. His understanding and encouragement are always the biggest support of my research.

CURRICULUM VITAE

Name: **Jin Zhao**
Date of birth: 28/09/1982
Place of birth: Shenyang, Liaoning Province, China
Nationality: Chinese
Marital status: Married

EDUCATION & RESEARCH EXPERIENCES

Since 08/2009: Graduate student in Biochemistry at Ludwig-Maximilians Universität München, Germany
Research topic: Roles of PIP aquaporins in lateral root development and stress responses in *Arabidopsis thaliana*.
Supervisor: PD Dr. Anton Schäffner, Institute of Biochemical Plant Pathology, Helmholtz Zentrum München, Germany

09/2005 – 07/2008: Master in Genetics at Beijing Normal University, China
Research topic: Changes of genomic DNA methylation of *Arabidopsis* treated by low energy ion implantation.
Supervisor: Prof. Genfa Zhang, College of Life Science, Beijing Normal University, China

09/2001 – 07/2005: Bachelor in Biology at Liaoning Normal University, China

PUBLICATIONS

Péret B, Li G, **Zhao J**, Band L R, Voss U, Postaire O, Luu D T, Da Ines O, Casimiro I, Lucas M, Wells D M, Lazzerini L, Nacry P, King J R, Jensen O E, Schäffner A R, Maurel C, and Bennett M J. Auxin regulates aquaporin function to facilitate lateral root emergence. *Nat. Cell Biol.* (2012) 14(10): 991-998.

Co-first authors

Yu H, **Zhao J**, Xu J, Li X, Zhang F, Wang Y, Carr C, Zhang J, and Zhang G. Detection of changes in DNA methylation induced by low-energy ion implantation in *Arabidopsis thaliana*. *Radiat. Res.* (2011) 175(5): 599-609.

Li K, Jiang S, Yu H, **Zhao J**, Zhang F, Carr C, Zhang J, and Zhang G. Analysis of charge and mass effects on peroxidase expressions and activities in *Arabidopsis thaliana* after low-energy ion irradiation. *Mutat. Res.* (2009) 680(1-2): 64-69.

MEETING/WORKSHOP PRESENTATIONS

- 06/2012
Talk Auxin-initiated regulation of PIP aquaporin expression is required to facilitate lateral root emergence.
SEB (Society of Experimental Biology) annual meeting 2012 in Salzburg (Austria)
- 09/2011
Poster Differential reactions of aquaporin mutants in *Arabidopsis thaliana* in response to drought.
Botanikertagung in Berlin (Germany)
- 10/2010
Poster Exposure chambers for controlled environmental simulation: Molecular and physiological reactions of aquaporin mutants in *Arabidopsis thaliana* in response to drought and enhanced temperature.
Systems Biology Workshop in Freiburg (Germany)

AWARDS

- 2012** Chinese Government Award for Outstanding Self-financed Students Abroad
- 2007** Excellent Academic Scholarship (Beijing Normal University)